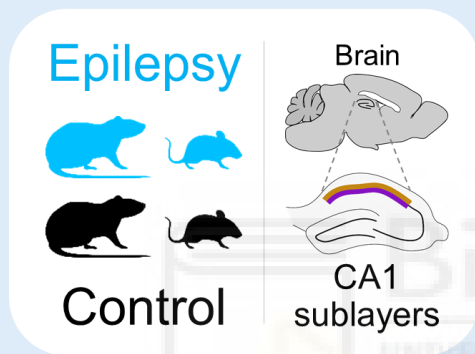# NEURODEGENERATIVE TRAJECTORIES IN A MODEL OF EPILEPSY WITH HIPPOCAMPAL SCLEROSIS

Ángel Márquez Galera
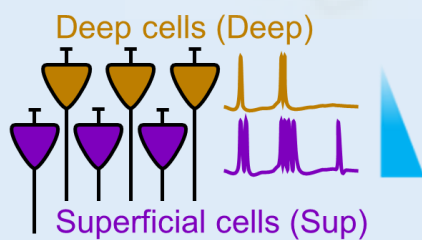**PhD Thesis**

Supervised by Dr. José Pascual López-Atalaya Martínez

PhD Program in Neuroscience
Universidad Miguel Hernández de Elche
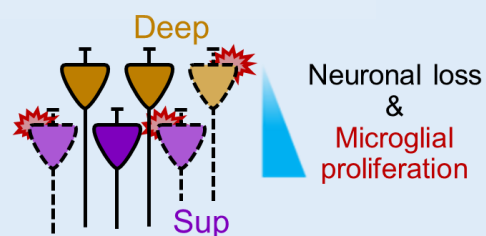**Campus de Sant Joan**

INSTITUTO DE NEUROCIENCIAS
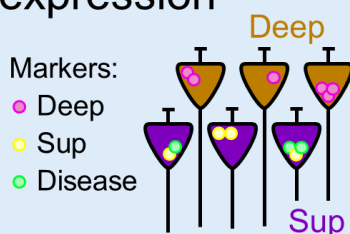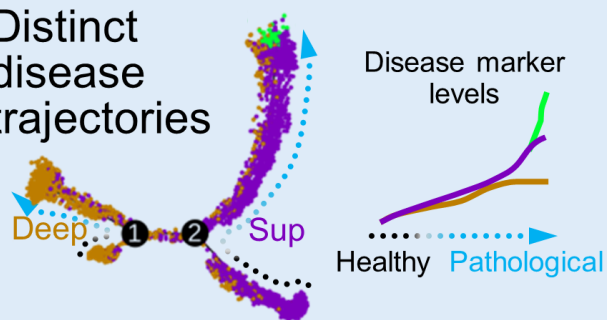
NEURODEGENERATIVE TRAJECTORIES IN A MODEL OF EPILEPSY WITH HIPPOCAMPAL SCLEROSIS

Doctoral Thesis presented by

Ángel Márquez Galera

Thesis Director:

Dr. José Pascual López-Atalaya Martínez

PhD Program in Neuroscience

Instituto de Neurociencias (UMH-CSIC)

Universidad Miguel Hernández de Elche

Campus de Sant Joan

- 2022 -

INSTITUTO DE NEUROCIENCIAS   UNIVERSITAS Miguel Hernández   EXCELENCIA SEVERO OCHOA   GOBIERNO DE ESPAÑA MINISTERIO DE CIENCIA E INNOVACIÓN

Sant Joan d'Alacant, 14th June, 2022

To whom it may concern,

The doctoral thesis entitled "***Neurodegenerative trajectories in a model of epilepsy with hippocampal sclerosis***" has been developed by myself, Ángel Márquez Galera. It is based on the studies carried out at the Instituto de Neurociencias in Alicante within the framework of the PhD Program in Neuroscience of the Universidad Miguel Hernández. This thesis is presented in a compendium of publications format and includes the following publication of which I am the first author:

- Elena Cid*, **Angel Marquez-Galera***, Manuel Valero, Beatriz Gal, Daniel C. Medeiros, Carmen M. Navarron, Luis Ballesteros-Esteban, Rita Reig-Viader, Aixa V. Morales, Ivan Fernandez-Lamo, Daniel Gomez-Dominguez, Masaaki Sato, Yasunori Hayashi, Alex Bayes, Angel Barco, Jose P. Lopez-Atalaya[#], Liset M. de la Prida[#]. Sublayer- and cell-type-specific neurodegenerative transcriptional trajectories in hippocampal sclerosis. *Cell Reports*, 2021 Jun 8; *35*(10):109229. ISSN: 2211-1247. doi: 10.1016/j.celrep.2021.109229

---

* These authors contributed equally.

[#] Corresponding authors.

As a complement and directly related to the scientific publication that forms the core of my thesis and its indication of quality, I have developed two interactive web applications that allows to explore the results of the transcriptomic analyses, and I have also contributed a step-by-step method that favors reproducibility of the computational analysis to extract cell-specific signatures from bulk-tissue RNA-seq reported in the main manuscript (Cid, Marquez-Galera, et al., 2021):

- Transcriptional profiling along the radial axis of normal and epileptic CA1: http://lopezatalayalab.in.umh-csic.es/CA1_Sublayers_&_Epilepsy

- Single-nuclei transcriptional profiling of normal and epileptic CA1: http://lopezatalayalab.in.umh-csic.es/CA1_SingleNuclei_&_Epilepsy

- **Angel Marquez-Galera**, Liset M. de la Prida, Jose P. Lopez-Atalaya (2022). A protocol to extract cell-type-specific gene expression signatures from differentially expressed genes in bulk-tissue RNA-seq. *STAR Protocols*, *3*(1), 101121. doi: 10.1016/j.xpro.2022.101121

Sant Joan d'Alacant, 14th June, 2022

Dr. José Pascual López-Atalaya Martínez, Tenured Scientist by the Spanish National Research Council (CSIC) at the Institute of Neurosciences in Alicante (UMH-CSIC) and Director of the Doctoral Thesis entitled "*Neurodegenerative trajectories in a model of epilepsy with hippocampal sclerosis*",

INFORMS:

That Mr. Ángel Márquez Galera has carried out under my supervision the work entitled "*Neurodegenerative trajectories in a model of epilepsy with hippocampal sclerosis*" in accordance with the terms and conditions defined in his Research Plan and in accordance with the Code of Good Practice of the University Miguel Hernández of Elche, satisfactorily fulfilling the objectives foreseen for its public defence as a Doctoral Thesis.

Which I sign for the appropriate purposes,

Dr. José Pascual López-Atalaya Martínez

Thesis Director

Sant Joan d'Alacant, 14th June, 2022

Dr. Elvira de la Peña García, Coordinator of the Neurosciences PhD programme at the Institute of Neurosciences in Alicante, a joint centre of the Miguel Hernández University (UMH) and the Spanish National Research Council (CSIC),

INFORMS:

That Mr. Ángel Márquez Galera has carried out under the supervision of our PhD Programme the work entitled "***Neurodegenerative trajectories in a model of epilepsy with hippocampal sclerosis***" in accordance with the terms and conditions defined in his Research Plan and in accordance with the Code of Good Practice of the University Miguel Hernández de Elche, satisfactorily fulfilling the objectives foreseen for its public defence as a Doctoral Thesis.

Which I sign for the appropriate purposes,

Dr. Elvira de la Peña García

Coordinator of the PhD Programme in Neurosciences

Sant Joan d'Alacant, 14th June, 2022

En primer lugar, quiero agradecer a mi director de tesis, Jose, me has dado la oportunidad de trabajar en este proyecto de tesis y en muchas otras colaboraciones, confiando en mí desde los inicios del establecimiento del grupo de investigación. Tu labor como mentor, y la orientación, el apoyo económico que me has brindado y el esfuerzo conjunto me ha permitido aportar mi granito de arena a este y otros proyectos muy relevantes en el panorama nacional e internacional. Además, me has dado la oportunidad de consolidar y ampliar mis conocimientos bioinformáticos y abrirme paso al mundo de la ciencia de datos, algo realmente valioso a nivel personal y profesional.

Quiero dar las gracias a Liset, Elena, Manuel y Carmen, así como al resto de autores de la publicación científica que constituye el núcleo de mi tesis, por vuestro apoyo y contribución a este proyecto, este trabajo es fruto del esfuerzo de todo el equipo.

También quiero agradecer a todos los amigos y compañeros del Instituto de Neurociencias que me han acompañado, han compartido su tiempo, sus problemas y sus metas, y me han escuchado y animado a seguir a lo largo de este periodo. A mis compañeros de batalla en el laboratorio, Aysha, Verónica, Alejandro y Daniel. A los que ya han comenzado una nueva etapa fuera del centro, Ana, Juan Medrano, Jeiny, Carmen, Sergio Valbuena y Michał. Y a los que aún siguen dándolo todo, Sergio Niñerola, Miguel, Marta Alaiz, Marilyn,

Lorenzo, Isabel, Juan Paraíso, Antonio Caler, Bea del Blanco, Marta Arumí, Carina, Beatriz Fernández, Khalil, Mayte, Román, Sonia, Lucía, Noemí, Óscar y Sergio del Olmo. No me olvido de aquellas personas que se dedican a servicios y tareas generales en el Instituto, con las que, aún estando ocupadas en otras tareas, han mostrado una sonrisa sincera y han dedicado parte de su tiempo a interesarse por cómo va todo, gracias Francis, Trini, Joan, Luís, Víctor Rodríguez, Maite y Enriqueta. Tampoco me olvido de Elvira, Cruz y Virtudes, por su voluntad y disposición para resolver dudas, orientarme y ayudarme con los temas administrativos del doctorado.

A mis amigos, Rubén, Jose, Isa, Melisa, Andrés, Patricia, Álex, Miguel, Alicia, Alba, Sandra, Ángel y Antonio, sois únicos y muy importantes para mí. Aunque apenas he tenido tiempo estos últimos años, sé que siempre he podido y podré contar con vosotros. Quiero que sepáis que vosotros también podéis contar conmigo. Gracias por ser así y por vuestro afecto, apoyo y dedicación.

Por último, quiero terminar agradeciendo a toda mi familia el apoyo, comprensión y cariño que me han dado. En especial a mis abuelos, mi tía Melina, mi tío Francis y mi primo Abel, por estar siempre ahí, a mis hermanos, por compartir tantos momentos, y a mis padres, por el esfuerzo que han realizado y los valores que me han transmitido, sin los cuales no habría podido llegar hasta aquí.

Table of contents

List of abbreviations

AC	Alternating current		CSD	Current source density
Ag	Silver		CT	Corticothalamic
AgCl	Silver chloride		CTX	Cortex
AHP	Afterhyperpolarization		c-Fos	Proto-Oncogene c-Fos
ANOVA	Analysis of variance		DAVID	Database for Annotation, Visualization and Integrated Discovery
AP	Anteroposterior			
Astro	Astrocytes		DDRTree	Discriminative dimensionality reduction with trees
ATP	Adenosine triphosphate			
AUC	Area under the curve			
Bdnf	Brain-derived neurotrophic factor		DEA	Differential expression analysis
BEAM	Branched expression analysis modeling		Deep	Deep CA1 layer/cells
			DEG	Differentially expressed genes
BH	Benjamini-Hochberg			
BSA	Bovine serum albumin		DG	Dentate gyrus
CA	Cornu Ammonis		DNA	Deoxyribonucleic acid
CA1	Cornu Ammonis region 1		DNase	Deoxyribonuclease
CA2	Cornu Ammonis region 2		DPSS	Diode pumped solid state
CA3	Cornu Ammonis region 3		DPX	Dibutylphthalate Polystyrene Xylene
CA3c	Cornu Ammonis region 3 division c			
CA4	Cornu Ammonis region 4		DREADD	Designer receptor exclusively activated by designer drugs
Calb	Calbindin			
Calb1	Calbindin-1		DsRed2	Red fluorescent protein
Casp3	Caspase-3		EDTA	Ethylenediaminetetra-acetic acid
CB	Calbindin			
cDNA	Complementary DNA		EEC	European Economic Community
CE	Conformité Européenne (French for "European conformity")			
			EEG	Electroencephalography
			Endo	Endothelial
CpG	DNA sequence in which a cytosine nucleotide is followed by a guanine nucleotide		ENT	Entorhinal cortex
			ENTl	Entorhinal cortex, lateral part
			ERDF	European Regional Development Fund
Cre	Cre recombinase			

Excit	Excitatory neurons		IgG	Immunoglobulin G
Fab	Antigen binding fragments		IGV	Integrative Genomics Viewer
FACS	Fluorescence-activated cell sorting		IID	Interictal discharges
FBS	Fetal bovine serum		III	3
FC	Fold change		IL	Interleukin
FDR	False discovery rate		ILAE	International League Against Epilepsy
Fig	Figure		Inc	Incorporated
FIR	Finite impulse response		Inter	Inhibitory neurons
GABA	Gamma-aminobutyric acid		IT	Intratelencephalic
GBD	Global burden of disease		kHz	Kilo-hertz
GEO	Gene Expression Omnibus		L2	Layer 2
GO	Gene Ontology		L3	Layer 3
GRCm38	Genome Reference Consortium Mouse Build 38		L5	Layer 5
			L6	Layer 6
			L6b	Layer 6b
GWAS	Genome-wide association studies		Lab	Laboratory
			LAS	Leica Application Suite
HBSS	Hank's balanced salt solution		LCM	Laser capture microdissection
HCl	Hydrogen chloride		LFP	Local field potential
HDAC	Histone deacetylase		MACS	Magnetic-activated cell sorting
HeNe	Helium-Neon			
HFO	High-frequency oscillation		$MgCl_2$	Magnesium chloride
HFSP	Human Frontiers Science Program		MICINN	Ministerio de Ciencia e Innovación
HS	Hippocampal sclerosis		MICIU	Ministerio de Ciencia, Innovación y Universidades
HTSeq	High-throughput sequence analysis		Micro	Microglia
HVGs	Highly variable genes		MINECO	Ministerio de Asuntos Económicos y Transformación Digital
Hz	Hertz			
ID	Identifier		ML	Mediolateral
IGEPAL	Octylphenoxy poly(ethyleneoxy)ethanol		Mm	Mus musculus
			mRNA	microRNA

MΩ	megohm		PVM	Brain perivascular macrophages
nA	nanoampere		Pyr	Pyramidal
NaCl	Sodium chloride		Pyr_CA1	CA1 pyramidal cells
NCBI	National Center for Biotechnology Information		Pyr_ES	Epilepsy-specific pyramidal cell population
NGS	Next Generation Sequencing		qPCR	Quantitative polymerase chain reaction
NIH	National Institutes of Health		RHP	Retrohippocampal region
			RIN	RNA integrity number
NMDAR	N-methyl-D-aspartate receptor		RMP	Resting membrane potential
NP	Near-projecting		RNA	Ribonucleic acid
ODC	Oligodendrocytes		RNase	Ribonuclease
Oligo	Oligodendrocytes		RNA-seq	Ribonucleic acid sequencing
OPCs	Oligodendrocyte progenitor cells		Rnor	Rattus norvegicus
P2ry12	Purinergic receptor gene P2ry12		ROC	Receiver operating characteristic
padj	Adjusted p value		ROI	Region of interest
PBC	Public Benefit Corporation		RRID	Research Resource Identifiers
PBS	Phosphate buffered saline		RT	Room temperature
PC	Principal component		RYC	Ramón y Cajal Programme
PCA	Principal component analysis		SC3	Single-cell Consensus Clustering
PCR	Polymerase chain reaction		scATAC	single-cell Assay for Transposase-Accessible Chromatin
PEN	Polyethylene naphthalate		scChIP	single-cell Chromatin Immunoprecipitation
Peri	Pericytes			
PFA	Paraformaldehyde		scRNA	single-cell RNA
pH	Potential of hydrogen		SDs	Standard deviations
PhD	Doctor of Philosophy		SEV	Severo Ochoa grant
ProS	Prosubiculum		SLM	Stratum lacunosum moleculare
PV	Parvalbumin			
Pvalb	Parvalbumin		SMART	Switching Mechanism At the end of the 5'-end of the RNA Transcript

SMC	Smooth Muscle Cells	TLE	Temporal lobe epilepsy
SNP	Single-nucleotide polymorphism	TPE	Temporal, perirhinal and ectorhinal
snRNA	single-nucleus RNA	Tris-HCL	Tris hydrochloride
snRNA-seq	single-nucleus RNA sequencing	tSNE	t-distributed stochastic neighbor embedding
SO	Stratum oriens	Tx	Triton X-100
SP	Stratum pyramidale	UMAP	Uniform manifold approximation and projection
SPW	Sharp waves		
SR	Stratum radiatum	UMI	Unique Molecular Identifier
Sst	Somatostatin		
STAR	Structured, Transparent, Accessible Reporting	UV	Ultraviolet
		VLMC	Vascular and leptomeningeal cells (Mural cells)
SUB	Subiculum		
Sup	Superficial CA1 layer/cells		
		Wfs1	Wolframin
SynCogDis	Synaptic Role in Cognitive Disabilities Network	WHO	World Health Organization

Summary

Temporal lobe epilepsy (TLE), the most common form of focal epilepsy, is a chronic disorder of the nervous system which is characterized by recurrent, unprovoked focal seizures that originate in the temporal lobe of the brain. Hippocampal sclerosis (HS), the major neuropathological hallmark of temporal lobe epilepsy, is characterized by different patterns of neuronal loss and is associated with cognitive impairment and drug resistance. One of the areas most affected by hippocampal sclerosis is the CA1 subfield, a layered structure consisting of a superficial and a deep sublayer. However, the mechanisms leading to CA1 hippocampal sclerosis are unknown. Using single-cell electrophysiology *in vivo* and immediate-early gene expression, we reveal that superficial CA1 pyramidal neurons are overactive in epileptic rodents. Bulk tissue and single-nucleus expression profiling disclose sublayer-specific transcriptomic signatures. These analyses reveal that superficial sublayer is more severely affected by epilepsy, showing a prominent neurodegeneration-associated transcriptomic signature that was characterized by upregulation of microglia reactive response and cell cycle genes, and downregulation of neuronal plasticity genes. Pseudotime analysis of gene expression in single nuclei and *in situ* validation reveal separated trajectories from health to epilepsy across cell types and identify a subset of superficial cells undergoing a later stage in neurodegeneration. Our findings indicate that sublayer- and cell-type-specific changes associated with selective neuronal damage in CA1 contribute to progression of hippocampal sclerosis, with neurons populating the superficial CA1 sublayer being much more vulnerable than those in the deep sublayer. In addition, we have introduced a protocol that leverages existing single-cell expression data to deconvolve lists of differentially expressed genes from highly heterogeneous tissues into cell-type-specific gene expression patterns. We have made all the data from this study accessible as public resources through interactive websites that facilitate exploration of analysis results.

Resumen

La epilepsia del lóbulo temporal (TLE), la forma más común de epilepsia focal, es un trastorno crónico del sistema nervioso que se caracteriza por convulsiones focales recurrentes y no provocadas que se originan en el lóbulo temporal del cerebro. La esclerosis del hipocampo (HS) es el principal signo neuropatológico de la epilepsia del lóbulo temporal y se caracteriza por diferentes patrones de pérdida neuronal que están asociados a deterioro cognitivo. Una de las zonas más afectadas por la esclerosis del hipocampo es la capa CA1, formada por una subcapa superficial y otra profunda. Sin embargo, se desconocen los mecanismos que subyacen a la esclerosis de la capa CA1 del hipocampo. Utilizando electrofisiología unicelular *in vivo* y la expresión génica inmediata y temprana, revelamos que las neuronas piramidales superficiales de CA1 son hiperactivas en roedores epilépticos. Los perfiles de expresión a nivel de tejido y de núcleo único revelan firmas transcriptómicas específicas de subcapa y respuestas microgliales proinflamatorias robustas asociadas a epilepsia afectando a la subcapa superficial. Los tránscritos que regulan los procesos neuronales como los canales de voltaje, la señalización sináptica y la adhesión celular se desregulan de manera diferente por la epilepsia en las subcapas, mientras que las firmas neurodegenerativas involucran principalmente células superficiales. El análisis de pseudotiempo de la expresión génica de núcleo único y la validación *in situ* revelan trayectorias separadas desde la salud hasta la epilepsia a través de los tipos celulares e identifican un subconjunto de células superficiales que atraviesan una etapa posterior de neurodegeneración. Nuestros hallazgos indican que los cambios específicos de subcapa y tipo celular asociados con el daño neuronal selectivo en CA1 contribuyen a la progresión de la esclerosis del hipocampo, siendo las neuronas que pueblan la subcapa superficial de CA1 mucho más vulnerables que las de la subcapa profunda. Además, hemos introducido un protocolo que aprovecha los datos de expresión unicelular existentes para deconvolucionar patrones de expresión génica específicos de tipo celular a partir de listas de genes expresados diferencialmente en tejidos altamente heterogéneos. Finalmente hemos hecho accesibles los datos de este estudio como recursos públicos a través de sitios web interactivos que facilitan la exploración de los resultados de los análisis.

Introduction

1. Epilepsy

Epilepsies are chronic brain disorders characterized by an enduring predisposition to generate seizures, triggered by abnormal electrical activity at neuronal level. Epilepsies have a broad spectrum of symptoms and clinical signs – from unusual sensations to seizures with loss of awareness with emotional and cognitive associated comorbidities.

Epilepsies are the common clinical manifestation of different diseases with very diverse etiology including structural, metabolic, immune, infectious, genetic, neurodegenerative and idiopathic causes, which are not mutually exclusive (Balestrini et al., 2021; Scheffer et al., 2017). The International League Against Epilepsy (ILAE) classifies seizure types by their onset, that can be focal, generalized or unknown, and with or without motor onset (Fisher et al., 2017). Diagnosis of the seizure type is followed by diagnosis of epilepsy type, which includes focal epilepsy, generalized epilepsy, combined generalized and focal epilepsy, and also unknown epilepsy type (Scheffer et al., 2017).

In 2016 epilepsies were the fifth largest contributor to global neurological disability-adjusted life-years (GBD 2016 Neurology Collaborators, 2019) and responsible for more than 0.5% of the global burden of disease (GBD 2016 Epilepsy Collaborators, 2019), with a socio-economic burden that in 2004 was estimated in 15.5 billion euros per year in Europe alone (Pugliatti et al., 2007). Epilepsies affect around 50 million people of all ages, sexes and income levels worldwide (WHO, 2019), although their onset are more frequent in childhood and late adulthood (England et al., 2012). With a combined incidence rate of 61.44 per 100,000 person-years, that is higher in low- and middle-income countries, 7.6 out of every 1,000 people suffer from epilepsy at some point during their lives (Fiest et al., 2017). Furthermore, recent evidence shows that epilepsy, commonly involving the temporal lobe, constitutes a pathophysiological element present in prodromal stages of the most common neurodegenerative diseases (Sen et al., 2020; Beagle et al., 2017; Cretin et al., 2017; Rao et al., 2009) including Alzheimer's disease (Palop and Mucke, 2009; Born, 2015), Lewy body disease (Marawar et al., 2020), vascular cognitive impairment (Imfeld et al., 2013), and fronto-temporal lobar degeneration (Beagle et al., 2017).

Despite significant therapeutic advances that have led to the availability of more than 20 anticonvulsant drugs (Kwan et al., 2011; Löscher et al., 2020), recent studies show that up to one third of affected individuals remain resistant to pharmacotherapy (Chen et al.,

2018; Kalilani et al., 2018). As such, there is a real clinical need to better understand the underlying biological processes in order to develop new treatments and to provide quality of life improvements to epileptic patients.

1.1. Temporal lobe epilepsy

Temporal lobe epilepsy (TLE) is the most common form of epilepsy with focal seizures and the most prevalent form of drug-resistant epilepsy (Abarrategui et al., 2021). A hallmark feature of TLE is hippocampal sclerosis (HS), a neuropathological condition characterized by neuronal loss and neuroinflammatory processes affecting the hippocampus (Blümcke et al., 2013; Blümcke et al., 2017) causing a strong cognitive, episodic and spatial memory alteration that dramatically impairs the quality of life of patients with drug-resistant TLE.

The only therapeutic alternative for these patients is an early resective surgery of the affected hippocampal formation (Riban et al., 2002; Kwan et al., 2011). In addition, prospective studies indicate that, although in the early postoperative years between 60 and 80% of patients are seizure-free, long-term outcomes are less favorable (Janszky et al., 2005; Blümcke et al., 2013) making the therapeutic management an unmet clinical need.

1.2. Experimental models of temporal lobe epilepsy

Distinct experimental models have been proposed to study epilepsy, such as chemical, electrical, hypoxic-ischemic and genetic models (Pitkänen et al., 2017).

To study the molecular, cellular and pharmacological mechanisms underlying TLE with HS, two experimental models have been widely used in rodents during the last decades due to their high level of similarity to human TLE (Sharma et al., 2007; Leite et al., 2002; Pitkänen et al., 2017). These experimental models are based on the activation of the two major excitatory neurotransmitter systems: the kainic acid model, which activates the glutamatergic system (Nadler et al., 1978; Ben-Ari et al., 1979; Rusina et al., 2021) and the pilocarpine or lithium-pilocarpine model, which activates the cholinergic system (Turski et al., 1983; Curia et al., 2008; Lévesque et al., 2021). These drugs are administered locally by intrahippocampal or intracerebroventricular injection, or systemically by intravenous, subcutaneous or intraperitoneal injection (Rusina et al., 2021; Lévesque et al., 2021). Epileptogenic drugs are administered with a single high dose or with repeated low doses until the development of *status epilepticus*, after which

the animals are usually treated with a single dose of diazepam, an anxiolytic with antiepileptic effects that prevents further seizures and increases their survival rate (Leite et al., 1995; Riban et al., 2002).

The aforementioned models develop chronic epilepsy in 3 phases, starting with *status epilepticus* followed by a latent period phase and chronifying in the recurrent phase (Riban et al., 2002; Pitkänen et al., 2015), mimicking the development observed in humans. The chronic epilepsy is characterized by recurrent paroxystic activity patterns in form of sharp-wave ripple and fast-ripple events (Valero et al., 2017) that appears after a latent period of two weeks (Riban et al., 2002; Pitkänen et al., 2015).

Although there are histopathological, seizure susceptibility and mortality differences at the species and strain level in rodents (McKhann et al., 2003; Löscher et al., 2017), both models induce very similar cytopathology that reproduces the neuroinflammation, neuronal loss and hippocampal sclerosis following *status epilepticus* – as seen in human patients with drug-resistant TLE. However, there are differences in the patterns of affectation in these models. Taking the glutamatergic model as a reference, the cholinergic model is characterized by a broader pattern of activated brain regions with slightly less damage to the hippocampus but more damage to the neocortex (Clifford et al., 1987; Covolan and Mello, 2000).

2. Hippocampus

The hippocampus is a temporal lobe structure that plays a key role in multiple cognitive functions, including learning and episodic and declarative memory (Scoville and Milner, 1957; Milner, 1972; Squire, 1992; Jarrard, 1993; Tulving and Markowitsch, 1998; Bird and Burgess, 2008). Its structure consists of two fields: the hippocampus proper and the dentate gyrus (DG). The hippocampus proper is composed of different layers, including CA1, CA2 and CA3, which are named after the acronym *cornu Ammonis* (CA), a name formerly used to refer to the hippocampus. In humans, the hippocampus proper also includes other layer termed CA4. Moreover, the hippocampal structure, function and connectivity is preserved across human and rodent brains (Clark and Squire, 2013; Bienkowski et al., 2021) (Figure I1).
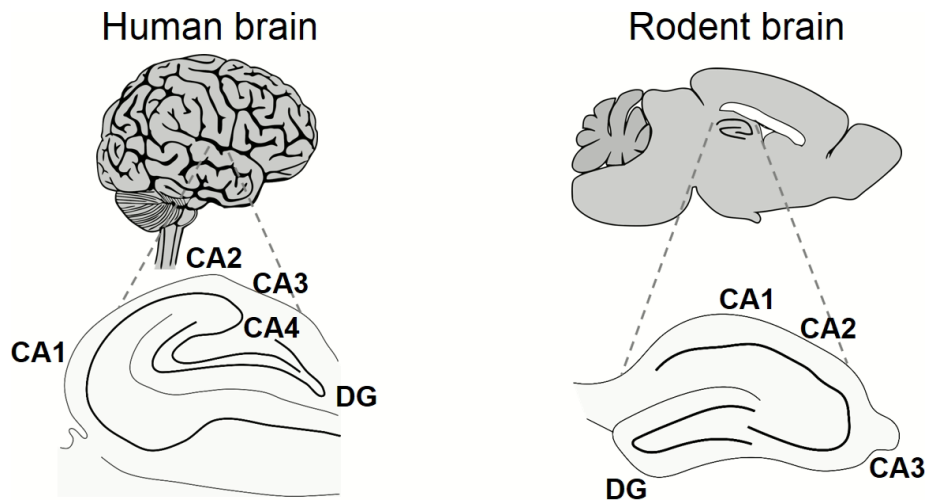
Figure I1. Schematic of the hippocampal structure in humans and rodents.

Major local connectivity within the hippocampus was first described in a publication by Santiago Ramón y Cajal in 1911. In this work he predicted the intrinsic connectivity of the hippocampus and even correctly inferred the directionality of neuronal impulses solely from histological data (Figure I2A). The hippocampus is mainly connected to the rest of the temporal lobe through connections with the subiculum and entorhinal cortex. Using the simplified schematic in Figure I2B as a reference, the circuit that connects hippocampal layers to each other and to adjacent structures is termed the trisynaptic circuit (Ramón y Cajal, 1911) and consists of the perforant pathway, which connects the entorhinal cortex to the DG, the mossy fibers, which connect the DG to the CA3 layer, and the Schaffer collaterals, which connect the CA3 layer to CA1 layer. Additionally, Ramón y Cajal (1911) also described the synapses and circuits in form of recurrent connections within the CA3 layer. More recent evidence has proposed a specific connectivity between the entorhinal cortex and the CA1 layer via the temporoammonic pathway (Steward and Scoville, 1976; Maccaferri and McBain, 1995).
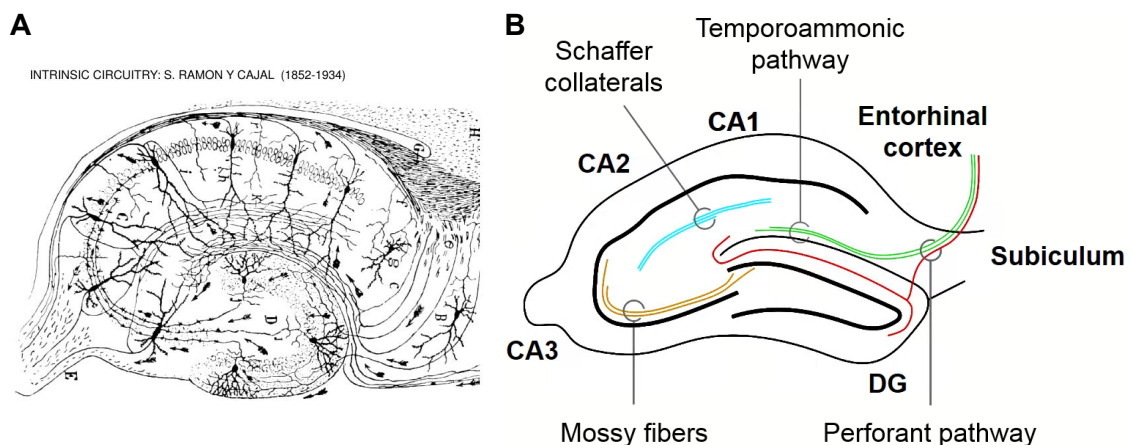
Figure I2. The hippocampal structure and major local connectivity in rodents. **A.** Illustration by Ramón y Cajal (1911) of the main cells, connections and directionality of neuronal impulses in hippocampal formation. **B.** Schematic of the hippocampal structure and trisynaptic circuit connectivity in rodents.

3. Hippocampal sclerosis

Historically, hippocampal sclerosis (HS) was coined by Sommer in 1880 in the autopsied brain of a patient with TLE as "Ammon's horn sclerosis". However, the presence of HS in the brains of epileptic patients had been observed earlier by Bouchet and Cazauvielh in 1825. HS is a hallmark feature of drug-resistant TLE and is a neuropathological condition characterized by loss of hippocampal volume, neuronal loss and neuroinflammatory processes affecting the hippocampus (Blümcke et al., 2013; Blümcke et al., 2017), causing severe cognitive, episodic and spatial memory impairment that dramatically deteriorates patients' quality of life.

HS is characterized by specific patterns of neuronal loss affecting different hippocampal subfields (Figure I3) from the CA1 to CA3/4 layers, the hilus of the DG and superficial layers of the entorhinal cortex (Blümcke et al., 2009; Du et al., 1995; de Lanerolle et al., 2003). Factors such as epilepsy history, age of onset, and the relationship with early precipitating events may all influence the degree and severity of HS (Davies et al., 1996; Janszky et al., 2005).
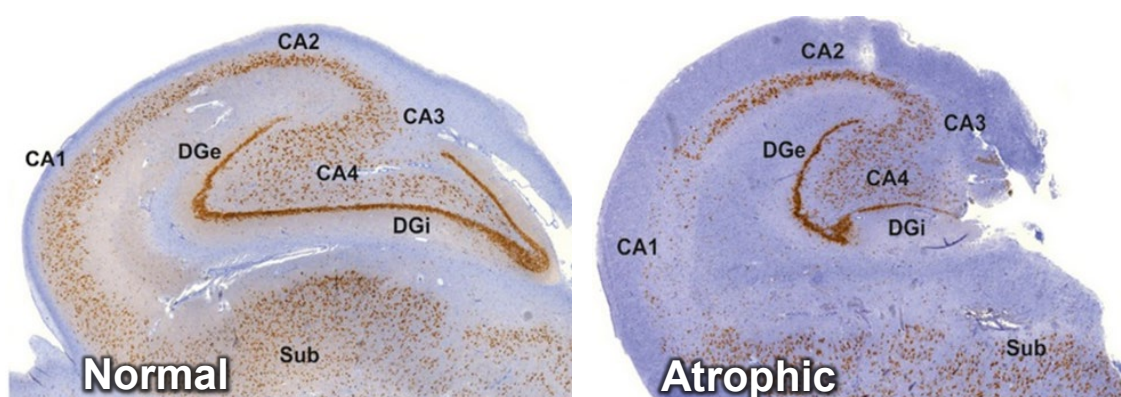
Figure I3. Resected hippocampal tissue from patients with TLE, showing a normal (left) and atrophic hippocampus (right). Note the strong neuronal loss affecting the CA1 layer of the hippocampus. Images adapted from Blümcke et al. (2013).

HS is also characterized by inflammatory processes leading to reactive gliosis, edema and glial scarring in the hippocampus (Blümcke et al., 2013; Pernot et al., 2011). This processes involve different cell types, including microglia and astrocytes (Blümcke et al., 2013; Devinsky et al., 2013; Morin-Brureau et al., 2018), that triggers the synthesis of cytokines, enzymes and trophic factors capable of worsening neurodegeneration (Crespel et al., 2002; McKenzie et al., 2020). Chronic neuroinflammation is a common feature of TLE in patients and in animal models, in which inflammatory processes are chronically active and can be reinduced by recurrent seizures (Pernot et al., 2011; Crespel et al., 2002; Gales et al., 2017). The role of chronic neuroinflammation and the contribution of the different glial populations to HS is not fully understood, but experimental and clinical evidence suggests that blockade of proinflammatory pathways reduces seizure duration and frequency (Radu et al., 2017; Maroso et al., 2010; Iori et al., 2017), and thus may protect against the development and progression of HS in TLE.

The most common form of HS (type 1; 60-80% of TLE cases) shows severe neuronal loss of CA1, CA3, and CA4 pyramidal neurons and milder loss in CA2 layer, with variability along the septotemporal or anteroposterior axis (Blümcke et al., 2013; Wyler et al., 1992). In contrast, type 2 HS (10-20% of TLE cases) is associated with predominant CA1 neurodegeneration and minimal loss in other layers (Blümcke et al., 2013). Given the disparities between clinical series, there is no consensus on neuronal loss progression over time (Blümcke et al., 2009; Davies et al., 1996). In addition, individual variabilities and anatomical inhomogeneities complicate classification (Coras et al., 2014; Rodrigues et al., 2015; Saghafi et al., 2018). For instance, patchy neuronal loss has been described in the CA1 layer in some cases, whereas in others, it seems to adopt a more laminar profile (Prada Jardim et al., 2018). In some affected individuals cell loss concentrates in the CA4 layer and the dentate gyrus, and is frequently integrated in dual pathologies – e.g., TLE and malformations of cortical development – classified as type 3 HS (3-7% of TLE cases) (Mathern et al., 1997). However, the mechanisms underlying specific vulnerability of diverse cells and their role in the histopathological landscape and clinical significance of TLE-HS remain unknown.

4. Laminar organization of the Hippocampal CA1 subfield

The CA1 layer of the hippocampus has a compact laminar structure whose layers are generated at different stages of development (Lorente de Nó, 1934). Recent techniques and methods operating at single-cell resolution point to an exquisite cell-type-specific organization that is instrumental for brain function (Habib et al., 2016; Zeisel et al., 2015).

Previous studies have shown that the CA1 layer of the rat and mouse hippocampus is populated by at least two distinct types of pyramidal cells that are different at molecular, neuroanatomical, morphological and functional levels, with characteristic gene expression gradients along the dorso-ventral and proximo-distal axes (Cembrowski et al., 2016a; Cembrowski and Spruston, 2019; Dong et al., 2009; Bannister and Larkman 1995; Slomianka et al., 2011). This pyramidal cells are also segregated along the CA1 radial axis, with one population expressing the cell marker *Calbindin* (*Calb*) located at the superficial sublayer of CA1 (closer to *stratum radiatum* (*SR*)), and cells at the deep sublayer (closer to *stratum oriens* (*SO*)) that are negative for this marker (Valero et al., 2015; Dong et al., 2009; Cembrowski et al., 2016a; Habib et al., 2016) (Figure I4).
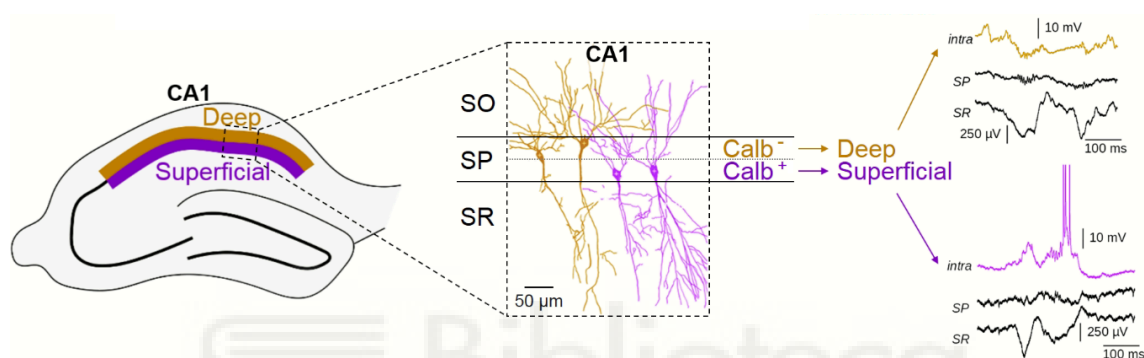
Figure I4. Schematic of the hippocampal CA1 superficial and deep sublayers (left), superficial and deep pyramidal cells segregation along the CA1 radial axis with *Calbindin* (*Calb*) staining, showing cell distribution along different *strata*, from top to bottom: *stratum oriens* (*SO*)*, stratum pyramidale* (*SP*) and *stratum radiatum* (*SR*) (center) and intracellular recordings showing that cells at deep sublayer hyperpolarize when superficial cells depolarize (right). Images adapted from Valero et al. (2015).

Functionally, superficial and deep CA1 pyramidal neurons project differentially and diverge in their participation of sharp-wave ripple activity (a rithmic activity that happens during sleeping and resting), theta-gamma oscillations (rhythmic oscillations that synchronize neurons within and across the brain's structure) and behavioral-cognitive correlates (Soltesz and Losonczy, 2018; Valero and de la Prida, 2018; Valero et al., 2015). Moreover, *Calbindin* negative cells at deep sublayer become hyperpolarized when superficial cells depolarize (Valero et al., 2015) (Figure I4). Differences in excitability are related to microcircuit mechanisms, which perisomatic inhibition by parvalbumin (PV) basket cells is markedly greater in deep compared to superficial cells (Soltesz and Losonczy, 2018; Valero et al., 2015), and a greater likelihood that superficial cells are driven by presynaptic CA3 activity through Schaeffer collaterals than deep cells (Valero et al., 2015). Similarly, direct inputs to CA1 from layer III pyramidal

neurons in the medial entorhinal cortex are biased by deep CA1 cells, whereas projections from the lateral entorhinal cortex are stronger in superficial cells (Masurkar et al., 2017). Consistent with this, there is recent evidence showing differential connectivity at the input and output levels between CA1 sublayers and the prefrontal cortex, with differentiated activation along approach and avoidance behavior (Sánchez-Bellot et al., 2022).

Despite data suggesting critical regionalization of CA1 neuronal responses to ischemia, anoxia, and epilepsy, in form of reduction of CA1 linear cell density consistent with HS type 2 (Morris et al., 1995; Valero et al., 2017; Wittner et al., 2002; Inostroza et al., 2011), little is known about their clinical relevance and potential relationship with neuronal vulnerability. We hypothesize that CA1 pyramidal neuron heterogeneity may be related to epilepsy progression and HS. Understanding the effect of this cellular diversity and transcriptional changes on these processes may provide insights into more specific mechanisms towards new diagnostic and therapeutic opportunities (Pfisterer et al., 2020).

5. Omics approaches to hippocampal sclerosis in epilepsy

The pathology of **TLE with hippocampal sclerosis (TLE-HS)** involves multiple processes in a complex and dynamic molecular environment that trigger neuroinflammation and neurodegeneration in the hippocampus. The study of the pathophysiological mechanisms underlying HS in epilepsy has been approached in recent decades from different fields of the life sciences, including anatomy, pathology, physiology, pharmacology and immunology. The recent incorporation of so-called "omics" techniques, which allow interrogation at different molecular levels with an unprecedented level of resolution, is generating valuable insights into the underlying mechanisms leading to TLE-HS (Bruxel et al., 2021). **Omics analyses** in samples from patients with TLE-HS and rodent models of TLE are contributing to our understanding of the underlying biological processes. However, analyses in tissue from patients with TLE-HS are limited by factors such as high inter-patient variability and the absence of adequate human controls (Becker, 2018; Ren and Curia, 2021). In addition, many of these samples are obtained by post-mortem autopsy with differences in collection time, temperature and their processing, which introduce undesirable effects for downstream analyses (Ferrer et al., 2007; Nagy et al., 2015). Despite the difficulties in translating the results to patients, experimental models of TLE allow control of these variables and

overcome some of the limitations of the molecular studies in humans (Ren and Curia, 2021).

Metabolomic techniques quantify diverse types of small molecules resulting from cellular metabolic functions. These approaches have demonstrated specific alterations in TLE-HS in neurotransmitter balance, increased metabolism and oxidative stress among others (Bruxel et al., 2021). A landmark study by Detour et al. (2018) has shown altered levels of specific metabolites in the brain of patients with TLE-HS. A small set of metabolites was studied in samples from patients of TLE with and without HS and revealed that sclerosis is associated to increased levels of glutamate, glutamine, and glutathione, and decreased concentration of glycine, choline, phosphocholine, N-acetylaspartate-acid, acetate, ascorbate, arginine, alanine, taurine and valine (Detour et al., 2018). This increase of metabolites in HS could be related to a higher neuronal activity burden in these samples, whereas the decrease was linked to phospholipid metabolic pathways and amino acid metabolism, possibly related to a decrease in metabolic density (Detour et al., 2018). In turn, the decrease in metabolic density could be due to the fact that the metabolic effects of neuronal loss are not compensated by the neuroinflammatory processes leading to gliosis (Detour et al., 2018). Additionally, samples from patients with TLE were segregated by HS subtype and compared by taking samples without signs of HS as a reference. This led to the identification of 3 highly discriminative metabolites between type 1 and type 2 HS – glutamate and N-acetylaspartate-acid were shown to be more concentrated exclusively in type 1 HS, while glutamine was shown to be more concentrated exclusively in type 2 HS (Detour et al., 2018). The field of metabolomics is making great strides. Future high-throughput studies analyzing broader sets of metabolites may help to better understand the array of metabolic alterations underlying TLE-HS pathology. These patterns of metabolic alteration could further be used as early predictors of drug response in epilepsy (Donatti et al., 2020).

Mass spectrometry has allowed proteomic and metabolomic studies to advance in terms of sensitivity, accuracy and resolution. The most recent **proteomic** studies use this technique to quantify the abundance of peptides, their interactions and post-translational modifications (Bruxel et al., 2021). Tissue proteomics by mass spectrometry imaging in samples from patients with TLE-HS has revealed enriched levels of neuropeptide precursors and receptors, and proteins implicated in axon regeneration, including neurotrophins, cell surface and membrane proteins, signal transduction proteins, cytoskeleton proteins and different tumor suppressors (Mériaux et al., 2014). Proteomic profiling by mass spectrometry and two-dimensional electrophoresis of hippocampal

samples from patients of TLE with and without HS disclosed that samples with signs of sclerosis had decreased synaptic protein levels and increased glia-related protein levels (Furukawa et al., 2020). A complementary histological analysis of the samples observed marked neuronal loss and astrocytic gliosis (Furukawa et al., 2020). Data from animal models of TLE-HS expand these observations, allowing longitudinal studies of different brain areas. A longitudinal proteomic profiling of the hippocampus, cortex and cerebellum has recently been performed surveying six time points spanning from the first minutes to two weeks after induction of *status epilepticus* (Ahmed et al., 2021). Protein expression alterations were found to be involved in different biological processes related to membrane trafficking, excitatory signaling, regulation of gene expression, cytoskeleton remodeling, immunity, apoptosis and cell survival, proliferation and differentiation – including the signaling pathways MAPK, MTOR, JAK/STAT, NMDAR receptor subunits, and cell death through STAT3 activation (Ahmed et al., 2021). Findings from different **proteomic approaches** in TLE-HS point to alterations in structural, synaptic and ion channel proteins, cytoskeleton remodeling and increased metabolism and oxidative stress (do Canto et al., 2021; Bruxel et al., 2021; Mériaux et al., 2014), while others further point to cell damage, inflammation, proliferation and cell death (Ahmed et al., 2021; Furukawa et al., 2020). This suggests that different biological processes in distinct cell types concur in tissue response to pathology, and highlights the need to study the different areas and populations separately in order to deconvolute the underlying responses associated with each process.

Genomic studies are a powerful tool to identify associations between genetic variants and disease, response to treatment and prognosis. In order to elucidate common mechanisms of susceptibility to TLE-HS, different genomic approaches have been applied to the analysis of patient samples. One of the most common types of genomic approaches are genome-wide association studies (GWAS). A GWAS of samples from a robust cohort of controls and patients for common genetic variation and susceptibility to focal epilepsies – including TLE-HS – was further analyzed by functional annotation, revealing glutamate receptor and ion channel genes among gene variations closest to significance (Kasperaviciūte et al., 2010). Genomic analysis of the polymorphisms in mitochondrial DNA of patients with TLE-HS and healthy controls revealed a significant relation of ATP-8, ND4 and ND5 genes with TLE-HS (Gurses et al., 2014). However, GWAS are often limited by the difficulty of explaining genetic risk for common diseases, of assessing rare genetic variants, and the small effect sizes of most associations (Manolio et al., 2009; McClellan and King, 2010). These limitations make it necessary to use a large number of samples that were representative of the general population and

the pathology to increase the statistical power and robustness of the analyses. Still, this does not avoid other common limitations of GWAS such as the difficulty in uncovering causal associations and the poor ability of the results to predict disease risk (Manolio et al., 2009; McClellan and King, 2010). On the other hand, **family genetic studies** have also proven useful in identifying mechanisms of susceptibility to TLE-HS. A genetic analysis of polymorphisms in two infant patients suffering from a common syndrome with TLE-HS revealed *de novo* mutations within the exon of the SCN1A gene (Tiefes et al., 2019). The study of genetic predisposition to TLE-HS related to polymorphisms in the proinflammatory cytokine genes encoding IL-1β, IL-1α and interleukin-1 receptor antagonist (IL-1RA) – modulators of the immune response and involved in glial scarring processes under central nervous system injury – suggests that homozygotes for IL-1B−511∗2 could develop HS under minor epileptogenic events in development (Kanemoto et al., 2000). Taken together, different **genetic and genomic approaches** have found mechanisms of susceptibility to TLE-HS in which again alterations in synaptic function, oxidative metabolism or immune response are observed.

The field of **epigenomics** aims at the genome-wide characterization of reversible modifications that affect gene expression without altering the DNA sequence through processes such as DNA methylation or histone acetylation (Friedman and Rando, 2015). There is evidence associating epilepsy with epigenetic modifications (Kobow et al., 2013; Citraro et al., 2020). In addition, several antiepileptic drugs are known to also induce epigenetic changes by inhibiting HDAC (histone deacetylase). These drugs include valproate (Göttlicher et al., 2001), carbamazepine (Beutler et al., 2005) and topiramate (Eyal et al., 2004). Furthermore, the induction of epigenetic changes has also been observed in antiepileptic treatments through DNA demethylation and untranslated RNA (Dong et al., 2010; Ni et al., 2015; Oikawa el al., 2015; Kong et al., 2020). Together, these studies suggest that epigenetic modifications may play a role in the development of epilepsy and its treatment. So far, the number of epigenomic approaches to investigate the role of epigenetic changes underlying HS in epilepsy is very limited and the few available references are related to DNA methylation studies (Bruxel et al., 2021). Dixit et al. (2020) has recently performed a genome-wide functional annotation of genes enriched in DNA methylation in samples from patients with TLE-HS compared to control post-mortem samples from individuals with no history of neurological disorders. These authors found that hypermethylated genes in TLE-HS are associated to the ionotropic glutamate receptor and axon guidance pathways, MAPK, TFAP2A-related regulatory activities, notch signaling and the immune response among others, highlighting ADAM17, CACNG2, MAP3K11, NRP1, SEMA3B and TFAP2A genes (Dixit et al., 2020).

Interestingly, they observed a high percentage of methylation changes associated with the gene body, and not with promoter sites or CpG islands. Methylation in microRNA gene regions has also been investigated in human TLE-HS (Miller-Delaney et al., 2015). The results show a high sensitivity to methylation at the promoter regions and transcription start site of several microRNAs. Furthermore, gene ontology analysis highlighted that most methylation occurred in genes associated with nuclear functions, including transcriptional regulation and DNA binding (Miller-Delaney et al., 2015). Finally, a very recent study shows that changes produced by DNA methylation in human TLE-HS correlate with transcriptomic changes driven by epilepsy, progressive alterations related to epilepsy duration and changes in inflammatory genes (Martins-Ferreira et al., 2022). The results of different **epigenetic approaches** in TLE-HS point to DNA methylation as a critical regulator of biological processes that again relate to synaptic function and immune response.

The biological processes underlying HS in epilepsy are diverse and operate at different molecular levels. Most omics approaches to HS in epilepsy interrogate these molecular levels separately, which limits the ability to obtain a complete and integrative view of the mechanisms involved. However, new **multi-omics approaches** – based on the analysis of the interaction between multiple biological levels – integrate the information from each level. The first multi-omics study on human TLE-HS samples was published by Schulz et al. in 2017. This study interrogated the effects of cis-regulatory single nucleotide polymorphisms (SNPs) on DNA methylation and gene expression in hippocampal biopsies from patients of drug-resistant TLE with pathological abnormalities affecting the hippocampus, including more than 65% with HS. A high number of cis-regulatory effects of SNPs were identified, affecting over 14,000 CpG methylation sites and more than 300 gene transcripts (Schulz et al., 2017). This initial study reports relevant points to address in studies with larger cohorts. An example is the identification of genes associated with neurodevelopmental disorders, including ADARB2, GABRA5, GABRB3, HDAC4, NRXN1, RBFOX3, RIMBP2, SLC2A1 and SLC6A1 by methylome and transcriptome correlation analysis (Schulz et al., 2017). However, the complexity in integrating the results from the different groups and biological levels studied limited the observations and conclusions. A posterior multi-omic study of tissue samples from patients with TLE-HS and post-mortem controls identified a cis-regulatory effect of SNPs affecting transcription of the METTL2 gene (Guelfi et al., 2019). The METTL2 gene encodes a protein of the methyltransferase family and is deleted in Williams-Beuren syndrome, a developmental disorder that sometimes presents with seizures (Schubert, 2009). In addition, the METTL2-DALRD3 complex dysfunction is related to epileptic

encephalopathy (Lentini et al., 2020). As in previous studies, most of the down-regulated genes were associated with neuronal development, cell differentiation, and synaptic transmission, and the up-regulated genes were associated with immune response. In addition, up-regulation was detected in genes associated with vascular development (Guelfi et al., 2019). Among the differentially expressed genes, they found genes previously linked to epilepsy, including GABRA1, GABRB2, ITPR1, SCN2A and SCN8A, and novel epilepsy candidate genes, such as CAP2, CADPS2, LDB2 or MYT1L (Guelfi et al., 2019). Interestingly, alternative RNA splicing events were detected in the form of shortened isoforms for ANK3 and NRXN3. According to the authors, the ANK3 isoform have unknown effects, while the NRXN3 isoform could lead to a decrease in sodium channel activity, predisposing to abnormal excitability (Guelfi et al., 2019). Multi-omics approaches have also been applied in animal models of TLE. In a pioneering study by Schouten et al. (2016), samples from the dentate gyrus of both hippocampi were analyzed three days after *status epilepticus* using microRNA profiling, transcriptomics and proteomics techniques. Results indicate that more than 300 microRNAs, 13,400 mRNAs and 2,300 proteins were modulated by epilepsy (Schouten et al., 2016). Many of these changes were further validated by complementary techniques. These data also revealed a novel regulatory role of microRNA-124 and microRNA-137 in BCL2L13 protein expression and downstream pro-apoptotic activity involving Caspase-3 (Schouten et al., 2015). This result suggest that microRNAs could play a role in regulating neuronal survival in HS in epilepsy.

Transcriptomics is the study of the complete set of RNA transcripts that are produced by the genome (i.e., transcriptome). Transcriptomic techniques have been widely applied in the study of TLE-HS. In neurons gene expression is tightly regulated by electrical activity and *de novo* gene expression is necessary for synaptic plasticity (Yap and Greenberg, 2018; Flavell and Greenberg, 2008; Kandel, 2001). On the other hand, transcriptional changes underlie phenotypic changes of glial cells from homeostatic to reactive states in response to environmental stimuli (Lopez-Atalaya et al., 2018; Holtman et al., 2017; Chen and Colonna, 2021; Escartin et al., 2021). During the first two decades of the twenty-first century, expression microarrays have been the technique of choice to study the transcriptome of TLE-HS in humans (de Lanerolle and Lee, 2005; Lee et al., 2007) and rodents (Aronica and Gorter, 2007; Gorter et al., 2006; Laurén et al., 2010). These studies, which in the vast majority of cases were performed using bulk homogenate tissue, show patterns of down-regulation of genes related to synaptic transmission and up-regulation of genes related to gliosis, immune and inflammatory responses (de Lanerolle and Lee, 2005; Lee et al., 2007; Aronica and Gorter, 2007;

Gorter et al., 2006; Laurén et al., 2010). Some of these studies further observed up-regulation patterns of genes associated with oxidative stress (Aronica and Gorter, 2007; Gorter et al., 2006; Laurén et al., 2010), neuronal loss and apoptosis (de Lanerolle and Lee, 2005; Aronica and Gorter, 2007; Gorter et al., 2006). This set of transcriptional signatures is consistent with the processes of neuroinflammation and neurodegeneration (Przedborski et al., 2003) underlying HS in epilepsy. Expression microarrays have been losing relevance with the advent of next-generation sequencing (NGS). RNA sequencing (RNA-seq), offers different advantages over microarrays, such as that measurements are discrete in RNA-seq while they are continuous in microarrays. Also, the dynamic range is wider in RNA-seq. In addition, sequencing is targeted in microarrays while it is unbiased in RNA-seq. This allows RNA-seq to offer accuracy at the transcript read level, complete coverage of the coding and non-coding transcriptome, as well as detection of low abundance transcripts (Wang et al., 2009; Wilhelm and Landry, 2009). Most transcriptomic approaches perform the analysis of bulk-tissue RNA-seq, a powerful method to reveal signature patterns of gene expression across different tissues or disease states. However, bulk RNA-seq produces an average gene transcript abundance that reflects the convoluted signal from several sources of variation, such as cell-type-specific gene expression levels. This limitation is especially relevant in the hippocampus – which is characterized by a highly heterogeneous cell type composition and is profoundly altered in TLE-HS – so a better understanding of the sources of transcriptional variation may help to identify new targets for novel and more effective therapies. Different RNA-seq transcriptomic approaches have been applied to the investigation of the biological processes underlying HS in human patients with TLE and rodent models of TLE. Gene expression changes in the epileptic hippocampal phenotype of a large cohort of pilocarpine-induced TLE and their control littermates were studied by bulk-tissue RNA-seq (Henkel et al., 2021). Interestingly, a cell-type deconvolution of the RNA-seq data was also performed, revealing altered proportions of neuronal and glial cells, with a sharp decrease of the relative proportion of CA1/CA2 pyramidal cells in epilepsy. In addition, non-neuronal cells and GABAergic interneurons were identified as possible mediators of neurodegeneration (Henkel et al., 2021). Whole tissue RNA-seq from samples of patients with TLE-HS was used to characterize the presence of different microglial phenotypes (Morin-Brureau et al., 2018). The microglia shape and transcriptomic profiling of regions with different neuronal death was compared. In addition, the pseudotemporal kinetics of the seizure response in a kainic acid mouse model of TLE was inferred. The results highlight an increased presence of amoeboid microglia in areas with increased neuronal loss, with local secretion of interleukin CXCL8, IL-1B and other cytokines, mediated in part by the NRLP3 inflammasome (Morin-Brureau

et al., 2018). On the other hand, RNA-seq and quantitative polymerase chain reaction (qPCR) analysis of cortex and hippocampus in a kainic acid rat model of TLE at different stages – acute damage, the onset of epileptogenesis, spontaneous epilepsy and cognitive impairment – identified an upregulation of immune response genes and a progressive neuronal loss that is earlier and stronger in the hippocampus (Dong et al., 2020). In brief, the common factor in the different **transcriptomic approaches** to the study of TLE-HS is the transcriptional signature of neuroinflammation and neurodegeneration associated to HS.

Previous research has found multiple associations and potential therapeutic targets for HS in epilepsy, including alterations at the level of ion channels and neurotransmission, inflammation and metabolism. However, one of the limitations of these studies is that they have been performed at the bulk-tissue or bulk-population level. Thus, further research is needed to better understand the causal mechanisms of neuronal loss and the contribution of neuron-glia interactions to HS. The advent of **single-cell omics approaches** has provided a new way to explore the underlying heterogeneity and responses with cell-level resolution. In addition, such approaches are enabling the study of differences at the cell type and subtype level between different conditions (Islam et al., 2011; Zeisel et al., 2015; Butler et al., 2018). Single-cell omics approaches are still very recent and are in constant evolution and improvement. Until a few years ago, these approaches were unfeasible due to limitations in terms of cell number, resolution, sequencing depth and high cost (Svensson et al., 2018). In fact, no studies related to single-cell omics approaches for HS in epilepsy have been published to date. The application of single-cell omics approaches to the study of hippocampal cellular heterogeneity and differences in the responses of distinct cell types to TLE-HS could help to advance the understanding of the biological mechanisms and processes leading to HS in epilepsy.

The **aim of my thesis** is to study for the first time how CA1 sublayer heterogeneity relates to epilepsy and development of HS. To do so, this thesis work takes advantage of genome-wide techniques to give new insights into HS in epilepsy. We combine analyses of cutting-edge gene expression profiling at the levels of single-nucleus and microdissected tissue with single-cell electrophysiology and gene expression *in situ* hybridization to disclose epileptogenic and neurodegenerative changes running differentially across superficial and deep CA1 sublayers in different rodent models of experimental epilepsy with HS. We have found that CA1 superficial pyramidal cells are particularly vulnerable in rat and mouse models of epilepsy. This finding has been in part made possible by a very precise approach (with laser microdissection and single cell

profiling). In addition, we have developed two open web applications that provide interactive visualization of our transcriptomic data analyses: laser capture microdissection RNA-seq of deep and superficial CA1 sublayers (http://lopezatalayalab.in.umh-csic.es/CA1_Sublayers_&_Epilepsy) and single nucleus RNA-seq of CA1 layer (http://lopezatalayalab.in.umh-csic.es/CA1_SingleNuclei_&_Epilepsy). These tools may facilitate cross-validation of results from resected samples of healthy and epileptic tissue from patients. Furthermore, we have also developed a simple and robust protocol that leverages single cell expression data to explore the contribution of distinct cell types to complex gene signatures obtained by differential gene expression analysis of bulk RNA-seq (Marquez-Galera et al., 2022). In contrast to the common tenet of adopting separated and static views of the underlying biological processes (e.g. microcircuit activity and inflammation), our study highlights the importance of leveraging cell type specificity to better understand the phenotypic complexities accompanying HS in epilepsy. These approaches may eventually determine new insights for future therapeutic interventions for TLE and HS.

Objectives

General aim

This thesis aims to study how CA1 sublayer heterogeneity is related to epilepsy and the development of hippocampal sclerosis by studying possible differences in sublayer response to epilepsy.

Specific objectives

1. To evaluate deep and superficial neuronal activity in epilepsy.

2. To assess neurodegeneration of deep and superficial cells in epilepsy.

3. To determine CA1 sublayer-specific transcriptomic signatures associated with epilepsy.

4. To explore the progression of transcriptomic signatures from health to neurodegenerative epilepsy at the single-cell level.
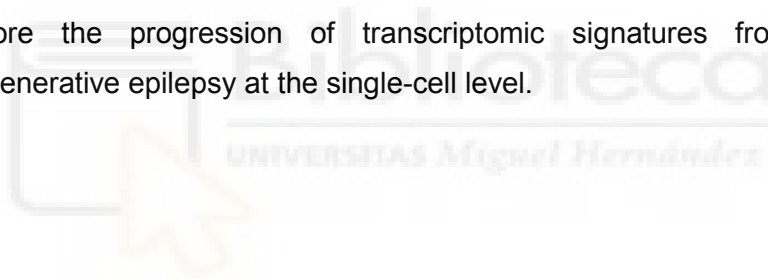
Materials and Methods

STAR★Methods

Key resources table

REAGENT or RESOURCE	SOURCE	IDENTIFIER
Antibodies		
Rabbit anti-calbindin D-28k	Swant	Cat# CB38; RRID: AB_10000340
Mouse anti-calbindin D-28k	Swant	Cat# 300; RRID: AB_10000347
Rabbit anti-Wfs1	Proteintech	Cat# 11558-1-AP; RRID: AB_2216046
Rabbit anti-Iba1	Wako	Cat# 019-19741; RRID: AB_839504
Rabbit anti-GFAP	Sigma	Cat# G9269; RRID: AB_477035
Rabbit anti-Olig2	Millipore	Cat# AB9610; RRID: AB_570666
Rabbit anti-cFos	Santa Cruz Biotechnology	Cat# sc-52; RRID: AB_2106783
Alexa Fluor633 goat anti-rabbit IgG	Thermo Fisher	Cat# A21070; RRID: AB_2535731
Alexa Fluor488 donkey anti-mouse IgG	Thermo Fisher	Cat# A21202; RRID: AB_141607
Alexa Fluor488 goat anti-mouse IgG	Jackson Immunoresearch	Cat# 115-545-003; RRID: AB_2338840
Rhodamine Red goat anti-mouse IgG	Jackson Immunoresearch	Cat# 115-295-003; RRID: AB_2338756
Alexa Fluor488-conjugated streptavidin	Jackson Immunoresearch	Cat# 016-540-084; RRID: AB_2337249
Chemicals, peptides, and recombinant proteins		
BSA	Sigma	A7906
EDTA	Sigma	607-429-00-8
PBS	VWR	E404-200 TABS
Tris-HCl	Sigma	T5941
NaCl	VWR	7647-14-5
$MgCl_2$	Sigma	M2670
IGEPAL	Sigma	I8896
ARCTURUS PicoPure RNA isolation kit	Thermo Fisher Scientific	KIT0204
RNase-free DNase set	QIAGEN	79254
Bisbenzimide H33258	Sigma-Aldrich	Cat# B2883; CAS: 23491-45-4
Neurobiotin tracer	Vector Labs	Cat# SP-1120
FluoroJade C dye	Sigma	AG325
DPX mountant	VWR	360294H
ProLong Gold antifade mountant	ThermoFisher Scientific	P10144
Critical commercial assays		
Chromium single cell 3′ library & gel bead kit v2	10x Genomics	Cat#: 120237 (v2)
Chromium i7 multiplex kit	10x Genomics	N/A
Chromium single cell A chip kit	10x Genomics	Cat#: 120236
TruSeq stranded mRNA library prep kit	Illumina	Cat#: RS-122-2101/2

REAGENT or RESOURCE	SOURCE	IDENTIFIER
HiSeq sequencing kit TruSeq v4	Illumina	Cat#: FC-401-4003
RNAscope fluorescent multiplex reagent kit	ACD	320850
Deposited data		
LCM-RNA-seq	Gene Expression Omnibus (NCBI)	GSE143555
snRNA-seq	Gene Expression Omnibus (NCBI)	GSE143560
Experimental models: organisms/strains		
Mouse: Thy1.2-G-CaMP7-DsRed2	RIKEN Bioresources Center	Stock: RBRCO6579
Mouse: Calb1-2A-dgCre-D	Jackson Labs	N/A
Mouse: TdTomato reporter line Ai9	Jackson Labs	Stock: 007905
Rat: Wistar	Instituto Cajal Animal facility	N/A
Mouse: C57BL/6	Instituto Cajal Animal facility	N/A
Oligonucleotides		
Wfs1-forw (5′CATCCCCAACAACCTGTTCC)	Sigma	NM_031823.1, bp 783-1631
Wfs1-rev (5′ACACCAGGTAGGGCACCACC)	Sigma	N/A
Ndst4-forw (5′ATACATCCAAAACTGATCCCAC)	Sigma	XM_006233274.2, bp 536-1024
Ndst4-rev (5′AAAAGCACTGGCTGGTAGGTAG)	Sigma	N/A
Syt17-forw (5′ACACATCCAAGTCCACATACAG)	Sigma	NM_138849.1, bp 378-1118
Syt17-rev (5′GTGTACCAGCTGGATTTTCACA)	Sigma	N/A
Hrt1a-forw (5′CTTTCTATATCCCGCTGTTGCT)	Sigma	J05276.1, bp 730-1663
Hrt1a-rev (5′CACACAGATACTAGTGGTTCTC)	Sigma	N/A
Scn7a-for (5′GATTATTTCTTCCCTTGTGTATGC)	Sigma	NM_131912.1, bp 2812-3550
Scn7a-rev (5′CTAAAGTCATCTTCGCTCAAGG)	Sigma	N/A
Recombinant DNA		
Mm-Spag5	ACD	505691
Mm-Dcc-C3	ACD	427491-C3
Mm-Dapk1-C3	ACD	880221-C3
RNAscope 3-plex positive control probe-Mm	ACD	320881
RNAscope 3-plex negative control probe	ACD	320871

REAGENT or RESOURCE	SOURCE	IDENTIFIER
Software and algorithms		
Sequencer Software HiSeq Control Software	Illumina, Inc	https://support.illumina.com/sequencing/sequencing_instruments/hiseq_2500/downloads.html
R	R Foundation for Statistical Computing	https://www.R-project.org/; RRID: SCR_001905
RStudio	RStudio, PBC	https://www.rstudio.com/; RRID: SCR_000432
FastQC	Simon Andrews	https://www.bioinformatics.babraham.ac.uk/projects/fastqc; RRID: SCR_014583
STAR	Dobin et al., 2013	https://code.google.com/archive/p/rna-star; RRID: SCR_004463
Samtools	Li et al., 2009	http://samtools.sourceforge.net; RRID: SCR_002105
HTSeq	Anders et al., 2015	https://htseq.readthedocs.io/en/master/; RRID: SCR_005514
DESeq2	Love et al., 2014	http://www.bioconductor.org/packages/release/bioc/html/DESeq2.html; RRID: SCR_015687
Cell Ranger	Zheng et al., 2017	https://support.10xgenomics.com/single-cell-gene-expression/; RRID: SCR_017344
Seurat	Butler et al., 2018; Stuart et al., 2019	http://satijalab.org/seurat/; RRID: SCR_016341
Monocle 2	Qiu et al., 2017a, 2017b	http://cole-trapnell-lab.github.io/monocle-release; RRID: SCR_016339
DAVID Bioinformatics	Huang et al., 2009	https://david.ncifcrf.gov; RRID: SCR_001881
Webgestalt	Liao et al., 2019	http://www.webgestalt.org; RRID: SCR_006786
MATLAB 2016b	Mathworks	https://www.mathworks.com; RRID: SCR_001622
ImageJ	NIH Image	https://imagej.net/ImageJ; RRID: SCR_003070
SPSS Statistics	IBM	https://www.ibm.com/products/spss-statistics; RRID: SCR_002865
Other		
Resource website for the LCM-RNA-seq data	This paper	http://lopezatalayalab.in.umh-csic.es/CA1_Sublayers_&_Epilepsy
Resource website for the snRNA-seq data	This paper	http://lopezatalayalab.in.umh-csic.es/CA1_SingleNuclei_&_Epilepsy
Silicon probes: 16-channel linear; 100 µm inter-spacing; 413 µm² electrode area	Neuronexus	A1x16-5mm-100-413

Resource availability

Lead contact

Further information and requests for reagents and resources may be directed to the lead contact, Dr. Liset M de la Prida (lmprida@cajal.csic.es).

Materials availability

This study did not generate any new unique reagents.

Data and code availability

No unpublished custom code, software or algorithm was used in this study. Freely available software and algorithms used for analysis are listed in the resource table. Some analyses were specifically designed for the purpose of this paper using routines written in MATLAB 7.10 (MathWorks). All custom scripts and data contained in this manuscript are available upon request from the Lead Contact. The accession number for the bulk-tissue transcriptome (LCM-RNA-seq) and single-nuclei RNA-seq (snRNA-seq) data reported in this paper is Gene Expression Omnibus (GEO) database: GSE143555   (LCM-RNA-seq) https://www.ncbi.nlm.nih.gov/geo/query/acc.cgi?acc=GSE143555;   GSE143560 (snRNA-seq) https://www.ncbi.nlm.nih.gov/geo/query/acc.cgi?acc=GSE143560.

Two open web applications provide visualization of transcriptomic data: LCM-RNA-seq data: http://lopezatalayalab.in.umh-csic.es/CA1_Sublayers_&_Epilepsy. snRNA-seq data: http://lopezatalayalab.in.umh-csic.es/CA1_SingleNuclei_&_Epilepsy.

The code developed to extract cell-type-specific gene expression signatures from differentially expressed genes in bulk-tissue RNA-seq is available as a protocol published in open access at STAR Protocols (Marquez-Galera et al., 2022). This protocol complements and expands on some of the information and analysis available in the article that forms the core of the thesis (Cid, Marquez-Galera, et al., 2021).

Experimental model and subject details

All experimental protocols and procedures were performed according to the Spanish legislation (R.D. 1201/2005 and L.32/2007), the European Communities Council Directives of 1986 (86/609/EEC) and 2003 (2003/65/CE) for animal research, and were approved by the Ethics Committee of the Instituto Cajal.

Adult male Wistar rats (180–200 g; 6-8 weeks postnatal), as well as wild-type C57 and transgenic mice (20-25 g; 8-9 weeks posnatal), were treated with multiple intraperitoneal injections of kainate (5 mg/kg) at hourly intervals until they reached *status epilepticus*. Transgenic mouse lines included the Thy1.2-G-CaMP7-DsRed2 (c57BL/6J-Tg(Thy1-G-CaMP7-DsRed2)492Bsi, stock RBRCO6579, RIKEN) and the Calb1-Cre (Jackson Lab, stock No:023531; Calb1-2A-dgCre-D) crossed with the tdTomato reporter line (Jackson Lab, stock No:007905; Ai9). The *status* was defined as a condition of continuous seizures lasting longer than 30 min. In a subset of rats, the lithium-pilocarpine model was used. These rats were i.p. injected with pilocarpine hydrochloride 12–24 h after the injection of lithium chloride (127 mg/kg, i.p.). Between one and four doses of 10 mg/kg pilocarpine were injected every 30 min until the *status epilepticus* was reached. Diazepam (4 mg/kg) was injected 1 h post-*status* to stop convulsions in all animals. They received intraperitoneal injections of 5% dextrose in saline (2.5 ml) and their diet was supplemented with fruit and powder milk during the following 2–3 days. After 3 days, animals behaved normally and were housed individually. Control animals were injected with saline and received treatments similar to epileptic animals.

Animals used in this study were examined in the chronic phase of the *status epilepticus* model of TLE (2-23 weeks post-*status*) when they already exhibited spontaneous seizures and interictal discharges (IID) (Figure S1A,B). In epileptic rats and mice, these events were typically associated with high-frequency oscillations (HFOs; Figure S1B), which are considered biomarkers of epileptogenesis (Jefferys et al., 2012; Valero et al., 2017). We focused on the dorsal hippocampus given the major role in associated cognitive comorbidities of epilepsy and more consistent neuronal loss as compared to ventral (Thom et al., 2012; Valero et al., 2017). In some epileptic animals, we aimed to induce convulsive seizures using high-pitched sounds (pulses of 95-100 dB and 1-20 s duration at random intervals of 1-20 s during 10 min). A convulsive motor seizure was defined according to clinical criteria, as sustained and repeated forelimbs automatisms with or without falling. Control animals did never exhibit convulsive seizures using this protocol.

Method details

EEG recordings and analysis

To evaluate epileptogenesis, some rats and mice were implanted with either intracranial 16-channel silicon probes or skull EEG-grid of 32-channels (Neuronexus) under

isoflurane anesthesia (1.5%–2% mixed in oxygen 400–800 ml/min). Jeweler's screws were inserted into the skull for providing additional anchoring and reference/ground connections (over the cerebellum). The implant was secured with dental cement. Animals were recovered from anesthesia and returned to home cages.

For recordings, EEG signals were pre-amplified (4x gain) and recorded with a 32-channel AC amplifier (Axona), further amplified by 100, filtered by analog means at 1 Hz to 5 kHz, and sampled at 20 kHz/channel with 12 bits precision. EEG recordings were synchronized with a ceiling video camera (30 frames/s) to track the animal position in space.

Analysis of electrophysiological signals was implemented in MATLAB 9.3 (MathWorks). EEG signals from the frontal and parietal electrodes were used to identify theta periods during running (band-pass 4-12 Hz) and periods of immobility characterized by low frequency delta activity (0.5-4 Hz). Forward-backward-zero-phase finite impulse response (FIR) filters of order 512 were used to preserve temporal relationships between channels and signals. Spectral values fitted to 1/f were similar between groups for frequencies > 150 Hz. HFO events were defined from the bandpass filtered signal (80-120 Hz) by thresholding (> 4 SDs). The power spectra were evaluated in a window of ± 0.2 ms around each detected event. Time-frequency analysis was performed by applying the multitaper spectral estimation in sliding windows with 97.7% overlap and frequency resolution of 10 Hz in the 90-600 Hz frequency range. HFO activity was evaluated as the power integral in the 80-120 Hz band.

We used a combination of features to identify HFO events automatically and to classify them in different categories (Valero et al., 2017) (Figure S1). First, we identified large amplitude transient (< 100 ms) discharges using LFP and current-source-density signals (CSD, i.e., the second spatial derivative) at the SR and SLM. Second, we identified HFO events at the SP by frequency thresholding over 100 Hz. Then we used spectral indices such as entropy and fast ripple indices from candidate HFO events at SP together with amplitude information from LFP and CSD signals at SR to classify events as: a) SPW-ripples (low amplitude; 100-150 Hz); b) SPW-fast ripples (medium amplitude, > 150 Hz) and IID-HFO (larger amplitude, > 100 Hz). Events not meeting criteria were left unclassified. Surface EEG recordings from mice were analyzed similarly, by using channels over the dorsal hippocampus or at the frontal cortex to identify HFO events and channels over the parietal cortex using selected segments of the EEG.

In vivo recording and labeling of single cells

Rats were anesthetized with urethane (1.2 g/kg, i.p.), fastened to the stereotaxic frame and warmed to keep their body temperature at 37°C. Two bilateral craniotomies of ~1 mm diameter were performed for CA3 stimulation (AP: −1.2 mm, ML: 2.9 mm) and CA1 recordings (AP: −3.7 mm; ML: 3 mm). The dura was gently removed, the *cisterna magna* was drained and the craniotomy covered with warm agar to reinforce stability.

A 16-channel silicon probes (NeuroNexus Tech; 100 µm interspaced, 413 µm^2 contact) was advanced perpendicular along the CA1-DG-CA3c axis guided by extracellular stimulation and electrophysiological hallmarks. Concentric bipolar electrodes were advanced 3.5 mm with 30° in the coronal plane to stimulate CA3. Stimulation consisted of biphasic square pulses (0.2 ms duration, 0.05-1.2 mA every 5 s). Extracellular signals were pre-amplified (4x gain) and recorded with a 16(32)-channel AC amplifier (Multichannel Systems), further amplified by 100, analogically filtered at 1Hz to 5 kHz, and sampled at 20 kHz/channel with 12 bits precision with a Digidata 1440. A subcutaneous Ag/AgCl wire in the neck served as reference. Recording and stimulus position was confirmed by post hoc histological analysis.

Intracellular recording and labeling were obtained in current-clamp mode using sharp pipettes (1.5 mm/0.86 mm outer/inner diameter borosilicate glass; A-M Systems, Inc) filled with 1.5 M potassium acetate and 2% Neurobiotin (Vector Labs, Inc; 50-100 MΩ) (Cid and de la Prida, 2019). Signals were acquired with an intracellular amplifier (Axoclamp 900A) at 100x gain. The resting potential, input resistance and amplitude of action potentials was monitored all over the course of experiments.

After data collection, Neurobiotin was ejected using 500 ms depolarizing pulses at 1-3 nA at 1 Hz for 10-45 min. Animals were perfused with 4% paraformaldehyde (PFA) and 15% saturated picric acid in 0.1 M, pH 7.4 phosphate buffered saline (PBS). Brains were postfixed overnight at room temperature (RT), washed in PBS and serially cut in 70 µm coronal sections (Leica VT 1000S vibratome). Sections containing the stimulus and probe tracks were identified with a stereomicroscope (S8APO, Leica). Sections containing Neurobiotin-labeled cells were localized by incubating them in 1:400 Alexa Fluor 488-conjugated streptavidin (Jackson ImmunoResearch 016-540-084) with 1% Triton X-100 in PBS (PBS-Tx) for 2 hours at room temperature (RT). To evaluate morphological features of single cells, sections containing the somata of recorded cells were processed with Triton 1% in PBS, blocked with 10% fetal bovine serum (FBS) in PBS-Tx and incubated overnight at RT with the primary antibody solution containing rabbit anti-Calbindin (1:500, CB D-28k, Swant CB-38) or mouse anti-Calbindin (1:1000,

CB D-28k, Swant 300) antibodies with 1% FBS in PBS-Tx. After three washes in PBS-Tx, sections were incubated for 2 hours at RT with appropriate secondary antibodies: goat anti-rabbit Alexa Fluor 633 (1:500, Invitrogen, A21070), and goat anti-mouse Alexa Fluor488 (Jackson Immunoresearch, 115-545-003) or goat anti-mouse Rhodamine Red (1:200, Jackson ImmunoResearch, 115-295-003) in PBS-Tx-1% FBS. Following 10 min incubation with bisbenzimide H33258 (1:10000 in PBS, Sigma, B2883) for nuclei labeling, sections were washed and mounted on glass slides in Mowiol (17% polyvinyl alcohol 4-88, 33% glycerin and 2% thimerosal in PBS).

All morphological analyses were performed blindly to electrophysiological data. The distance from the cell soma to radiatum was measured from confocal images using information from Calbindin and bisbenzimide staining. All pyramidal cells included in this study were localized within the CA1 region. Calbindin immunostaining was used to estimate the width of the superficial sub-layer from the border to the stratum radiatum. Superficial cells were defined based on the location of the soma within the calbindin sublayer, independently on their immunoreactivity (Valero et al., 2015). The border with radiatum was estimated for each section and the distance from the recorded cell somata was measured using ImageJ (NIH Image).

Analysis of intracellular single-cell recordings

Interictal discharges and sharp-waves associated with HFO events (ripples or fast ripples) recorded simultaneously to the intracellular membrane potential were detected as explained before. The timing of these events was used to identify the corresponding membrane potential deflections. Time-frequency analysis of HFO events was performed by applying the multitaper spectral estimation in sliding windows with 97.7% overlap and frequency resolution of 10 Hz in the 90-600 Hz frequency range (only the 100-600 Hz range is shown) to data sweeps aligned by sharp-wave ripple events (±1 s). Membrane potential responses of single-cells were evaluated in peri-event plots before (−200 to −150 ms), during (±50 ms) and after (150 to 200 ms) HFO events.

Passive electrophysiological properties (input resistance, membrane decay and capacitance) of neurons recorded intracellularly *in vivo* were measured using 500 ms currents step in current-clamp mode. Cells with intracellular action potential amplitude smaller than 40 mV were excluded. Resting membrane potential and input resistance were estimated by linear regression between baseline potential data and the associated holding current. Intrinsic firing properties, including action potential threshold, half-width duration and AHP were estimated from the first spike in response to depolarizing current pulses of 0.2 nA amplitude and 500 ms duration. The sag and maximal firing rate were

calculated from current pulses of ± 0.3 nA amplitude. A bursting index was defined as the ratio of the number of complex spikes (minimum of 3 spikes < 8 ms inter-spike interval) over the total number of spikes recorded during theta activity.

c-Fos immunostaining and analysis

To evaluate immediate-early gene expression associated to sound-induced convulsive seizures, animals were perfused 1 hour after and their brains cut in 70 µm coronal sections. Selected sections were stained against c-Fos using a polyclonal antibody at 1:250 (Santa Cruz Biotechnology sC-52) and bisbenzimide. Using one 20x confocal mosaic per animal, we quantified c-Fos intensity at CA1 pyramidal cells by delineating single-cell nuclei stained with bisbenzimide in one confocal plane (ImageJ). The mean intensity of c-Fos signal from each cell was then normalized by subtracting the background (set at 0) and dividing by the maximal positive signal in the mosaic, which was always at granule cell level (set at 1). No significant differences of background were observed across sections. Delineated cells were ranked by their distance to radiatum to classify them as deep or superficial, according to standard measurements of Calb1-layer thickness.

Laser capture microdissection (LCM) and RNA isolation

Brains from 3 control and 3 epileptic rats were dissected, longitudinally cut in half (separating both hemispheres), wrapped in aluminum foil and immediately frozen in liquid nitrogen. To avoid circadian effects on gene expression all samples were collected in the morning before noon and conserved at −80°C until use. The hippocampal region of each hemisphere was cut in 20 µm slices in a cryostat (Leica) (chamber temperature: −20°C; block temperature: −30°C) and placed on 1.0 mm PEN-membrane covered slides (Carl Zeiss). Slides were conserved at −20°C until use. Right before microdissection, slides were dried with vapor of liquid nitrogen. The CA1 cell layer was microdissected with a Leica 6000 laser microdissector through a 40x non-oil immersion objective to obtain cell bodies of superficial and deep sublayers separately (Figure 2A). Microdissected deep and superficial areas were collected in different empty caps of 0.5 mL Eppendorf tubes. After microdissection, samples were processed following ARCTURUS PicoPure RNA Isolation Kit (Thermo Fisher Scientific) instructions in order to extract and isolate total RNA. Briefly, 50 µl of extraction buffer was added into the cap, incubated at 42°C for 30 min, centrifuged at 800 x G for 2 min and stored at −80°C. The same volume of 70% ethanol was added to the cell extract and the mixture was pipetted into a pre-conditioned RNA purification column. The column was centrifuged 2 min at 100 x G and 30 s at 16000 x G, and washed with 100 µl of Wash Buffer 1. To completely

eliminate DNA, the purification column was treated with 40 µl of DNase (diluted 1/8 in RDD Buffer) (QIAGEN), incubated 15 min and centrifuged at 8000 x G for 15 s. Then the column was washed twice with 100 µl of Wash Buffer 2, and centrifuged at 8000 x G after the first wash and at 16000 x G after the second one. Finally, RNA was eluted into a new 0.5 µl Eppendorf tube by adding 11 µl of elution buffer onto the column membrane, incubating the column for 1 min at room temperature, and centrifuging the column for 1 min at 1000 x G and at 16000 x G immediately after. Total RNA samples were stored at −80°C. RNA integrity number (RIN) was similar in control (4.7 ± 0.8) and epileptic rats (5.7 ± 0.5; p = 0.07; 3 replicates x 2 sublayers per group), as well as for deep (5.2 ± 0.9) and superficial sublayers (5.3 ± 0.1; p = 0.81; n = 6 replicates per sublayers).

LCM-RNA-seq library construction and sequencing

RNA preparation for sequencing deep and superficial CA1 sublayers from control and epileptic rats was performed as described in Scandaglia et al. (2017). The twelve samples were sequenced according to manufacturer instructions in a HiSeq2500 sequencer (Illumina, Inc). Libraries were strand specific (reverse) and sequenciation was performed in paired-end configuration with a read length of 75 bp. Library size of read pairs for the different samples analyzed was between 47 and 59 Million reads. RNA-seq data can be accessed at the GEO repository (GSE143555).

LCM-RNA-seq data analysis

Alignment quality control of sequenced samples (LCM-RNA-seq) was assessed with FastQC (v.0.11.3) (Babraham Institute) and RNA-seq tracks were visualized using IGV (v.2.3.57) (Thorvaldsdóttir et al., 2013). LCM-RNA-seq reads were mapped to the rat genome (Rnor_6.0.83) using STAR (v.2.5.0c) (Dobin et al., 2013), and files were further processed with Samtools (v.0.1.19). Aligned reads were counted to gene transcripts using HTSeq (v.0.6.1) (Anders et al., 2015). Differential expression analysis was performed using DESeq2 (v.1.10.0) (Love et al., 2014) of the bioconductor suite (Huber et al., 2015) in the R (v.3.2.2) statistical computing platform. The experimental design consisted in two factors (treatment and anatomical area) and there was also grouped samples (samples from different anatomical areas (minus (deep) and plus (superficial) that were obtained from individual mice). Genes were considered differentially expressed at Benjamini-Hochberg (BH) adj. p < 0.05 and FC > 0.3 (Benjamini and Hochberg, 1995), except otherwise specified. GO analysis was performed using DAVID (v.6.8) bioinformatics platform (Huang et al., 2009).

LCM-RNA-seq single-cell informed data analysis

Single-cell RNA-seq data from Zeisel et al. (2015) was reanalyzed with consensus cluster SC3 algorithm (Kiselev et al., 2017). From the original 3,005 cells, pyramidal and interneurons were removed from somatosensory cortex, resulting in a total of 2,442 cells. Remaining cells were re-analyzed downstream with SC3. Clustering stability was optimal for 6 clusters. One cluster presented high heterogeneity (mixed population cluster), and was reanalyzed with the optimal clustering stability (5 clusters). Marker genes were tested for every cluster with Wilcoxon signed rank test. Top 10 genes with the area under the receiver operating characteristic (ROC) curve (AUC) power > 0.85 and with the adj. p < 0.01 from both cluster analyses were selected, with a total of 69 bona fide population markers. Based on the markers, populations were fused/splitted and 3 populations were isolated in the first clustering (pyramidal neurons, interneurons and oligodendrocytes) and 4 more in the second (astrocytes, endothelial cells, microglia and mural cells). Sixteen outlier cells were removed by total_counts, total_features or pct_counts_spike criteria, remaining 2,426 cells with a high correspondence with the original classification: Astrocytes (155 cells), Endothelial (177 cells), Interneurons (174 cells), Microglia (85 cells), Mural (56 cells), Oligodendrocytes (804 cells) and Pyramidal (975 cells). Next, to capture convoluted gene signatures on LCM-RNA-seq we used gene sets of equal size that were differentially regulated between superficial and deep sublayers of control and epileptic rats. To obtain these gene sets, we first filtered the genes by significance (adj. p < 0.1), then significantly differentially regulated genes were ranked by fold-change, and top 250 differentially regulated genes for each sublayer and condition, were retained for further analysis. We then, obtained normalized gene expression from scRNA-seq data for these gene sets and performed linear dimensionality reduction by principal component analysis to summarize and visualize the cells in the low-dimensional space. We also performed Pearson pairwise correlation and hierarchical clustering for these gene sets across all cells, to capture cell-type specific gene signatures that were mapped to major cell types in CA1 by using previously identified cell markers.

Single-cell RNA-seq data from Allen Brain Map portal - Mouse Whole Cortex and Hippocampus SMART-seq (2019) with 10x-SMART-seq taxonomy (2020) (Yao et al., 2021) was downloaded (http://portal.brain-map.org/atlases-and-data/rnaseq/mouse-whole-cortex-and-hippocampus-smart-seq) and subsetted as follows: from the original 76,533 cells, cells from hippocampal region were retained, and subsequently, cells from CA2, CA3, DG or empty subclass were removed. Then, cells of subclasses Astro, Micro-PVM, Endo, Oligo or VLMC were added. This initial filtering led a total of 5,506 cells. Of these, cells tagged by subclass as CA1-ProS (1,592 cells), Astro (976 cells), Lamp5 (864

cells), Vip (462 cells), Sncg (416 cells), Sst (266 cells), Oligo (236 cells), Endo (213 cells), Micro-PVM (176 cells), VLMC (159 cells), Pvalb (69 cells) were retained for further analysis, while cells tagged by subclass as SUB-ProS (29 cells), L2 IT RHP (21), NP SUB (9), L2/3 IT CTX-1 (3), L5 IT TPE-ENT (3), Sst Chodl (3), L2/3 IT ENTI (2), L6 CT CTX (2), Meis2 (2), L2/3 IT CTX-2 (1), L2/3 IT PPP (1), L6b CTX (1) were removed because of their low cell number and/or mismatch with CA1 or glial cells. The remaining 5,429 cells were grouped in their corresponding major cell populations as follows: Astrocytes (Astro) (976 cells), Endothelial (Endo) (213 cells), Interneurons (Lamp5, Pvalb, Sncg, Sst, Vip) (2077 cells), Microglia (Micro-PVM) (176 cells), Mural (VLMC) (159 cells), Oligodendrocytes (Oligo) (236 cells) and Pyramidal (CA1-ProS) (1,592 cells). Next, we proceed as indicated before to capture convoluted gene signatures on LCM-RNA-seq by using normalized expression data from this scRNA-seq dataset, for differentially regulated between superficial and deep sublayers of control and epileptic rats.

Single-nuclei isolation

We accurately isolated single nuclei from 2 control and 2 epileptic Calb1::CrexTdTomato young adult mice. We used these animals to facilitate identification of the CA1 region under a fluorescent scope. Animals were sacrificed 12 weeks after the kainate/saline administration by cervical dislocation and brains were dissected and cut in 300 μm thick slices in a vibratome covered by ice cold Hank's balanced salt solution (HBSS) 1x. As in LCM studies, samples were collected before noon to avoid circadian effects. The dorsal CA1 region were manually dissected from 4 consecutive slices and put altogether into 400 μL of ice-cold Magnetic-activated cell sorting (MACS) buffer (0.5% BSA, 2 mM EDTA, PBS 1x). CA1 portions were transferred to a dounce homogenizer (20404 Lab Unlimited) containing 400 μL of MACS buffer and were homogenized 12-15 times each with the pestle. The cell suspension was transferred to a 2 mL Eppendorf tube and centrifuge 15 min 500 x G 4°C. Cell pellets were resuspended in 500 μL of lysis buffer (10 mM Tris-HCl, 10 mM NaCl, 3 mM $MgCl_2$, 0,1% IGEPAL) and kept 5 min on ice. Samples were then spun down at 500 x G for 30 min in a pre-chilled centrifuge. The nuclei pellet was resuspended in PBS 1x 1% BSA and then 15,000 nuclei were purified by flow cytometry in a BD FACS Aria III. The whole process was carried out at 4°C.

Single-nucleus RNA sequencing

Purified intact nuclei from mouse hippocampal CA1 area were processed through all steps to generate stable cDNA libraries as previously described (Lipinski et al., 2020). For every sample, 15,000 nuclei were loaded into a Chromium Single Cell A Chip (10x

Genomics) and processed following the manufacturer's instructions. Single-nuclei RNA-seq libraries were prepared using the Chromium Single Cell 3′ Library & Gel Bead kit v2 and i7 Multiplex kit (10x Genomics). Pooled libraries were then loaded on a HiSeq2500 instrument (Illumina) and sequenced to obtain 75 bp paired-end reads following manufacturer instructions. On sequencing depth, 262 million fragments were generated for the control condition and 296 for the epileptic dataset. Libraries reached a sequencing saturation of 86.9% for control and 91.2% for epilepsy condition. snRNA-seq data can be accessed at the GEO repository (GSE143560).

snRNA-seq analysis

Quality control of sequenced reads was performed using FastQC (Babraham Institute). Sequenced samples were processed using the Cell Ranger (v.2.2.0) pipeline (10x Genomics) (Zheng et al., 2017) and aligned to the GRCm38 (mm10) mouse reference genome customized to count reads in introns (pre-mRNA) over the Ensembl gene annotation version 94. Barcodes with total unique molecular identifier (UMI) count > 10% of the 99th percentile of the expected recovered cells were selected for further analysis. Using this criterion, we retrieved 3,661 (control), 3,078 (epileptic) high quality nuclei per sample. Mean reads per nucleus were 71,449 (control) and 96,150 (epileptic). Median genes per nucleus were 1,599 (control) and 1,256 (epileptic). Minimum UMI count per nucleus were 710 (control), 540 (epileptic), well above the typical quality standards in single-cell/nucleus sequencing. Single-nucleus RNA-seq data were subsequently pre-processed and further analyzed in R (v.3.4.4) using Seurat (v.2.3.4) (Butler et al., 2018; Stuart et al., 2019), following the same steps that we applied in Lipinski et al. (2020). Filtering parameters were as follows: genes, nCell < 5; cells, nGene < 200. Data were then normalized using global-scaling normalization (method: LogNormalize, scale.factor = 10,000).

An initial exploratory analysis was performed on each dataset separately. This analysis retrieved a similar number of clusters in each dataset that were approximately equal in size. We next combined both datasets using the function MergeSeurat. Highly variable genes (HVGs) were detected using FindVariableGenes function with default parameters. Then, normalized counts on HVGs were scaled and centered using ScaleData function with default parameters. Principal component analysis (PCA) was performed over the first ranked 1,000 HVGs. Plots of the two principal components of the PCA, where cells were colored by dataset, excluded the presence of batch effects. Cluster detection was carried out with Louvain algorithm in FindClusters function, using 20 first PCA dimensions and resolution of 0.6 (the default number in Seurat and the optimal according

to cell number, data dispersion and co-expression of previously reported cell markers). Plots of the two principal components of the PCA where cells were colored by dataset of origin excluded the presence of batch effects.

This analysis identified 13 clusters. CA1 pyramidal neurons populated three of these clusters: one cluster was enriched in bona fide gene markers of deep cells (*Ndst4*, *Col11a1*) whereas a second one was enriched in canonical markers of superficial cells (*Calb1*, *Epha3*). The third cluster showed a mixed identity. An additional round of clustering segmented this population in three additional clusters that were enriched in deep and superficial markers, respectively, and a third cluster that could not be annotated based on the presence of gene markers of CA1 sublayer neurons. The vast majority of cells within this cluster (66/67) were from epileptic mice (Pyr_ES). Next, the FindMarkers function was used to identify gene markers and to determine the cell populations represented by each cluster. Finally, cell subtypes were manually aggregated based on the presence of canonical markers of known cell types into six distinct major cell types: excitatory neurons (Excit); inhibitory neurons (Inter); oligodendrocytes (ODC); oligodendrocyte progenitor cells (OPCs); microglia (Microglia); astrocytes (Astro).

Visualization and embedding were performed using stochastic nearest neighbors (tSNE) (van der Maaten and Hinton, 2008) and uniform manifold approximation and projection (UMAP) (McInnes et al., 2018) methods over PCA using the 20 first PCA dimensions. UMAP plots of gene expression show normalized count (UMIs) per nucleus. The equalized expression between fixed percentiles was plotted according to the following criterion: the minimum expression was adjusted to 5% and the maximum expression was adjusted to 95% in all UMAP expression plots. To evaluate effects of epilepsy, datasets from both conditions were merged and HVGs were identified for each dataset as above indicated. Only HVGs that were detected in all datasets were used to perform visualization and embedding as described above. Clustering was performed on merged dataset from both conditions and populations were identified combining these results with clustering information obtained in control and epileptic datasets separately, together with co-expression of population markers.

Differential expression analysis (DEA) was used to identify population gene markers. For DEA, the nuclei of each population were contrasted against all the other nuclei in the merged dataset using Wilcoxon Rank Sum test on normalized counts. For epilepsy effect analysis, in the merged dataset, the nuclei of each population from the epileptic dataset were contrasted against all the other nuclei of the same population in control using

Wilcoxon Rank Sum test on normalized counts. GO functional enrichment analyses were performed using DAVID (v.6.8) bioinformatics platform (Huang et al., 2009). All DEA and functional enrichment analyses applies False Discovery Rate (FDR) method by BH post hoc p adjustment, except otherwise specified.

Cell trajectories and pseudotime analysis

The disease pseudotime analysis was performed using Monocle 2 (v.2.8.0) (Qiu et al., 2017a, 2017b). First, the Seurat merged dataset was transformed to Monocle object and cells from Pyr_CA1 were subset. The size factor and dispersion of the subset was estimated, and data was normalized and preprocessed. Genes under the minimum level detection threshold of 0.1 and detected in less than 10 cells were filtered with the function setOrderingFilter. Genes defining how a cell progress through a pseudo-time disease trajectory were selected with the function differentialGeneTest (Monocle's main differential analysis routine). 2,579 genes (64,68% of a total of 3,987 genes considered as expressed) were significative with FDR adj. p < 1% for the combination of factors: ~SeuratCluster+Condition, and thus, defined the high dimensional space for pseudotemporal trajectory analysis.

Discriminative dimensionality reduction with trees (DDRTree) reduction algorithm learns the principal graph and specifies the trajectory. DDRTree was applied inside the function reduceDimension, and got the default parameters: norm_method = "log", pseudo_expr = 1, relative_expr = TRUE, auto_param_selection = TRUE (automatically calculate the proper value for the ncenter (number of centroids)) and scaling = TRUE (scale each gene before running trajectory reconstruction). Prior the dimensional reduction, the function reduceDimension also performed a variance-stabilization of the data (because the expressionFamily of the data was negbinomial.size). Finally, the cells were ordered according to pseudo-time with the function orderCells, which added a pseudo-time value and state for each cell; together encode where each cell maps to the trajectory.

For enrichment analysis on pseudotime trajectories, top-ranked 250 branched expression analysis modeling (BEAM) significant changes through the progression across the disease trajectory for each sublayer were clusterized and GO enrichment analyses on upregulated and downregulated clusters were performed using DAVID (v.6.8) bioinformatics platform (Huang et al., 2009).

Cell-type immunostaining and analysis

To evaluate the contribution of different cell-types to hippocampal sclerosis, control and epileptic rats and mice were perfused with 4% paraformaldehyde (PFA) and 15%

saturated picric acid in 0.1 M PBS, pH 7.4. Brains were postfixed overnight and cut in 70 µm coronal sections (Leica VT 1000S vibratome). Sections containing the dorsal-intermediate hippocampus were processed with Triton 1% in PBS and blocked with 10% fetal bovine serum (FBS) in PBS-Tx. Sections were incubated overnight at RT with 1% FBS PBS-Tx solution containing primary antibodies against a battery of cell-type specific markers. The list of antibodies includes: rabbit anti-calbindin (1:1000, CB D-28k, Swant CB-38) or mouse anti-calbindin (1:500, CB D-28k, Swant 300) to identify superficial CA1 pyramidal cells; rabbit anti-Wfs1 (1:500, Protein Tech, 11558-1-AP) for CA1 pyramidal cells; rabbit anti-Iba1 (1:1000, Wako, 019-19741) for microglia; rabbit anti-GFAP (1:1000, Sigma, G9269) for astrocytes; rabbit anti-Olig2 (1:200, Millipore, AB9610) for oligodendrocytes. After three washes in PBS-Tx, sections were incubated for 2 hours at RT with appropriate secondary antibodies: goat anti-rabbit Alexa Fluor633 (1:200, ThermoFisher, A-21070), and donkey anti-mouse Alexa Fluor488 (1:200, ThermoFisher, A-21202) or goat anti-mouse Rhodamine Red (1:200, Jackson ImmunoResearch, 115-295-003) in PBS-Tx-1%FBS. Following 10 min incubation with bisbenzimide H33258 (1:10000 in PBS, Sigma, B2883) for nuclei labeling, sections were washed and mounted on glass slides in Mowiol (17% polyvinyl alcohol 4-88, 33% glycerin and 2% thimerosal in PBS).

To acquire multichannel fluorescence stacks from recorded cells, a confocal microscope (Leica SP5) with LAS AF software v.2.6.0 build 7266 (Leica) was used. The following channels (fluorophore, laser and excitation wavelength, emission spectral filter) were used: a) bisbenzimide, Diode 405 nm, 415–485 nm; b) Alexa Fluor 488 nm, Argon 488 nm, 499–535 nm; c) Rhodamine Red / Alexa Fluor 568 / Texas Red, DPSS 561 nm, 571–620 nm; d) Alexa Fluor 633, HeNe 633 nm, 652–738 nm; and objectives HC PL APO CS 10.0 × 0.40 DRY UV, HCX PL APO lambda blue 20.0 × 0.70 IMM UV and HCX PL APO CS 40.0 × 1.25 OIL UV were used.

FluoroJade staining

To evaluate neurodegenerating neurons we used coronal sections from epileptic rats perfused at different time points post-*status*. Selected sections were immunostained against Wfs1 followed by FluoroJade staining. To this purpose, sections were pretreated for 5 min with 1% sodium hydroxide in 80% ethanol, followed by 70% ethanol (2 min) and distilled water (2 min). Sections were then incubated 10 min in 0.06% potassium permanganate, rinsed in distilled water and immersed into 0.0001% solution of FluoroJade C dye (Sigma AG325) in 0.1% acetic acid (pH 3.5) for 10 min. After a brief wash in distilled water, they were mounted on gelatin-coated slides, air-dried,

coverslipped with DPX and examined under a confocal microscope as described above. FluoroJade positive cells exhibited bright green fluorescence.

In situ hybridization analysis

Selected sections from control and epileptic rats were processed for *in situ* hybridization using standard methods. Briefly, riboprobes were prepared from Rat *Enpp2* cDNA (Image clone ID 7115236) and using RT-PCR from rat adult hippocampus to prepare *Wfs1* (NM_031823.1, from bp 783 to 1631), *Ndst4* (XM_006233274.2, from bp 536 to 1024), *Syt17* (NM_138849.1, from bp 378 to 1118), *Hrt1a* (J05276.1, from bp 730 to 1663) and *Scn7a* (NM_131912.1, from bp 2812 to 3550) cDNAs. Similar riboprobes were used in sections from normal and epileptic mice. Riboprobe hybridization was detected using alkaline phosphatase–coupled anti-digoxigenin Fab fragments (Sigma). Hybridized sections were mounted in glycerol and photographed using a Nikon stereoscope and a DCC Nikon camera.

RNAscope analysis

Control and epileptic mice were perfused with 4% paraformaldehyde (PFA) and 15% saturated picric acid in 0.1 M PBS, pH 7.4. Brains were post-fixed overnight and cut in 50 µm coronal sections (Leica VT 1000S vibratome) which were kept at −20°C in a solution of 30% glycerol and 30% etylenglycol in PBS. RNAscope Fluorescent Multiplex Assay (Advanced Cell Diagnostics) was carried out according to the manufacturer's protocols. Briefly, sections containing the dorsal-intermediate hippocampus (around −2 µm AP from Bregma) were washed in PBS-Tx, and mounted onto SuperFrost Plus microscope slides (10149870, ThermoFisher Scientific). They were then dehydrated at 60°C follow by ethanol, pretreated with a target retrieval solution (322000, ACD) and protease III (322340, ACD), and co-hybridized with *Spag5* (Mm-Spag5, 505691, ACD) and *Dcc* (Mm-Dcc-C3, 427491, ACD) or *Dapk1* (Mm-Dapk1-C3, 880221-C3, ACD) probes. Finally, the amplification steps (RNAscope Fluorescent Multiplex Detection reagents, 320851, ACD) were followed, using Atto 550 for *Spag5* and Atto 647 for *Dcc* or *Dapk1* as fluorescent labels. The RNAscope 3-plex positive control probe set (320881, ACD), with probes to Polr2a, PPIB and UBC, was used to confirm preservation of sample RNA. The negative control probe to bacterial DapB (320871) was used to establish non-specific labeling.

Following the RNAscope protocol, sections were blocked for 30 min with 10% FBS in PBS-Tx, and incubated overnight at RT with rabbit anti-Wfs1 (1:500, Protein Tech, 11558-1-AP) in 1% FBS PBS-Tx. After three washes in PBS, sections were incubated for 2 h with donkey anti-rabbit Alexa Fluor488 (1:200, ThermoFisher Scientific, A-21206)

in 1% FBS PBS-Tx, washed twice in PBS and mounted using ProLong Gold Antifade mountant (ThermoFisher Scientific, P10144).

Multichannel fluorescence stacks were achieved in a confocal microscope (Leica SP5) with LAS AF software v.2.6.0 build 7266 (Leica), with a 40x objective (HCX PL APO CS 40.0 × 1.25 OIL UV), at 0.5 µm z-interval. Pinhole was set at 1 Airy, and following channels settings were applied for each fluorophore (excitation wavelength, emission spectral filter): Argon (488 nm, 499–553 nm) for Alexa Fluor488, DPSS (561 nm, 570–630 nm) for Atto 550, and HeNe (633 nm, 645–740 nm) for Atto 647. Diode (405 nm, 415–485 nm) was used as an unstained channel to identify autofluorescent material, which can be abundant in epileptic tissue. Images were acquired at 8 bits, 387.5 × 387.5 µm (1024 × 1024 pixels) in size. Brightness and contrast were adjusted with the ImageJ Fiji software (NIH Image).

To estimate the amount of *Dapk1*, *Spag5* and *Dcc* transcripts per cell, a total of 5 control and 5 epileptic animals (12 cells per animal) were analyzed. Each ROI was drawn in one confocal plane as the outline of a pyramidal cell soma at their maximum diameter based on Wfs1 immunoreactivity, using ImageJ. Only those cells focused within the first 10 µm were selected to avoid reduction of the signal due to depth in the section. In either *Dapk1*, *Spag5* or *Dcc* channels, single signal dots were counted, and clusters were converted to dot number as suggested by the manufacturer (ACD): (total intensity - average background intensity x area)/single dot average intensity.

Quantification and statistical analysis

Statistical analyses were performed with MATLAB, SPSS and using the computing environment R (R Development Core Team, 2005, http://www.R-project.org). No statistical method was used to predetermine sample sizes. Normality and homoscedasticity were evaluated with the Kolmogorov–Smirnov and Levene's tests, respectively. The exact number of replications for each experiment is detailed in text and figures. Several ways ANOVAs or Friedman tests were applied. Post hoc comparisons were evaluated with the Tukey-Kramer, Student or Wilcoxon tests. Deep-superficial trends were evaluated using Spearman correlation and tested against 0 (i.e., no correlation was the null hypothesis) at $p < 0.05$ (two sided).

Discussion

Temporal lobe epilepsy (TLE) is the most common type of focal epilepsy in adults, and hippocampal sclerosis (HS) its most frequent underlying pathology (Babb and Brown, 1987). HS is a heterogeneous histopathological entity classified in different subtypes with distinct clinical relevance (Blümcke et al., 2013). HS affects specific temporal lobe regions with major roles in learning and memory, as evidenced by the correlation with cognitive co-morbidities in some clinical studies (Coras et al., 2014; Rodrigues et al., 2015). The prognosis value of certain subtypes has been largely debated, but emerging data suggest that it deserves further consideration in light of cell-type specificity (Prada Jardim et al., 2018). It is becoming increasingly clear that the pattern of sclerosis is quite complex and that a better understanding could improve diagnosis. Thus, neuropathological studies on post-surgical and post-mortem human brain samples call for the need to better rely on cell-type-specific markers and more clear segmentation between regions (DeKraker et al., 2019; Thom, 2014). Unfortunately, our understanding of the mechanisms leading to different subtypes of HS and their clinical value remains elusive.

The area most affected by the different subtypes of HS is the CA1 layer, which consist of a deep and superficial sublayer. Superficial CA1 pyramidal cells are located toward the *stratum radiatum*, characteristically express *Calbindin* amongst other specific markers and are developed later during embryogenesis, as compared with deep pyramidal cells located closer to the *stratum oriens* (Slomianka et al., 2011; Valero et al., 2015). Deep and superficial CA1 pyramidal cells are innervated differently by local-circuit GABAergic interneurons, express different neuromodulatory receptors, project differentially to cortical and subcortical regions and participate distinctly in hippocampal oscillations (Cembrowski et al., 2016a; Soltesz and Losonczy, 2018; Valero and de la Prida, 2018). In experimental models of acquired epilepsy with type 2 HS – characterized by profound selective neuronal loss in the CA1 layer – we found specific effects in the superficial sublayer. During epileptiform activity, *in vivo* single-cell recordings showed that superficial CA1 pyramidal cells exhibit a larger and sustained post-event depolarization and increased firing rate after interictal discharges. In addition, superficial CA1 cells show increased expression of the immediate-early gene-associated protein c-Fos after individual seizures. Taken together, these data indicate that conversely to deep cells, superficial neurons of CA1 undergo a larger activity burden in epilepsy (Figure 1). Our snRNA-seq analysis identified many transcripts differentially regulated between deep and superficial CA1 pyramidal cells in the basal state. Deep pyramidal

cells show an enrichment in genes (i.e., *Bdnf*, *Gabrg3*, *Htr4* and *Gabra5*) associated with the gamma-aminobutyric acid signaling pathway, which is related to inhibition of synaptic transmission (Figure S5B). In contrast, superficial pyramidal cells show an enrichment in genes (i.e., *Grm1*, *Grm7*, *Kcnc2*, *Kcnab1*, *Cacna1c* and *Cacng3*) associated with glutamatergic signaling, and potassium and calcium ion transport pathways, related to increased excitability and synaptic transmission (Figure S5C). These distinct patterns at the level of gene expression may contribute to the observed differences in excitability between deep and superficial cells in epilepsy. While these changes can reflect a distinct developmental origin of the two subtypes of principal neurons populating CA1, they may also be shaped by hippocampal microcircuitry. First, perisomatic inhibition by parvalbumin (PV) basket cells is remarkably higher in deep compared with superficial cells (Soltesz and Losonczy, 2018; Valero et al., 2015). Second, superficial cells are more likely to be driven by presynaptic CA3 activity through Schaeffer collaterals than deep cells (Valero et al., 2015). Similarly, direct inputs to CA1 from layer III pyramidal neurons in the medial entorhinal cortex are biased towards deep CA1 cells, whereas projections from the lateral entorhinal cortex are stronger in superficial cells (Masurkar et al., 2017). Given the loss of medial layer III inputs and sprouting of lateral inputs together with specific cannabinoid type 1 receptors pathways (Laurent et al., 2015; Maroso et al., 2016), it is very likely that these changes contribute to more sustained activation of superficial cells in the epilepsy context.

Our transcriptional profiling of laser-microdissected deep and superficial CA1 sublayers (LCM-RNA-seq) revealed strong regionalized responses to acquired epilepsy. The sublayer-specific transcriptional effect in epilepsy may arise from a combination of cell type-specific responses and changes in the cellular composition of the tissue. In fact, transcriptional dysregulation is a central feature of most prevalent neurodegenerative diseases – such as Alzheimer's and Parkinson's disease (Gjoneska et al., 2015; Nido et al., 2020) – were the combination of cell type-specific responses and changes in cell-type composition are common sources of variation driven by the complex cellular phase associated with disease (De Strooper and Karran, 2016). We found many more significantly differentially expressed transcripts in the superficial sublayer (Figure 2). Notably, these genes are associated with GO terms related to immune and inflammatory processes, cytokine production, and programmed cell death (Figure 2). These findings are in line with recent reports in human temporal lobe epilepsy (Morin-Brureau et al., 2018). Indeed, the analysis of bulk-tissue LCM-RNA-seq data revealed that a significant proportion of the upregulated genes in the superficial CA1 sublayer in response to epilepsy are related to microglia (Figure 2; Figure S2F,G). Accordingly, we found

sublayer-specific deregulation of several genes associated to the microglial sensome (Hickman et al., 2013) and alteration of neuron-microglia signalling pathways in epilepsy (Ali et al., 2015; Eyo et al., 2014; Vezzani and Baram, 2007) (Figure S3). Some of the genes that were significantly differentially upregulated in superficial CA1 sublayer include the specific purinergic receptor gene *P2ry12* that is involved in microglial motility and migration, an early step of neuroinflammation process (Eyo et al., 2018), and the tyrosine kinase receptor gene *Csf1r* that is involved in microglia proliferation and whose blockade has been shown to attenuate epileptic seizures in three preclinical models of epilepsy (Srivastava et al., 2018). On the other hand, genes constitutively expressed at the neuronal membrane playing relevant roles in neuron-microglia communication such as *Cd200* and *Cx3cl1*, were downregulated in epilepsy. Among these genes, the transcript levels of CX3CL1 (fractalkine) a transmembrane chemokine that acts as a "find me" signal to promote phagocytic clearance of dying cells (Zabel et al., 2016; Butler et al., 2021), were downregulated in deep and superficial CA1 sublayers in epilepsy. Notably, the immunoglobulin superfamily gene *Cd200*, that acts as a "don't eat me" signal that negatively regulates phagocytosis (Biber et al., 2007), was selectively downregulated in superficial CA1 sublayer. To better understand the changes in gene expression identified in a highly complex and heterogeneous tissue, we deconvolved differentially expressed gene lists from bulk LCM-RNA-seq into cell-type-specific gene expression patterns. To do so, we leveraged publicly available single-cell expression data from CA1 layer in the adult brain. This analysis unveiled a significant response of microglia cells in the superficial sublayer of epileptic animals (Figure 3). The presence of regionalized responses in epilepsy was further confirmed by immunofluorescence (Figure 4). These results suggest the existence of progressive interactions between microglia and superficial pyramidal cells in epilepsy that may contribute to HS. In support of this interpretation, immunofluorescence analyses revealed a negative correlation between microglia and pyramidal cell density in superficial CA1 sublayer in epilepsy (Figure 4). Moreover, we found that most of the degenerating neurons (positive to fluoro-jade staining) were located in the CA1 superficial sublayer (Figure 4). Taken together, our results reveal sublayer-specific neurodegeneration in epilepsy that primarily affects superficial CA1 sublayer, and suggest that neuron-microglia interactions represent a relevant event underlying type 2 HS.

Regionalized responses in acquired epilepsy identified in our study open new questions such as the role that cellular interaction hierarchies at the neuronal microcircuit level and the relevance of neuron-microglia interactions in differentiated vulnerability at the sublayer level underlying type 2 HS. These questions would be addressed by interfering

with each cell type independently. Our data indicates that superficial pyramidal cells compared to deep pyramidal cells sustain the greatest depolarization burden in epilepsy (Figure 1). However, whether this observation has a causal relationship to their increased vulnerability to neurodegeneration remains unknown. This question would be tackled by modulating neuronal activity in specific neuronal populations. Designer receptor exclusively activated by designer drugs (DREADD) chemogenetic technology is ideally suited for prolonged modulation of cell activity in the range of hours to days (Goossens et al., 2021a; Goossens et al., 2021b). This can be achieved by using a combination of viral vectors and intersectional genetics to target superficial CA1 neurons (i.e., Cre/loxP system to target Gi-coupled inhibitory DREADD expression in superficial-layer Calb1-postive neurons). By doing so, it would be possible to test whether the increased burden of activity observed in superficial CA1 cells in epilepsy is a necessary event in the cascade leading to neuronal loss underlying HS. On the other hand, we have found that the death of superficial pyramidal cells in epilepsy is associated to increased density of activated microglia in the superficial CA1 sublayer (Figure 3). The increased abundance of microglia in superficial sublayer could be consequence of neuronal cell death in this region. However, it is also possible that microglia would be actively attracted to this area by signals emitted from unhealthy or dysfunctional neurons, where they would actively contribute to HS by promoting the death of functionally compromised neurons by specific mechanisms. In line with this, it has been shown that microglia causes neuronal death by different mechanisms including cytolysis (Ding et al., 2020) and phagoptosis – cell death by phagocytosis (Brown and Neher, 2014; Brown et al., 2015). Therefore, experiments aimed at modulating microglia activity would contribute to answer these relevant questions. In this line, pharmacological agents such as the irreversible P2RY12-receptor antagonist clopidrogrel (Lou et a., 2016) and the unspecific anti-inflammatory antibiotic minocycline (Kobayashi et al., 2013) could represent valuable tools to investigate the role of microglia in TLE-HS. It should be noted that minocycline and clopidogrel are commonly used in the clinic. Should these or related drugs show neuroprotective effects towards HS, they could open the design of new therapeutic interventions in TLE, in combination with modern antiepileptic agents. While the electrical and pro-inflammatory manifestations of epilepsy are interrelated, they proceed across different levels in the hierarchy, since microglial activation is dependent on signals emitted by hyperexcitable and excitotoxic neurons (Biber et al., 2007; Eyo et al., 2014; Eyo et al., 2018). Should the pharmacological approach be effective in rescuing neuronal loss, the fact that sclerosis can actually dissociate from epileptiform activities would not necessarily demonstrate that they are totally independent processes, but rather that they are different sides of a more complex interactive manifold. Finally,

should any of the strategies discussed above be able to preserve neuronal integrity, it would be critical to assess cognitive function since experimental TLE-HS has extensively show to be associated to impairment in hippocampal-dependent memory functions such as episodic memory (Valero et al., 2017).

To better understand the mechanisms leading to neuronal death, we explored and characterized the transcriptomic differences between CA1 pyramidal cells and epilepsy effects at the single-cell level (Figure 5). Unsupervised branched expression learning unveiled cell-type specific transcriptional trajectories that deviate from health to epilepsy in deep and superficial CA1 pyramidal cells (Figure 6). Gene ontology analysis of the genes underlying cell-type specific trajectories in experimental TLE-HS suggests that transition from the normal to the epileptic condition in deep cells is more likely associated with changes in synaptic signaling and excitability (i.e., they reflect microcircuit alterations), whereas transcriptional changes observed in superficial cells along distinct cell states are related to cell-cell communication (i.e., neuron-microglia interactions). Such different latent trends might be caused by different kinetics of deep and superficial cells along the neurodegenerative process. However, it could be also possible that each subpopulation is affected by distinct pathways leading to the observed differential vulnerability of superficial and deep CA1 neurons in experimental TLE-HS. For instance, while we found deregulated expression of genes associated with apoptotic pathways that were common to both cell types in response to epilepsy (i.e., *Akt3*, *Nrg3*, and *Camk2a*) (Ashpole and Hudmon, 2011; He et al., 2020; Kanekura et al., 2005; Tawarayama et al., 2018; Vest et al., 2010), we also identified genes related to cell death that were deregulated specifically in superficial or deep neurons. Thus, in superficial cells, epilepsy resulted in decreased expression of brain-derived neurotrophic factor (*Bdnf*) and increased transcript levels of the pro-apoptotic pathway activator *Dapk1* (Bialik and Kimchi, 2006). Conversely, in deep pyramidal neurons, epilepsy led to a robust increase in expression of the gene encoding the pro-survival receptors TrkB (*Ntrk2*) and TrkC (*Ntrk3*) (Huang and Reichardt, 2001; Pfisterer and Khodosevich, 2017) (Figure 6E-G; Figure S6F). Interestingly, pseudotime analysis mapped some control cells along the epileptic branches in both sublayers, suggesting that latent sublayer-specific transcriptional processes might actually be running along life (Bishop et al., 2010) (Figure 6C,D).

Our snRNA-seq analysis also disclosed an epilepsy-specific pyramidal cell population, Pyr_ES (Figure 5B; Figure S4E), which accumulated at the end of the superficial trajectory branch, suggesting they could also represent a subset of superficial cells (Figure 6B, arrowhead). This subset of pyramidal cells displayed remarkable expression

of neurodegeneration-related transcripts such as *Cdk5*, *Ckb*, *Matk*, *Chl1*, and *Spag5* (Patrick et al., 1999). The presence of cells with very high numbers of *Spag5* molecules in the superficial sublayer of the epileptic CA1 was confirmed by combined immunofluorescence and single-molecule amplification methods (Figure 5I,J; Figure S6D,E). Our results suggest that genes with an exacerbated response to epilepsy are expressed specifically by a vulnerable subset of pyramidal neurons undergoing later stages of neurodegeneration by the time of sampling. We propose that Pyr_ES cells reflect the accumulated pro-epileptic transitional changes leading to epileptogenesis and neurodegeneration, as suggested by their extreme location along disease trajectories.

The advent of new high-throughput techniques that allow transcriptome profiling of thousands of individual cells simultaneously is unfolding cellular heterogeneity in the central nervous system with an unprecedented resolution (Islam et al., 2011; Lein et al., 2017; Zeisel et al., 2018; Ortiz et al., 2020; La Manno et al., 2021; Yao et al., 2021). However, little is still known on how this heterogeneity affects disease development and how it is affected in pathological conditions. Here, we identify for the first time heterogeneity in the neuronal patterns of activity of deep and superficial CA1 pyramidal neurons in epilepsy, show specific gene expression signatures across deep and superficial CA1 sublayers that are associated with neuronal loss and HS, reveal disease trajectories of deep and superficial CA1 pyramidal neurons in epilepsy, and uncover their underlying transcriptional programs. In addition, to our knowledge, we provide the most comprehensive characterization of the transcriptome of deep and superficial pyramidal cells of CA1 area of the adult mouse hippocampus in basal (healthy) conditions (Figure 5C,D). By dissecting the transcriptional landscape across CA1 sublayers in epilepsy, our work offers insights into the mechanisms regulating epileptogenesis, the biological processes occurring across resident cellular types segregated across CA1 sublayers, and highlights the importance of leveraging cell-type specificity to better understand the phenotypic complexities accompanying HS in epilepsy.

Our work reveals the neurodegenerative component that progresses over time in the pathology of TLE-HS. Still, additional efforts are needed to further advance in understanding the processes underlying neurodegeneration in epilepsy. The continuous advances in single-cell technology are allowing to scale up the number of cells that can be sequenced while reducing costs (Svensson et al., 2018; Rosenberg et al., 2018; Ding et al., 2020; Datlinger et al., 2021; Mamanova et al., 2021). Increasing the number of samples and cells would allow more robust results to be obtained and also to study the effects on smaller populations. Possible new analyses would include the study of ligand-receptor communication between hippocampal populations (Efremova et al., 2020;

Armingol et al., 2021; Hu et al., 2021; Lummertz da Rocha et al., 2022) and a detailed study of the neurons most affected in epilepsy and undergoing advanced stages of neurodegeneration. In addition, a longitudinal study of TLE-HS progression would reveal a more complete picture of the neurodegenerative component of epilepsy through a real temporal dimension. On the other hand, the application of state-of-the-art *in situ* transcriptomic techniques (Ke et al., 2013; Qian et al., 2020; Gyllborg et al., 2020; Langseth et al., 2021) would spatially resolve specific and differentiated cellular responses to TLE-HS at CA1 sublayers. *In situ* profiling would help connect the observations of intercellular communication, neuroinflammation and neuronal loss with spatial dimension (Longo et al., 2021; La Manno et al., 2021; Lummertz da Rocha et al., 2022). Finally, it is necessary to translate these analyses to human tissue samples. However, the main limitations of using human brain tissue samples cannot be avoided. Limitations include lack of proper control samples, high inter-individual variability and high heterogeneity in tissue status (Becker, 2018; Ren and Curia, 2021). Furthermore, differences in processing, temperature and collection time of post-mortem and *ex vivo* samples (e.g., those obtained after resective treatment of drug-resistant TLE) introduce variability that affect downstream analyses (Ferrer et al., 2007; Nagy et al., 2015). Therefore, standardization in the processing of human samples would be key to mitigate differences due to external causes and to obtain robust and generalizable results to TLE-HS pathology.

Conclusions

General conclusion

Our results support the conclusion that superficial pyramidal cells of the CA1 sublayer are more vulnerable to epilepsy.

Specific conclusions

1. Using single-cell electrophysiology *in vivo* and immediate early gene expression, we reveal that superficial CA1 pyramidal neurons are overactive in epileptic rodents.

2. Bulk tissue and single-nucleus expression profiling disclosed sublayer-specific transcriptomic signatures, and robust microglial pro-inflammatory response in superficial sublayer of CA1 that was associate to higher vulnerability of these cells to epilepsy.

3. Transcripts regulating neuronal processes such as voltage-channels, synaptic signalling and cell adhesion molecules were deregulated by epilepsy differently across sublayers, while neurodegenerative signatures primarily involved superficial cells.

4. Pseudotime analysis of gene expression in single-nuclei and *in situ* validation revealed separated trajectories from health to epilepsy across cell types, and identified a subset of superficial cells undergoing a later stage in neurodegeneration.

5. Our findings indicate sublayer- and cell-type-specific changes associated with selective CA1 neuronal damage contributing to the progression of hippocampal sclerosis.

Conclusiones

Conclusión general

Nuestros resultados sustentan la conclusión de que las células piramidales superficiales de la subcapa CA1 son más vulnerables a la epilepsia.

Conclusión específica

1. Utilizando la electrofisiología *in vivo* y la expresión génica temprana inmediata, revelamos que las neuronas piramidales de la subcapa superficial de CA1 son hiperactivas en los roedores epilépticos.

2. Los perfiles de expresión del tejido y de los núcleos individuales revelan firmas transcriptómicas específicas de las subcapas y respuesta proinflamatoria de microglía que es más acusada en la capa superficial y que se asocia a una mayor vulnerabilidad de estas células a la epilepsia.

3. Los transcritos que regulan los procesos neuronales, como los canales de voltaje, la señalización sináptica y las moléculas de adhesión celular, están desregulados por la epilepsia de forma diferente en las subcapas, mientras que las firmas neurodegenerativas implican principalmente a las células superficiales.

4. El análisis de pseudotiempo de la expresión génica en núcleos individuales y la validación *in situ* revelan trayectorias separadas de la salud a la epilepsia a través de los tipos de células, e identifican un subgrupo de células superficiales que experimentan una etapa posterior en la neurodegeneración.

5. Nuestros hallazgos indican que los cambios específicos de subcapa y tipo celular asociados con el daño neuronal selectivo en CA1 contribuyen a la progresión de la esclerosis del hipocampo.

References

Abarrategui, B., Mai, R., Sartori, I., Francione, S., Pelliccia, V., Cossu, M., & Tassi, L. (2021). Temporal lobe epilepsy: A never-ending story. *Epilepsy & behavior: E&B*, *122*, 108122. https://doi.org/10.1016/j.yebeh.2021.108122

Ahmed, M. M., Carrel, A. J., Cruz Del Angel, Y., Carlsen, J., Thomas, A. X., González, M. I., Gardiner, K. J., & Brooks-Kayal, A. (2021). Altered Protein Profiles During Epileptogenesis in the Pilocarpine Mouse Model of Temporal Lobe Epilepsy. *Frontiers in neurology*, *12*, 654606. https://doi.org/10.3389/fneur.2021.654606

Ali, I., Chugh, D., & Ekdahl, C. T. (2015). Role of fractalkine-CX3CR1 pathway in seizure-induced microglial activation, neurodegeneration, and neuroblast production in the adult rat brain. *Neurobiology of disease*, *74*, 194–203. https://doi.org/10.1016/j.nbd.2014.11.009

Anders, S., Pyl, P. T., & Huber, W. (2015). HTSeq--a Python framework to work with high-throughput sequencing data. *Bioinformatics (Oxford, England)*, *31*(2), 166–169. https://doi.org/10.1093/bioinformatics/btu638

Armingol, E., Officer, A., Harismendy, O., & Lewis, N. E. (2021). Deciphering cell-cell interactions and communication from gene expression. *Nature reviews. Genetics*, *22*(2), 71–88. https://doi.org/10.1038/s41576-020-00292-x

Aronica, E., & Gorter, J. A. (2007). Gene expression profile in temporal lobe epilepsy. *The Neuroscientist: a review journal bringing neurobiology, neurology and psychiatry*, *13*(2), 100–108. https://doi.org/10.1177/1073858406295832

Ashpole, N. M., & Hudmon, A. (2011). Excitotoxic neuroprotection and vulnerability with CaMKII inhibition. *Molecular and cellular neurosciences*, *46*(4), 720–730. https://doi.org/10.1016/j.mcn.2011.02.003

Babb, T., & Brown, W. (1987). Pathological findings in epilepsy. In J. Engel, Jr. (Ed.), *Surgical treatment of the epilepsies* (pp. 511–540). New York: Raven Press.

Balestrini, S., Arzimanoglou, A., Blümcke, I., Scheffer, I. E., Wiebe, S., Zelano, J. and Walker, M. C. (2021), The aetiologies of epilepsy. *Epileptic Disorders, 23*: 1–16. https://doi.org/10.1684/epd.2021.1255

Bannister, N. J., & Larkman, A. U. (1995). Dendritic morphology of CA1 pyramidal neurones from the rat hippocampus: I. Branching patterns. *The Journal of comparative neurology*, *360*(1), 150–160. https://doi.org/10.1002/cne.903600111

Beagle, A. J., Darwish, S. M., Ranasinghe, K. G., La, A. L., Karageorgiou, E., & Vossel, K. A. (2017). Relative Incidence of Seizures and Myoclonus in Alzheimer's Disease, Dementia with Lewy Bodies, and Frontotemporal Dementia. *Journal of Alzheimer's disease: JAD, 60*(1), 211–223. https://doi.org/10.3233/JAD-170031

Becker A. J. (2018). Review: Animal models of acquired epilepsy: insights into mechanisms of human epileptogenesis. *Neuropathology and applied neurobiology*, *44*(1), 112–129. https://doi.org/10.1111/nan.12451

Ben-Ari, Y., Tremblay, E., Ottersen, O. P., & Naquet, R. (1979). Evidence suggesting secondary epileptogenic lesion after kainic acid: pre treatment with diazepam reduces distant but not local brain damage. *Brain research*, *165*(2), 362–365.

https://doi.org/10.1016/0006-8993(79)90571-7

Benjamini, Y., & Hochberg, Y. (1995). Controlling the false discovery rate: a practical and powerful approach to multiple testing. *Journal of the Royal statistical society: series B (Methodological)*, *57*(1), 289-300. https://doi.org/10.1111/j.2517-6161.1995.tb02031.x

Beutler, A. S., Li, S., Nicol, R., & Walsh, M. J. (2005). Carbamazepine is an inhibitor of histone deacetylases. *Life sciences*, *76*(26), 3107–3115. https://doi.org/10.1016/j.lfs.2005.01.003

Bialik, S., & Kimchi, A. (2006). The death-associated protein kinases: structure, function, and beyond. *Annual review of biochemistry*, *75*, 189–210. https://doi.org/10.1146/annurev.biochem.75.103004.142615

Biber, K., Neumann, H., Inoue, K., & Boddeke, H. W. (2007). Neuronal 'On' and 'Off' signals control microglia. *Trends in neurosciences*, *30*(11), 596–602. https://doi.org/10.1016/j.tins.2007.08.007

Bienkowski, M. S., Sepehrband, F., Kurniawan, N. D., Stanis, J., Korobkova, L., Khanjani, N., Clark, K., Hintiryan, H., Miller, C. A., & Dong, H. W. (2021). Homologous laminar organization of the mouse and human subiculum. *Scientific reports*, *11*(1), 3729. https://doi.org/10.1038/s41598-021-81362-w

Bird, C. M., & Burgess, N. (2008). The hippocampus and memory: insights from spatial processing. *Nature reviews. Neuroscience*, *9*(3), 182–194. https://doi.org/10.1038/nrn2335

Bishop, N. A., Lu, T., & Yankner, B. A. (2010). Neural mechanisms of ageing and cognitive decline. *Nature*, *464*(7288), 529–535. https://doi.org/10.1038/nature08983

Blümcke, I., Kistner, I., Clusmann, H., Schramm, J., Becker, A. J., Elger, C. E., Bien, C. G., Merschhemke, M., Meencke, H. J., Lehmann, T., Buchfelder, M., Weigel, D., Buslei, R., Stefan, H., Pauli, E., & Hildebrandt, M. (2009). Towards a clinico-pathological classification of granule cell dispersion in human mesial temporal lobe epilepsies. *Acta neuropathologica*, *117*(5), 535–544. https://doi.org/10.1007/s00401-009-0512-5

Blümcke, I., Spreafico, R., Haaker, G., Coras, R., Kobow, K., Bien, C. G., Pfäfflin, M., Elger, C., Widman, G., Schramm, J., Becker, A., Braun, K. P., Leijten, F., Baayen, J. C., Aronica, E., Chassoux, F., Hamer, H., Stefan, H., Rössler, K., Thom, M., … EEBB Consortium (2017). Histopathological Findings in Brain Tissue Obtained during Epilepsy Surgery. *The New England journal of medicine*, *377*(17), 1648–1656. https://doi.org/10.1056/NEJMoa1703784

Blümcke, I., Thom, M., Aronica, E., Armstrong, D. D., Bartolomei, F., Bernasconi, A., Bernasconi, N., Bien, C. G., Cendes, F., Coras, R., Cross, J. H., Jacques, T. S., Kahane, P., Mathern, G. W., Miyata, H., Moshé, S. L., Oz, B., Özkara, Ç., Perucca, E., Sisodiya, S., … Spreafico, R. (2013). International consensus classification of hippocampal sclerosis in temporal lobe epilepsy: a Task Force report from the ILAE Commission on Diagnostic Methods. *Epilepsia*, *54*(7), 1315–1329. https://doi.org/10.1111/epi.12220

Born H. A. (2015). Seizures in Alzheimer's disease. *Neuroscience, 286*, 251–263. https://doi.org/10.1016/j.neuroscience.2014.11.051

Brown, G. C., & Neher, J. J. (2014). Microglial phagocytosis of live neurons. *Nature reviews. Neuroscience*, *15*(4), 209–216. https://doi.org/10.1038/nrn3710

Brown, G. C., Vilalta, A., & Fricker, M. (2015). Phagoptosis - Cell Death By Phagocytosis - Plays Central Roles in Physiology, Host Defense and Pathology. *Current molecular medicine*, *15*(9), 842–851. https://doi.org/10.2174/1566524015091151105130628

Bruxel, E. M., Bruno, D., do Canto, A. M., Geraldis, J. C., Godoi, A. B., Martin, M., & Lopes-Cendes, I. (2021). Multi-omics in mesial temporal lobe epilepsy with hippocampal sclerosis: Clues into the underlying mechanisms leading to disease. *Seizure*, *90*, 34–50. https://doi.org/10.1016/j.seizure.2021.03.002

Bouchet C., & Cazauvielh J. B. (1825). De l'épilepsie considerée dans ses rapports avec l'aliénation mentale. *Arch Gen Med*. 9, 510–542.

Butler, A., Hoffman, P., Smibert, P., Papalexi, E., & Satija, R. (2018). Integrating single-cell transcriptomic data across different conditions, technologies, and species. *Nature biotechnology*, *36*(5), 411–420. https://doi.org/10.1038/nbt.4096

Butler, C. A., Popescu, A. S., Kitchener, E., Allendorf, D. H., Puigdellívol, M., & Brown, G. C. (2021). Microglial phagocytosis of neurons in neurodegeneration, and its regulation. *Journal of neurochemistry*, *158*(3), 621–639. https://doi.org/10.1111/jnc.15327

Cembrowski, M. S., & Spruston, N. (2019). Heterogeneity within classical cell types is the rule: lessons from hippocampal pyramidal neurons. *Nature reviews. Neuroscience, 20*(4), 193–204. https://doi.org/10.1038/s41583-019-0125-5

Cembrowski, M. S., Bachman, J. L., Wang, L., Sugino, K., Shields, B. C., & Spruston, N. (2016a). Spatial Gene-Expression Gradients Underlie Prominent Heterogeneity of CA1 Pyramidal Neurons. *Neuron*, *89*(2), 351–368. https://doi.org/10.1016/j.neuron.2015.12.013

Cembrowski, M. S., Wang, L., Sugino, K., Shields, B. C., & Spruston, N. (2016b). Hipposeq: a comprehensive RNA-seq database of gene expression in hippocampal principal neurons. *eLife*, *5*, e14997. https://doi.org/10.7554/eLife.14997

Chen, Y., & Colonna, M. (2021). Microglia in Alzheimer's disease at single-cell level. Are there common patterns in humans and mice?. *The Journal of experimental medicine*, *218*(9), e20202717. https://doi.org/10.1084/jem.20202717

Chen, Z., Brodie, M. J., Liew, D., & Kwan, P. (2018). Treatment Outcomes in Patients With Newly Diagnosed Epilepsy Treated With Established and New Antiepileptic Drugs: A 30-Year Longitudinal Cohort Study. *JAMA neurology*, *75*(3), 279–286. https://doi.org/10.1001/jamaneurol.2017.3949

Cid, E., & de la Prida, L. M. (2019). Methods for single-cell recording and labeling in vivo. *Journal of neuroscience methods*, *325*, 108354. https://doi.org/10.1016/j.jneumeth.2019.108354

Cid, E., Marquez-Galera, A., Valero, M., Gal, B., Medeiros, D. C., Navarron, C. M., Ballesteros-Esteban, L., Reig-Viader, R., Morales, A. V., Fernandez-Lamo, I., Gomez-Dominguez, D., Sato, M., Hayashi, Y., Bayés, À., Barco, A., Lopez-Atalaya, J. P., & de la Prida, L. M. (2021). Sublayer- and cell-type-specific neurodegenerative transcriptional trajectories in hippocampal sclerosis. *Cell reports*, *35*(10), 109229. https://doi.org/10.1016/j.celrep.2021.109229

Citraro, R., Leo, A., De Caro, C., Nesci, V., Gallo Cantafio, M. E., Amodio, N., Mattace Raso, G., Lama, A., Russo, R., Calignano, A., Tallarico, M., Russo, E., & De Sarro, G.

(2020). Effects of Histone Deacetylase Inhibitors on the Development of Epilepsy and Psychiatric Comorbidity in WAG/Rij Rats. *Molecular neurobiology*, *57*(1), 408–421. https://doi.org/10.1007/s12035-019-01712-8

Clark, R. E., & Squire, L. R. (2013). Similarity in form and function of the hippocampus in rodents, monkeys, and humans. *Proceedings of the National Academy of Sciences of the United States of America*, *110 Suppl 2*(Suppl 2), 10365–10370. https://doi.org/10.1073/pnas.1301225110

Clifford, D. B., Olney, J. W., Maniotis, A., Collins, R. C., & Zorumski, C. F. (1987). The functional anatomy and pathology of lithium-pilocarpine and high-dose pilocarpine seizures. *Neuroscience*, *23*(3), 953–968. https://doi.org/10.1016/0306-4522(87)90171-0

Coras, R., Pauli, E., Li, J., Schwarz, M., Rössler, K., Buchfelder, M., Hamer, H., Stefan, H., & Blumcke, I. (2014). Differential influence of hippocampal subfields to memory formation: insights from patients with temporal lobe epilepsy. *Brain: a journal of neurology*, *137*(Pt 7), 1945–1957. https://doi.org/10.1093/brain/awu100

Covolan, L., & Mello, L. E. (2000). Temporal profile of neuronal injury following pilocarpine or kainic acid-induced status epilepticus. *Epilepsy research*, *39*(2), 133–152. https://doi.org/10.1016/s0920-1211(99)00119-9

Crespel, A., Coubes, P., Rousset, M. C., Brana, C., Rougier, A., Rondouin, G., Bockaert, J., Baldy-Moulinier, M., & Lerner-Natoli, M. (2002). Inflammatory reactions in human medial temporal lobe epilepsy with hippocampal sclerosis. *Brain research*, *952*(2), 159–169. https://doi.org/10.1016/s0006-8993(02)03050-0

Cretin, B., Philippi, N., Dibitonto, L., & Blanc, F. (2017). Epilepsy at the prodromal stages of neurodegenerative diseases. Épilepsie aux stades débutants des maladies neurodégénératives. *Geriatrie et psychologie neuropsychiatrie du vieillissement, 15*(1), 75–82. https://doi.org/10.1684/pnv.2017.0652

Curia, G., Longo, D., Biagini, G., Jones, R. S., & Avoli, M. (2008). The pilocarpine model of temporal lobe epilepsy. *Journal of neuroscience methods*, *172*(2), 143–157. https://doi.org/10.1016/j.jneumeth.2008.04.019

Datlinger, P., Rendeiro, A. F., Boenke, T., Senekowitsch, M., Krausgruber, T., Barreca, D., & Bock, C. (2021). Ultra-high-throughput single-cell RNA sequencing and perturbation screening with combinatorial fluidic indexing. *Nature methods*, *18*(6), 635–642. https://doi.org/10.1038/s41592-021-01153-z

Davies, K. G., Hermann, B. P., Dohan, F. C., Jr, Foley, K. T., Bush, A. J., & Wyler, A. R. (1996). Relationship of hippocampal sclerosis to duration and age of onset of epilepsy, and childhood febrile seizures in temporal lobectomy patients. *Epilepsy research*, *24*(2), 119–126. https://doi.org/10.1016/0920-1211(96)00008-3

de Lanerolle, N. C., & Lee, T. S. (2005). New facets of the neuropathology and molecular profile of human temporal lobe epilepsy. *Epilepsy & behavior: E&B*, *7*(2), 190–203. https://doi.org/10.1016/j.yebeh.2005.06.003

de Lanerolle, N. C., Kim, J. H., Williamson, A., Spencer, S. S., Zaveri, H. P., Eid, T., & Spencer, D. D. (2003). A retrospective analysis of hippocampal pathology in human temporal lobe epilepsy: evidence for distinctive patient subcategories. *Epilepsia*, *44*(5), 677–687. https://doi.org/10.1046/j.1528-1157.2003.32701.x

De Strooper, B., & Karran, E. (2016). The Cellular Phase of Alzheimer's Disease. *Cell*, *164*(4), 603–615. https://doi.org/10.1016/j.cell.2015.12.056

DeKraker, J., Lau, J. C., Ferko, K. M., Khan, A. R., & Köhler, S. (2020). Hippocampal subfields revealed through unfolding and unsupervised clustering of laminar and morphological features in 3D BigBrain. *NeuroImage, 206*, 116328. https://doi.org/10.1016/j.neuroimage.2019.116328

Detour, J., Bund, C., Behr, C., Cebula, H., Cicek, E. A., Valenti-Hirsch, M. P., Lannes, B., Lhermitte, B., Nehlig, A., Kehrli, P., Proust, F., Hirsch, E., & Namer, I. J. (2018). Metabolomic characterization of human hippocampus from drug-resistant epilepsy with mesial temporal seizure. *Epilepsia*, *59*(3), 607–616. https://doi.org/10.1111/epi.14000

Devinsky, O., Vezzani, A., Najjar, S., De Lanerolle, N. C., & Rogawski, M. A. (2013). Glia and epilepsy: excitability and inflammation. *Trends in neurosciences*, *36*(3), 174–184. https://doi.org/10.1016/j.tins.2012.11.008

Ding, J., Adiconis, X., Simmons, S. K., Kowalczyk, M. S., Hession, C. C., Marjanovic, N. D., Hughes, T. K., Wadsworth, M. H., Burks, T., Nguyen, L. T., Kwon, J., Barak, B., Ge, W., Kedaigle, A. J., Carroll, S., Li, S., Hacohen, N., Rozenblatt-Rosen, O., Shalek, A. K., Villani, A. C., … Levin, J. Z. (2020). Systematic comparison of single-cell and single-nucleus RNA-sequencing methods. *Nature biotechnology*, *38*(6), 737–746. https://doi.org/10.1038/s41587-020-0465-8

Ding, X., Yang, W., Ren, Q., Hu, J., Yang, S., Han, W., Wang, J., Wang, X., & Wang, H. (2020). Serum IgG-induced microglial activation enhances neuronal cytolysis via the NO/sGC/PKG pathway in children with opsoclonus-myoclonus syndrome and neuroblastoma. *Journal of neuroinflammation*, *17*(1), 190. https://doi.org/10.1186/s12974-020-01839-9

Dixit, A. B., Banerjee, J., Srivastava, A., Tripathi, M., Sarkar, C., Kakkar, A., Jain, M., & Chandra, P. S. (2016). RNA-seq analysis of hippocampal tissues reveals novel candidate genes for drug refractory epilepsy in patients with MTLE-HS. *Genomics*, *107*(5), 178–188. https://doi.org/10.1016/j.ygeno.2016.04.001

Dixit, A. B., Srivastava, A., Sharma, D., Tripathi, M., Paul, D., Lalwani, S., Doddamani, R., Sharma, M. C., Banerjee, J., & Chandra, P. S. (2020). Integrated Genome-Wide DNA Methylation and RNAseq Analysis of Hippocampal Specimens Identifies Potential Candidate Genes and Aberrant Signalling Pathways in Patients with Hippocampal Sclerosis. *Neurology India*, *68*(2), 307–313. https://doi.org/10.4103/0028-3886.280649

do Canto, A. M., Donatti, A., Geraldis, J. C., Godoi, A. B., da Rosa, D. C., & Lopes-Cendes, I. (2021). Neuroproteomics in Epilepsy: What Do We Know so Far?. *Frontiers in molecular neuroscience*, *13*, 604158. https://doi.org/10.3389/fnmol.2020.604158

Dobin, A., Davis, C. A., Schlesinger, F., Drenkow, J., Zaleski, C., Jha, S., Batut, P., Chaisson, M., & Gingeras, T. R. (2013). STAR: ultrafast universal RNA-seq aligner. *Bioinformatics (Oxford, England)*, *29*(1), 15–21. https://doi.org/10.1093/bioinformatics/bts635

Donatti, A., Canto, A. M., Godoi, A. B., da Rosa, D. C., & Lopes-Cendes, I. (2020). Circulating Metabolites as Potential Biomarkers for Neurological Disorders-Metabolites in Neurological Disorders. *Metabolites*, *10*(10), 389. https://doi.org/10.3390/metabo10100389

Dong, E., Chen, Y., Gavin, D. P., Grayson, D. R., & Guidotti, A. (2010). Valproate induces DNA demethylation in nuclear extracts from adult mouse brain. *Epigenetics*, *5*(8), 730–735. https://doi.org/10.4161/epi.5.8.13053

Dong, H. W., Swanson, L. W., Chen, L., Fanselow, M. S., & Toga, A. W. (2009). Genomic-anatomic evidence for distinct functional domains in hippocampal field CA1. *Proceedings of the National Academy of Sciences of the United States of America*, *106*(28), 11794–11799. https://doi.org/10.1073/pnas.0812608106

Dong, X., Hao, X., Xu, P., Fan, M., Wang, X., Huang, X., Jiang, P., Zeng, L., & Xie, Y. (2020). RNA sequencing analysis of cortex and hippocampus in a kainic acid rat model of temporal lobe epilepsy to identify mechanisms and therapeutic targets related to inflammation, immunity and cognition. *International immunopharmacology*, *87*, 106825. https://doi.org/10.1016/j.intimp.2020.106825

Du, F., Eid, T., Lothman, E. W., Köhler, C., & Schwarcz, R. (1995). Preferential neuronal loss in layer III of the medial entorhinal cortex in rat models of temporal lobe epilepsy. *The Journal of neuroscience: the official journal of the Society for Neuroscience*, *15*(10), 6301–6313. https://doi.org/10.1523/JNEUROSCI.15-10-06301.1995

Efremova, M., Vento-Tormo, M., Teichmann, S. A., & Vento-Tormo, R. (2020). CellPhoneDB: inferring cell-cell communication from combined expression of multi-subunit ligand-receptor complexes. *Nature protocols*, *15*(4), 1484–1506. https://doi.org/10.1038/s41596-020-0292-x

England, M. J., Liverman, C. T., Schultz, A. M., & Strawbridge, L. M. (2012). Epilepsy across the spectrum: promoting health and understanding. A summary of the Institute of Medicine report. *Epilepsy & behavior: E&B, 25*(2), 266–276. https://doi.org/10.1016/j.yebeh.2012.06.016

Escartin, C., Galea, E., Lakatos, A., O'Callaghan, J. P., Petzold, G. C., Serrano-Pozo, A., Steinhäuser, C., Volterra, A., Carmignoto, G., Agarwal, A., Allen, N. J., Araque, A., Barbeito, L., Barzilai, A., Bergles, D. E., Bonvento, G., Butt, A. M., Chen, W. T., Cohen-Salmon, M., Cunningham, C., … Verkhratsky, A. (2021). Reactive astrocyte nomenclature, definitions, and future directions. *Nature neuroscience*, *24*(3), 312–325. https://doi.org/10.1038/s41593-020-00783-4

Eyal, S., Yagen, B., Sobol, E., Altschuler, Y., Shmuel, M., & Bialer, M. (2004). The activity of antiepileptic drugs as histone deacetylase inhibitors. *Epilepsia*, *45*(7), 737–744. https://doi.org/10.1111/j.0013-9580.2004.00104.x

Eyo, U. B., Mo, M., Yi, M. H., Murugan, M., Liu, J., Yarlagadda, R., Margolis, D. J., Xu, P., & Wu, L. J. (2018). P2Y12R-Dependent Translocation Mechanisms Gate the Changing Microglial Landscape. *Cell reports, 23*(4), 959–966. https://doi.org/10.1016/j.celrep.2018.04.001

Eyo, U. B., Peng, J., Swiatkowski, P., Mukherjee, A., Bispo, A., & Wu, L. J. (2014). Neuronal hyperactivity recruits microglial processes via neuronal NMDA receptors and microglial P2Y12 receptors after status epilepticus. *The Journal of neuroscience: the official journal of the Society for Neuroscience*, *34*(32), 10528–10540. https://doi.org/10.1523/JNEUROSCI.0416-14.2014

Ferrer, I., Santpere, G., Arzberger, T., Bell, J., Blanco, R., Boluda, S., Budka, H., Carmona, M., Giaccone, G., Krebs, B., Limido, L., Parchi, P., Puig, B., Strammiello, R., Ströbel, T., & Kretzschmar, H. (2007). Brain protein preservation largely depends on the

postmortem storage temperature: implications for study of proteins in human neurologic diseases and management of brain banks: a BrainNet Europe Study. *Journal of neuropathology and experimental neurology*, *66*(1), 35–46. https://doi.org/10.1097/nen.0b013e31802c3e7d

Fiest, K. M., Sauro, K. M., Wiebe, S., Patten, S. B., Kwon, C. S., Dykeman, J., Pringsheim, T., Lorenzetti, D. L., & Jetté, N. (2017). Prevalence and incidence of epilepsy: A systematic review and meta-analysis of international studies. *Neurology, 88*(3), 296–303. https://doi.org/10.1212/WNL.0000000000003509

Fisher, R. S., Cross, J. H., French, J. A., Higurashi, N., Hirsch, E., Jansen, F. E., Lagae, L., Moshé, S. L., Peltola, J., Roulet Perez, E., Scheffer, I. E. and Zuberi, S. M. (2017), Operational classification of seizure types by the International League Against Epilepsy: Position Paper of the ILAE Commission for Classification and Terminology. *Epilepsia, 58*: 522–530. https://doi.org/10.1111/epi.13670

Flavell, S. W., & Greenberg, M. E. (2008). Signaling mechanisms linking neuronal activity to gene expression and plasticity of the nervous system. *Annual review of neuroscience*, *31*, 563–590. https://doi.org/10.1146/annurev.neuro.31.060407.125631

Friedman, N., & Rando, O. J. (2015). Epigenomics and the structure of the living genome. *Genome research*, *25*(10), 1482–1490. https://doi.org/10.1101/gr.190165.115

Furukawa, A., Kakita, A., Chiba, Y., Kitaura, H., Fujii, Y., Fukuda, M., Kameyama, S., & Shimada, A. (2020). Proteomic profile differentiating between mesial temporal lobe epilepsy with and without hippocampal sclerosis. *Epilepsy research*, *168*, 106502. https://doi.org/10.1016/j.eplepsyres.2020.106502

Gales, J. M., & Prayson, R. A. (2017). Chronic inflammation in refractory hippocampal sclerosis-related temporal lobe epilepsy. *Annals of diagnostic pathology*, *30*, 12–16. https://doi.org/10.1016/j.anndiagpath.2017.05.009

GBD 2016 Epilepsy Collaborators (2019). Global, regional, and national burden of epilepsy, 1990-2016: a systematic analysis for the Global Burden of Disease Study 2016. *The Lancet. Neurology, 18*(4), 357–375. https://doi.org/10.1016/S1474-4422(18)30454-X

GBD 2016 Neurology Collaborators (2019). Global, regional, and national burden of neurological disorders, 1990-2016: a systematic analysis for the Global Burden of Disease Study 2016. *The Lancet. Neurology, 18*(5), 459–480. https://doi.org/10.1016/S1474-4422(18)30499-X

Gjoneska, E., Pfenning, A. R., Mathys, H., Quon, G., Kundaje, A., Tsai, L. H., & Kellis, M. (2015). Conserved epigenomic signals in mice and humans reveal immune basis of Alzheimer's disease. *Nature*, *518*(7539), 365–369. https://doi.org/10.1038/nature14252

Goossens, M. G., Boon, P., Wadman, W., Van den Haute, C., Baekelandt, V., Verstraete, A. G., Vonck, K., Larsen, L. E., Sprengers, M., Carrette, E., Desloovere, J., Meurs, A., Delbeke, J., Vanhove, C., & Raedt, R. (2021). Long-term chemogenetic suppression of seizures in ac multifocal rat model of temporal lobe epilepsy. *Epilepsia*, *62*(3), 659–670. https://doi.org/10.1111/epi.16840

Goossens, M. G., Larsen, L. E., Vergaelen, M., Wadman, W., Van den Haute, C., Brackx, W., Proesmans, S., Desloovere, J., Christiaen, E., Craey, E., Vanhove, C., Vonck, K., Boon, P., & Raedt, R. (2021). Level of hM4D(Gi) DREADD Expression Determines

Inhibitory and Neurotoxic Effects in the Hippocampus. *eNeuro*, *8*(6), ENEURO.0105-21.2021. https://doi.org/10.1523/ENEURO.0105-21.2021

Gorter, J. A., van Vliet, E. A., Aronica, E., Breit, T., Rauwerda, H., Lopes da Silva, F. H., & Wadman, W. J. (2006). Potential new antiepileptogenic targets indicated by microarray analysis in a rat model for temporal lobe epilepsy. *The Journal of neuroscience: the official journal of the Society for Neuroscience*, *26*(43), 11083–11110. https://doi.org/10.1523/JNEUROSCI.2766-06.2006

Göttlicher, M., Minucci, S., Zhu, P., Krämer, O. H., Schimpf, A., Giavara, S., Sleeman, J. P., Lo Coco, F., Nervi, C., Pelicci, P. G., & Heinzel, T. (2001). Valproic acid defines a novel class of HDAC inhibitors inducing differentiation of transformed cells. *The EMBO journal*, *20*(24), 6969–6978. https://doi.org/10.1093/emboj/20.24.6969

Guelfi, S., Botia, J. A., Thom, M., Ramasamy, A., Perona, M., Stanyer, L., Martinian, L., Trabzuni, D., Smith, C., Walker, R., Ryten, M., Reimers, M., Weale, M. E., Hardy, J., & Matarin, M. (2019). Transcriptomic and genetic analyses reveal potential causal drivers for intractable partial epilepsy. *Brain: a journal of neurology*, *142*(6), 1616–1630. https://doi.org/10.1093/brain/awz074

Gurses, C., Azakli, H., Alptekin, A., Cakiris, A., Abaci, N., Arikan, M., Kursun, O., Gokyigit, A., & Ustek, D. (2014). Mitochondrial DNA profiling via genomic analysis in mesial temporal lobe epilepsy patients with hippocampal sclerosis. *Gene*, *538*(2), 323–327. https://doi.org/10.1016/j.gene.2014.01.030

Gyllborg, D., Langseth, C. M., Qian, X., Choi, E., Salas, S. M., Hilscher, M. M., Lein, E. S., & Nilsson, M. (2020). Hybridization-based in situ sequencing (HybISS) for spatially resolved transcriptomics in human and mouse brain tissue. *Nucleic acids research*, *48*(19), e112. https://doi.org/10.1093/nar/gkaa792

Habib, N., Li, Y., Heidenreich, M., Swiech, L., Avraham-Davidi, I., Trombetta, J. J., Hession, C., Zhang, F., & Regev, A. (2016). Div-Seq: Single-nucleus RNA-Seq reveals dynamics of rare adult newborn neurons. *Science (New York, N.Y.)*, *353*(6302), 925–928. https://doi.org/10.1126/science.aad7038

He, J., Green, A. R., Li, Y., Chan, S., & Liu, D. X. (2020). SPAG5: An Emerging Oncogene. *Trends in cancer*, *6*(7), 543–547. https://doi.org/10.1016/j.trecan.2020.03.006

Henkel, N. D., Smail, M. A., Wu, X., Enright, H. A., Fischer, N. O., Eby, H. M., McCullumsmith, R. E., & Shukla, R. (2021). Cellular, molecular, and therapeutic characterization of pilocarpine-induced temporal lobe epilepsy. *Scientific reports*, *11*(1), 19102. https://doi.org/10.1038/s41598-021-98534-3

Hickman, S. E., Kingery, N. D., Ohsumi, T. K., Borowsky, M. L., Wang, L. C., Means, T. K., & El Khoury, J. (2013). The microglial sensome revealed by direct RNA sequencing. *Nature neuroscience*, *16*(12), 1896–1905. https://doi.org/10.1038/nn.3554

Hoek, R. M., Ruuls, S. R., Murphy, C. A., Wright, G. J., Goddard, R., Zurawski, S. M., Blom, B., Homola, M. E., Streit, W. J., Brown, M. H., Barclay, A. N., & Sedgwick, J. D. (2000). Down-regulation of the macrophage lineage through interaction with OX2 (CD200). *Science (New York, N.Y.)*, *290*(5497), 1768–1771. https://doi.org/10.1126/science.290.5497.1768

Holtman, I. R., Skola, D., & Glass, C. K. (2017). Transcriptional control of microglia phenotypes in health and disease. *The Journal of clinical investigation*, *127*(9), 3220–3229. https://doi.org/10.1172/JCI90604

Hu, Y., Peng, T., Gao, L., & Tan, K. (2021). CytoTalk: De novo construction of signal transduction networks using single-cell transcriptomic data. *Science advances*, *7*(16), eabf1356. https://doi.org/10.1126/sciadv.abf1356

Huang, d., Sherman, B. T., & Lempicki, R. A. (2009). Systematic and integrative analysis of large gene lists using DAVID bioinformatics resources. *Nature protocols*, *4*(1), 44–57. https://doi.org/10.1038/nprot.2008.211

Huang, E. J., & Reichardt, L. F. (2001). Neurotrophins: roles in neuronal development and function. *Annual review of neuroscience*, *24*, 677–736. https://doi.org/10.1146/annurev.neuro.24.1.677

Huber, W., Carey, V. J., Gentleman, R., Anders, S., Carlson, M., Carvalho, B. S., Bravo, H. C., Davis, S., Gatto, L., Girke, T., Gottardo, R., Hahne, F., Hansen, K. D., Irizarry, R. A., Lawrence, M., Love, M. I., MacDonald, J., Obenchain, V., Oleś, A. K., Pagès, H., … Morgan, M. (2015). Orchestrating high-throughput genomic analysis with Bioconductor. *Nature methods*, *12*(2), 115–121. https://doi.org/10.1038/nmeth.3252

Iacopino, A. M., & Christakos, S. (1990). Specific reduction of calcium-binding protein (28-kilodalton calbindin-D) gene expression in aging and neurodegenerative diseases. *Proceedings of the National Academy of Sciences of the United States of America*, *87*(11), 4078–4082. https://doi.org/10.1073/pnas.87.11.4078

Imfeld, P., Bodmer, M., Schuerch, M., Jick, S. S., & Meier, C. R. (2013). Seizures in patients with Alzheimer's disease or vascular dementia: a population-based nested case-control analysis. *Epilepsia, 54*(4), 700–707. https://doi.org/10.1111/epi.12045

Inostroza, M., Cid, E., Brotons-Mas, J., Gal, B., Aivar, P., Uzcategui, Y. G., Sandi, C., & Menendez de la Prida, L. (2011). Hippocampal-dependent spatial memory in the water maze is preserved in an experimental model of temporal lobe epilepsy in rats. *PloS one*, *6*(7), e22372. https://doi.org/10.1371/journal.pone.0022372

Iori, V., Iyer, A. M., Ravizza, T., Beltrame, L., Paracchini, L., Marchini, S., Cerovic, M., Hill, C., Ferrari, M., Zucchetti, M., Molteni, M., Rossetti, C., Brambilla, R., Steve White, H., D'Incalci, M., Aronica, E., & Vezzani, A. (2017). Blockade of the IL-1R1/TLR4 pathway mediates disease-modification therapeutic effects in a model of acquired epilepsy. *Neurobiology of disease*, *99*, 12–23. https://doi.org/10.1016/j.nbd.2016.12.007

Islam, S., Kjällquist, U., Moliner, A., Zajac, P., Fan, J. B., Lönnerberg, P., & Linnarsson, S. (2011). Characterization of the single-cell transcriptional landscape by highly multiplex RNA-seq. *Genome research*, *21*(7), 1160–1167. https://doi.org/10.1101/gr.110882.110

Janszky, J., Janszky, I., Schulz, R., Hoppe, M., Behne, F., Pannek, H. W., & Ebner, A. (2005). Temporal lobe epilepsy with hippocampal sclerosis: predictors for long-term surgical outcome. *Brain: a journal of neurology*, *128*(Pt 2), 395–404. https://doi.org/10.1093/brain/awh358

Jarrard L. E. (1993). On the role of the hippocampus in learning and memory in the rat. *Behavioral and neural biology*, *60*(1), 9–26. https://doi.org/10.1016/0163-1047(93)90664-4

Jefferys, J. G., Menendez de la Prida, L., Wendling, F., Bragin, A., Avoli, M., Timofeev, I., & Lopes da Silva, F. H. (2012). Mechanisms of physiological and epileptic HFO generation. *Progress in neurobiology*, *98*(3), 250–264. https://doi.org/10.1016/j.pneurobio.2012.02.005

Kalilani, L., Sun, X., Pelgrims, B., Noack-Rink, M., & Villanueva, V. (2018). The epidemiology of drug-resistant epilepsy: A systematic review and meta-analysis. *Epilepsia*, *59*(12), 2179–2193. https://doi.org/10.1111/epi.14596

Kandel E. R. (2001). The molecular biology of memory storage: a dialogue between genes and synapses. *Science (New York, N.Y.)*, *294*(5544), 1030–1038. https://doi.org/10.1126/science.1067020

Kanekura, K., Hashimoto, Y., Kita, Y., Sasabe, J., Aiso, S., Nishimoto, I., & Matsuoka, M. (2005). A Rac1/phosphatidylinositol 3-kinase/Akt3 anti-apoptotic pathway, triggered by AlsinLF, the product of the ALS2 gene, antagonizes Cu/Zn-superoxide dismutase (SOD1) mutant-induced motoneuronal cell death. *The Journal of biological chemistry*, *280*(6), 4532–4543. https://doi.org/10.1074/jbc.M410508200

Kanemoto, K., Kawasaki, J., Miyamoto, T., Obayashi, H., & Nishimura, M. (2000). Interleukin (IL)1beta, IL-1alpha, and IL-1 receptor antagonist gene polymorphisms in patients with temporal lobe epilepsy. *Annals of neurology*, *47*(5), 571–574. https://doi.org/10.1002/1531-8249(200005)47:5%3C571::AID-ANA3%3E3.0.CO;2-A

Kasperaviciūte, D., Catarino, C. B., Heinzen, E. L., Depondt, C., Cavalleri, G. L., Caboclo, L. O., Tate, S. K., Jamnadas-Khoda, J., Chinthapalli, K., Clayton, L. M., Shianna, K. V., Radtke, R. A., Mikati, M. A., Gallentine, W. B., Husain, A. M., Alhusaini, S., Leppert, D., Middleton, L. T., Gibson, R. A., Johnson, M. R., … Sisodiya, S. M. (2010). Common genetic variation and susceptibility to partial epilepsies: a genome-wide association study. *Brain: a journal of neurology*, *133*(Pt 7), 2136–2147. https://doi.org/10.1093/brain/awq130

Katic, J., Loers, G., Tosic, J., Schachner, M., & Kleene, R. (2017). The cell adhesion molecule CHL1 interacts with patched-1 to regulate apoptosis during postnatal cerebellar development. *Journal of cell science*, *130*(15), 2606–2619. https://doi.org/10.1242/jcs.194563

Ke, R., Mignardi, M., Pacureanu, A., Svedlund, J., Botling, J., Wählby, C., & Nilsson, M. (2013). In situ sequencing for RNA analysis in preserved tissue and cells. *Nature methods*, *10*(9), 857–860. https://doi.org/10.1038/nmeth.2563

Kiselev, V. Y., Kirschner, K., Schaub, M. T., Andrews, T., Yiu, A., Chandra, T., Natarajan, K. N., Reik, W., Barahona, M., Green, A. R., & Hemberg, M. (2017). SC3: consensus clustering of single-cell RNA-seq data. *Nature methods*, *14*(5), 483–486. https://doi.org/10.1038/nmeth.4236

Kobayashi, K., Imagama, S., Ohgomori, T., Hirano, K., Uchimura, K., Sakamoto, K., Hirakawa, A., Takeuchi, H., Suzumura, A., Ishiguro, N., & Kadomatsu, K. (2013). Minocycline selectively inhibits M1 polarization of microglia. *Cell death & disease*, *4*(3), e525. https://doi.org/10.1038/cddis.2013.54

Kobow, K., El-Osta, A., & Blümcke, I. (2013). The methylation hypothesis of pharmacoresistance in epilepsy. *Epilepsia*, *54 Suppl 2*, 41–47. https://doi.org/10.1111/epi.12183

Kong, F. C., Ma, C. L., & Zhong, M. K. (2020). Epigenetic Effects Mediated by Antiepileptic Drugs and their Potential Application. *Current neuropharmacology*, *18*(2), 153–166. https://doi.org/10.2174/1570159X17666191010094849

Kwan, P., Schachter, S. C., & Brodie, M. J. (2011). Drug-resistant epilepsy. *The New England journal of medicine, 365*(10), 919–926. https://doi.org/10.1056/NEJMra1004418

La Manno, G., Siletti, K., Furlan, A., Gyllborg, D., Vinsland, E., Mossi Albiach, A., Mattsson Langseth, C., Khven, I., Lederer, A. R., Dratva, L. M., Johnsson, A., Nilsson, M., Lönnerberg, P., & Linnarsson, S. (2021). Molecular architecture of the developing mouse brain. *Nature*, *596*(7870), 92–96. https://doi.org/10.1038/s41586-021-03775-x

Langseth, C. M., Gyllborg, D., Miller, J. A., Close, J. L., Long, B., Lein, E. S., Hilscher, M. M., & Nilsson, M. (2021). Comprehensive in situ mapping of human cortical transcriptomic cell types. *Communications biology*, 4(1), 998. https://doi.org/10.1038/s42003-021-02517-z

Laurén, H. B., Lopez-Picon, F. R., Brandt, A. M., Rios-Rojas, C. J., & Holopainen, I. E. (2010). Transcriptome analysis of the hippocampal CA1 pyramidal cell region after kainic acid-induced status epilepticus in juvenile rats. *PloS one*, *5*(5), e10733. https://doi.org/10.1371/journal.pone.0010733

Laurent, F., Brotons-Mas, J. R., Cid, E., Lopez-Pigozzi, D., Valero, M., Gal, B., & de la Prida, L. M. (2015). Proximodistal structure of theta coordination in the dorsal hippocampus of epileptic rats. *The Journal of neuroscience: the official journal of the Society for Neuroscience*, *35*(11), 4760–4775. https://doi.org/10.1523/JNEUROSCI.4297-14.2015

Lee, T. S., Mane, S., Eid, T., Zhao, H., Lin, A., Guan, Z., Kim, J. H., Schweitzer, J., King-Stevens, D., Weber, P., Spencer, S. S., Spencer, D. D., & de Lanerolle, N. C. (2007). Gene expression in temporal lobe epilepsy is consistent with increased release of glutamate by astrocytes. *Molecular medicine (Cambridge, Mass.)*, *13*(1-2), 1–13. https://doi.org/10.2119/2006-00079.Lee

Lein, E., Borm, L. E., & Linnarsson, S. (2017). The promise of spatial transcriptomics for neuroscience in the era of molecular cell typing. *Science* (New York, N.Y.), *358*(6359), 64–69. https://doi.org/10.1126/science.aan6827

Leite, J. P., & Cavalheiro, E. A. (1995). Effects of conventional antiepileptic drugs in a model of spontaneous recurrent seizures in rats. *Epilepsy research*, *20*(2), 93–104. https://doi.org/10.1016/0920-1211(94)00070-d

Leite, J. P., Garcia-Cairasco, N., & Cavalheiro, E. A. (2002). New insights from the use of pilocarpine and kainate models. *Epilepsy research*, *50*(1-2), 93–103. https://doi.org/10.1016/s0920-1211(02)00072-4

Lentini, J. M., Alsaif, H. S., Faqeih, E., Alkuraya, F. S., & Fu, D. (2020). DALRD3 encodes a protein mutated in epileptic encephalopathy that targets arginine tRNAs for 3-methylcytosine modification. *Nature communications*, *11*(1), 2510. https://doi.org/10.1038/s41467-020-16321-6

Lévesque, M., Biagini, G., de Curtis, M., Gnatkovsky, V., Pitsch, J., Wang, S., & Avoli, M. (2021). The pilocarpine model of mesial temporal lobe epilepsy: Over one decade later, with more rodent species and new investigative approaches. *Neuroscience and biobehavioral reviews*, *130*, 274–291. https://doi.org/10.1016/j.neubiorev.2021.08.020

Li, H., Handsaker, B., Wysoker, A., Fennell, T., Ruan, J., Homer, N., Marth, G., Abecasis, G., Durbin, R., & 1000 Genome Project Data Processing Subgroup (2009). The Sequence Alignment/Map format and SAMtools. *Bioinformatics (Oxford, England)*, *25*(16), 2078–2079. https://doi.org/10.1093/bioinformatics/btp352

Liao, Y., Wang, J., Jaehnig, E. J., Shi, Z., & Zhang, B. (2019). WebGestalt 2019: gene set analysis toolkit with revamped UIs and APIs. *Nucleic acids research*, *47*(W1), W199–W205. https://doi.org/10.1093/nar/gkz401

Lipinski, M., Muñoz-Viana, R., Del Blanco, B., Marquez-Galera, A., Medrano-Relinque, J., Caramés, J. M., Szczepankiewicz, A. A., Fernandez-Albert, J., Navarrón, C. M., Olivares, R., Wilczyński, G. M., Canals, S., Lopez-Atalaya, J. P., & Barco, A. (2020). KAT3-dependent acetylation of cell type-specific genes maintains neuronal identity in the adult mouse brain. *Nature communications*, *11*(1), 2588. https://doi.org/10.1038/s41467-020-16246-0

Longo, S. K., Guo, M. G., Ji, A. L., & Khavari, P. A. (2021). Integrating single-cell and spatial transcriptomics to elucidate intercellular tissue dynamics. *Nature reviews. Genetics*, *22*(10), 627–644. https://doi.org/10.1038/s41576-021-00370-8

Lopez-Atalaya, J. P., Askew, K. E., Sierra, A., & Gomez-Nicola, D. (2018). Development and maintenance of the brain's immune toolkit: Microglia and non-parenchymal brain macrophages. *Developmental neurobiology*, *78*(6), 561–579. https://doi.org/10.1002/dneu.22545

Lorente de Nó, R. (1934). Studies on the structure of the cerebral cortex. II: Continuatiuon of the study of the Ammonic system. *J Psychol Neurol, 46*, 113–177.

Löscher, W., Ferland, R. J., & Ferraro, T. N. (2017). The relevance of inter- and intrastrain differences in mice and rats and their implications for models of seizures and epilepsy. *Epilepsy & behavior: E&B*, *73*, 214–235. https://doi.org/10.1016/j.yebeh.2017.05.040

Löscher, W., Potschka, H., Sisodiya, S. M., & Vezzani, A. (2020). Drug Resistance in Epilepsy: Clinical Impact, Potential Mechanisms, and New Innovative Treatment Options. *Pharmacological reviews, 72*(3), 606–638. https://doi.org/10.1124/pr.120.019539

Lou, N., Takano, T., Pei, Y., Xavier, A. L., Goldman, S. A., & Nedergaard, M. (2016). Purinergic receptor P2RY12-dependent microglial closure of the injured blood-brain barrier. *Proceedings of the National Academy of Sciences of the United States of America*, *113*(4), 1074–1079. https://doi.org/10.1073/pnas.1520398113

Love, M. I., Huber, W., & Anders, S. (2014). Moderated estimation of fold change and dispersion for RNA-seq data with DESeq2. *Genome biology*, *15*(12), 550. https://doi.org/10.1186/s13059-014-0550-8

Lummertz da Rocha, E., Kubaczka, C., Sugden, W. W., Najia, M. A., Jing, R., Markel, A., LeBlanc, Z. C., Dos Santos Peixoto, R., Falchetti, M., Collins, J. J., North, T. E., & Daley, G. Q. (2022). CellComm infers cellular crosstalk that drives haematopoietic stem and progenitor cell development. *Nature cell biology*, 10.1038/s41556-022-00884-1. Advance online publication. https://doi.org/10.1038/s41556-022-00884-1

Luo, J., Elwood, F., Britschgi, M., Villeda, S., Zhang, H., Ding, Z., Zhu, L., Alabsi, H., Getachew, R., Narasimhan, R., Wabl, R., Fainberg, N., James, M. L., Wong, G., Relton, J., Gambhir, S. S., Pollard, J. W., & Wyss-Coray, T. (2013). Colony-stimulating factor 1

receptor (CSF1R) signaling in injured neurons facilitates protection and survival. *The Journal of experimental medicine*, *210*(1), 157–172. https://doi.org/10.1084/jem.20120412

Maccaferri, G., & McBain, C. J. (1995). Passive propagation of LTD to stratum oriens-alveus inhibitory neurons modulates the temporoammonic input to the hippocampal CA1 region. *Neuron*, *15*(1), 137–145. https://doi.org/10.1016/0896-6273(95)90071-3

Mamanova, L., Miao, Z., Jinat, A., Ellis, P., Shirley, L., & Teichmann, S. A. (2021). High-throughput full-length single-cell RNA-seq automation. Nature protocols, 16(6), 2886–2915. https://doi.org/10.1038/s41596-021-00523-3

Manolio, T. A., Collins, F. S., Cox, N. J., Goldstein, D. B., Hindorff, L. A., Hunter, D. J., McCarthy, M. I., Ramos, E. M., Cardon, L. R., Chakravarti, A., Cho, J. H., Guttmacher, A. E., Kong, A., Kruglyak, L., Mardis, E., Rotimi, C. N., Slatkin, M., Valle, D., Whittemore, A. S., Boehnke, M., … Visscher, P. M. (2009). Finding the missing heritability of complex diseases. *Nature*, *461*(7265), 747–753. https://doi.org/10.1038/nature08494

Marawar, R., Wakim, N., Albin, R. L., & Dodge, H. (2020). Seizure occurrence and related mortality in dementia with Lewy bodies. *Epilepsy & behavior: E&B, 111*, 107311. https://doi.org/10.1016/j.yebeh.2020.107311

Maroso, M., Balosso, S., Ravizza, T., Liu, J., Aronica, E., Iyer, A. M., Rossetti, C., Molteni, M., Casalgrandi, M., Manfredi, A. A., Bianchi, M. E., & Vezzani, A. (2010). Toll-like receptor 4 and high-mobility group box-1 are involved in ictogenesis and can be targeted to reduce seizures. *Nature medicine*, *16*(4), 413–419. https://doi.org/10.1038/nm.2127

Maroso, M., Szabo, G. G., Kim, H. K., Alexander, A., Bui, A. D., Lee, S. H., Lutz, B., & Soltesz, I. (2016). Cannabinoid Control of Learning and Memory through HCN Channels. *Neuron*, *89*(5), 1059–1073. https://doi.org/10.1016/j.neuron.2016.01.023

Marquez-Galera, A., de la Prida, L. M., & Lopez-Atalaya, J. P. (2022). A protocol to extract cell-type-specific signatures from differentially expressed genes in bulk-tissue RNA-seq. *STAR protocols*, *3*(1), 101121. https://doi.org/10.1016/j.xpro.2022.101121

Martins-Ferreira, R., Leal, B., Chaves, J., Li, T., Ciudad, L., Rangel, R., Santos, A., Martins da Silva, A., Pinho Costa, P., & Ballestar, E. (2022). Epilepsy progression is associated with cumulative DNA methylation changes in inflammatory genes. *Progress in neurobiology*, *209*, 102207. https://doi.org/10.1016/j.pneurobio.2021.102207

Masurkar, A. V., Srinivas, K. V., Brann, D. H., Warren, R., Lowes, D. C., & Siegelbaum, S. A. (2017). Medial and Lateral Entorhinal Cortex Differentially Excite Deep versus Superficial CA1 Pyramidal Neurons. *Cell reports*, *18*(1), 148–160. https://doi.org/10.1016/j.celrep.2016.12.012

Mathern, G. W., Kuhlman, P. A., Mendoza, D., & Pretorius, J. K. (1997). Human fascia dentata anatomy and hippocampal neuron densities differ depending on the epileptic syndrome and age at first seizure. *Journal of neuropathology and experimental neurology*, *56*(2), 199–212. https://doi.org/10.1097/00005072-199702000-00011

McClellan, J., & King, M. C. (2010). Genetic heterogeneity in human disease. *Cell*, *141*(2), 210–217. https://doi.org/10.1016/j.cell.2010.03.032

McInnes, L., Healy, J., & Melville, J. (2018). Umap: Uniform manifold approximation and projection for dimension reduction. *arXiv*. https://doi.org/10.48550/arXiv.1802.03426

McKenzie, B. A., Dixit, V. M., & Power, C. (2020). Fiery Cell Death: Pyroptosis in the Central Nervous System. *Trends in neurosciences*, *43*(1), 55–73. https://doi.org/10.1016/j.tins.2019.11.005

McKhann, G. M., 2nd, Wenzel, H. J., Robbins, C. A., Sosunov, A. A., & Schwartzkroin, P. A. (2003). Mouse strain differences in kainic acid sensitivity, seizure behavior, mortality, and hippocampal pathology. *Neuroscience*, *122*(2), 551–561. https://doi.org/10.1016/s0306-4522(03)00562-1

Mériaux, C., Franck, J., Park, D. B., Quanico, J., Kim, Y. H., Chung, C. K., Park, Y. M., Steinbusch, H., Salzet, M., & Fournier, I. (2014). Human temporal lobe epilepsy analyses by tissue proteomics. *Hippocampus*, *24*(6), 628–642. https://doi.org/10.1002/hipo.22246

Miller-Delaney, S. F., Bryan, K., Das, S., McKiernan, R. C., Bray, I. M., Reynolds, J. P., Gwinn, R., Stallings, R. L., & Henshall, D. C. (2015). Differential DNA methylation profiles of coding and non-coding genes define hippocampal sclerosis in human temporal lobe epilepsy. *Brain: a journal of neurology*, *138*(Pt 3), 616–631. https://doi.org/10.1093/brain/awu373

Milner B. (1972). Disorders of learning and memory after temporal lobe lesions in man. *Clinical neurosurgery*, *19*, 421–446. https://doi.org/10.1093/neurosurgery/19.cn_suppl_1.421

Morin-Brureau, M., Milior, G., Royer, J., Chali, F., Le Duigou, C., Savary, E., Blugeon, C., Jourdren, L., Akbar, D., Dupont, S., Navarro, V., Baulac, M., Bielle, F., Mathon, B., Clemenceau, S., & Miles, R. (2018). Microglial phenotypes in the human epileptic temporal lobe. *Brain: a journal of neurology*, *141*(12), 3343–3360. https://doi.org/10.1093/brain/awy276

Morris, M. E., Baimbridge, K. G., el-Beheiry, H., Obrocea, G. V., & Rosen, A. S. (1995). Correlation of anoxic neuronal responses and calbindin-D28k localization in stratum pyramidale of rat hippocampus. *Hippocampus*, *5*(1), 25–39. https://doi.org/10.1002/hipo.450050105

Nadler, J. V., Perry, B. W., & Cotman, C. W. (1978). Intraventricular kainic acid preferentially destroys hippocampal pyramidal cells. *Nature*, *271*(5646), 676–677. https://doi.org/10.1038/271676a0

Nagy, C., Maheu, M., Lopez, J. P., Vaillancourt, K., Cruceanu, C., Gross, J. A., Arnovitz, M., Mechawar, N., & Turecki, G. (2015). Effects of postmortem interval on biomolecule integrity in the brain. *Journal of neuropathology and experimental neurology*, *74*(5), 459–469. https://doi.org/10.1097/NEN.0000000000000190

Ni, G., Qin, J., Li, H., Chen, Z., Zhou, Y., Fang, Z., Chen, Y., Zhou, J., Huang, M., & Zhou, L. (2015). Effects of antiepileptic drug monotherapy on one-carbon metabolism and DNA methylation in patients with epilepsy. *PloS one*, *10*(4), e0125656. https://doi.org/10.1371/journal.pone.0125656

Nido, G. S., Dick, F., Toker, L., Petersen, K., Alves, G., Tysnes, O. B., Jonassen, I., Haugarvoll, K., & Tzoulis, C. (2020). Common gene expression signatures in Parkinson's disease are driven by changes in cell composition. *Acta neuropathologica communications*, *8*(1), 55. https://doi.org/10.1186/s40478-020-00932-7

Oikawa, H., Goh, W. W., Lim, V. K., Wong, L., & Sng, J. C. (2015). Valproic acid mediates miR-124 to down-regulate a novel protein target, GNAI1. *Neurochemistry international*, *91*, 62–71. https://doi.org/10.1016/j.neuint.2015.10.010

Ortiz, C., Navarro, J. F., Jurek, A., Märtin, A., Lundeberg, J., & Meletis, K. (2020). Molecular atlas of the adult mouse brain. *Science advances*, *6*(26), eabb3446. https://doi.org/10.1126/sciadv.abb3446

Palop, J. J., & Mucke, L. (2009). Epilepsy and cognitive impairments in Alzheimer disease. *Archives of neurology, 66*(4), 435–440. https://doi.org/10.1001/archneurol.2009.15

Patrick, G. N., Zukerberg, L., Nikolic, M., de la Monte, S., Dikkes, P., & Tsai, L. H. (1999). Conversion of p35 to p25 deregulates Cdk5 activity and promotes neurodegeneration. *Nature*, *402*(6762), 615–622. https://doi.org/10.1038/45159

Peñagarikano, O., Abrahams, B. S., Herman, E. I., Winden, K. D., Gdalyahu, A., Dong, H., Sonnenblick, L. I., Gruver, R., Almajano, J., Bragin, A., Golshani, P., Trachtenberg, J. T., Peles, E., & Geschwind, D. H. (2011). Absence of CNTNAP2 leads to epilepsy, neuronal migration abnormalities, and core autism-related deficits. *Cell, 147*(1), 235–246. https://doi.org/10.1016/j.cell.2011.08.040

Pernot, F., Heinrich, C., Barbier, L., Peinnequin, A., Carpentier, P., Dhote, F., Baille, V., Beaup, C., Depaulis, A., & Dorandeu, F. (2011). Inflammatory changes during epileptogenesis and spontaneous seizures in a mouse model of mesiotemporal lobe epilepsy. *Epilepsia*, *52*(12), 2315–2325. https://doi.org/10.1111/j.1528-1167.2011.03273.x

Pfisterer, U., & Khodosevich, K. (2017). Neuronal survival in the brain: neuron type-specific mechanisms. *Cell death & disease*, *8*(3), e2643. https://doi.org/10.1038/cddis.2017.64

Pfisterer, U., Petukhov, V., Demharter, S., Meichsner, J., Thompson, J. J., Batiuk, M. Y., Asenjo-Martinez, A., Vasistha, N. A., Thakur, A., Mikkelsen, J., Adorjan, I., Pinborg, L. H., Pers, T. H., von Engelhardt, J., Kharchenko, P. V., & Khodosevich, K. (2020). Identification of epilepsy-associated neuronal subtypes and gene expression underlying epileptogenesis. *Nature communications*, *11*(1), 5038. https://doi.org/10.1038/s41467-020-18752-7

Pitkänen, A., Buckmaster, P., Galanopoulou, A. S., & Moshé, S. L. (Eds.). (2017). *Models of seizures and epilepsy*. Academic Press. https://doi.org/10.1016/B978-0-12-804066-9.00079-1

Pitkänen, A., Lukasiuk, K., Dudek, F. E., & Staley, K. J. (2015). Epileptogenesis. *Cold Spring Harbor perspectives in medicine*, *5*(10), a022822. https://doi.org/10.1101/cshperspect.a022822

Prada Jardim, A., Liu, J., Baber, J., Michalak, Z., Reeves, C., Ellis, M., Novy, J., de Tisi, J., McEvoy, A., Miserocchi, A., Targas Yacubian, E. M., Sisodiya, S., Thompson, P., & Thom, M. (2018). Characterising subtypes of hippocampal sclerosis and reorganization: correlation with pre and postoperative memory deficit. *Brain pathology (Zurich, Switzerland)*, *28*(2), 143–154. https://doi.org/10.1111/bpa.12514

Przedborski, S., Vila, M., & Jackson-Lewis, V. (2003). Neurodegeneration: what is it and where are we?. *The Journal of clinical investigation*, *111*(1), 3–10. https://doi.org/10.1172/JCI17522

Pugliatti, M., Beghi, E., Forsgren, L., Ekman, M., & Sobocki, P. (2007). Estimating the cost of epilepsy in Europe: a review with economic modeling. *Epilepsia, 48*(12), 2224–2233. https://doi.org/10.1111/j.1528-1167.2007.01251.x

Qian, X., Harris, K. D., Hauling, T., Nicoloutsopoulos, D., Muñoz-Manchado, A. B., Skene, N., Hjerling-Leffler, J., & Nilsson, M. (2020). Probabilistic cell typing enables fine mapping of closely related cell types in situ. *Nature methods*, *17*(1), 101–106. https://doi.org/10.1038/s41592-019-0631-4

Qiu, X., Mao, Q., Tang, Y., Wang, L., Chawla, R., Pliner, H. A., & Trapnell, C. (2017a). Reversed graph embedding resolves complex single-cell trajectories. *Nature methods*, *14*(10), 979–982. https://doi.org/10.1038/nmeth.4402

Qiu, X., Hill, A., Packer, J., Lin, D., Ma, Y. A., & Trapnell, C. (2017b). Single-cell mRNA quantification and differential analysis with Census. *Nature methods*, *14*(3), 309–315. https://doi.org/10.1038/nmeth.4150

Radu, B. M., Epureanu, F. B., Radu, M., Fabene, P. F., & Bertini, G. (2017). Nonsteroidal anti-inflammatory drugs in clinical and experimental epilepsy. *Epilepsy research*, *131*, 15–27. https://doi.org/10.1016/j.eplepsyres.2017.02.003

Ramón y Cajal, S. (1911). Histologie du système nerveux de l'homme et des vertébrés. *Vol II. Maloine: Paris*. https://doi.org/10.5962/bhl.title.48637

Rao, S. C., Dove, G., Cascino, G. D., & Petersen, R. C. (2009). Recurrent seizures in patients with dementia: frequency, seizure types, and treatment outcome. *Epilepsy & behavior: E&B, 14*(1), 118–120. https://doi.org/10.1016/j.yebeh.2008.08.012

Ren, E., & Curia, G. (2021). Synaptic Reshaping and Neuronal Outcomes in the Temporal Lobe Epilepsy. *International journal of molecular sciences*, *22*(8), 3860. https://doi.org/10.3390/ijms22083860

Riban, V., Bouilleret, V., Pham-Lê, B. T., Fritschy, J. M., Marescaux, C., & Depaulis, A. (2002). Evolution of hippocampal epileptic activity during the development of hippocampal sclerosis in a mouse model of temporal lobe epilepsy. *Neuroscience*, *112*(1), 101–111. https://doi.org/10.1016/s0306-4522(02)00064-7

Rodrigues, G. R., Kandratavicius, L., Peixoto-Santos, J. E., Monteiro, M. R., Gargaro, A. C., Geraldi, C., Velasco, T. R., & Leite, J. P. (2015). Increased frequency of hippocampal sclerosis ILAE type 2 in patients with mesial temporal lobe epilepsy with normal episodic memory. *Brain: a journal of neurology*, *138*(Pt 6), e359. https://doi.org/10.1093/brain/awu340

Rosenberg, A. B., Roco, C. M., Muscat, R. A., Kuchina, A., Sample, P., Yao, Z., Graybuck, L. T., Peeler, D. J., Mukherjee, S., Chen, W., Pun, S. H., Sellers, D. L., Tasic, B., & Seelig, G. (2018). Single-cell profiling of the developing mouse brain and spinal cord with split-pool barcoding. *Science (New York, N.Y.)*, *360*(6385), 176–182. https://doi.org/10.1126/science.aam8999

Rusina, E., Bernard, C., & Williamson, A. (2021). The Kainic Acid Models of Temporal Lobe Epilepsy. *eNeuro*, *8*(2), ENEURO.0337-20.2021. https://doi.org/10.1523/ENEURO.0337-20.2021

Saghafi, S., Ferguson, L., Hogue, O., Gales, J. M., Prayson, R., & Busch, R. M. (2018). Histopathologic subtype of hippocampal sclerosis and episodic memory performance before and after temporal lobectomy for epilepsy. *Epilepsia*, *59*(4), 825–833. https://doi.org/10.1111/epi.14036

Sánchez-Bellot, C., AlSubaie, R., Mishchanchuk, K., Wee, R., & MacAskill, A. F. (2022). Two opposing hippocampus to prefrontal cortex pathways for the control of approach and avoidance behaviour. *Nature communications*, *13*(1), 339. https://doi.org/10.1038/s41467-022-27977-7

Scandaglia, M., Lopez-Atalaya, J. P., Medrano-Fernandez, A., Lopez-Cascales, M. T., Del Blanco, B., Lipinski, M., Benito, E., Olivares, R., Iwase, S., Shi, Y., & Barco, A. (2017). Loss of Kdm5c Causes Spurious Transcription and Prevents the Fine-Tuning of Activity-Regulated Enhancers in Neurons. *Cell reports*, *21*(1), 47–59. https://doi.org/10.1016/j.celrep.2017.09.014

Scheffer, I. E., Berkovic, S., Capovilla, G., Connolly, M. B., French, J., Guilhoto, L., Hirsch, E., Jain, S., Mathern, G. W., Moshé, S. L., Nordli, D. R., Perucca, E., Tomson, T., Wiebe, S., Zhang, Y.-H. and Zuberi, S. M. (2017), ILAE classification of the epilepsies: Position paper of the ILAE Commission for Classification and Terminology. *Epilepsia, 58*: 512–521. https://doi.org/10.1111/epi.13709

Schouten, M., Bielefeld, P., Fratantoni, S. A., Hubens, C. J., Piersma, S. R., Pham, T. V., Voskuyl, R. A., Lucassen, P. J., Jimenez, C. R., & Fitzsimons, C. P. (2016). Multi-omics profile of the mouse dentate gyrus after kainic acid-induced status epilepticus. *Scientific data*, *3*, 160068. https://doi.org/10.1038/sdata.2016.68

Schouten, M., Fratantoni, S. A., Hubens, C. J., Piersma, S. R., Pham, T. V., Bielefeld, P., Voskuyl, R. A., Lucassen, P. J., Jimenez, C. R., & Fitzsimons, C. P. (2015). MicroRNA-124 and -137 cooperativity controls caspase-3 activity through BCL2L13 in hippocampal neural stem cells. *Scientific reports*, *5*, 12448. https://doi.org/10.1038/srep12448

Schubert C. (2009). The genomic basis of the Williams-Beuren syndrome. *Cellular and molecular life sciences: CMLS*, *66*(7), 1178–1197. https://doi.org/10.1007/s00018-008-8401-y

Schulz, H., Ruppert, A. K., Herms, S., Wolf, C., Mirza-Schreiber, N., Stegle, O., Czamara, D., Forstner, A. J., Sivalingam, S., Schoch, S., Moebus, S., Pütz, B., Hillmer, A., Fricker, N., Vatter, H., Müller-Myhsok, B., Nöthen, M. M., Becker, A. J., Hoffmann, P., Sander, T., … Cichon, S. (2017). Genome-wide mapping of genetic determinants influencing DNA methylation and gene expression in human hippocampus. *Nature communications*, *8*(1), 1511. https://doi.org/10.1038/s41467-017-01818-4

Scoville, W. B., & Milner, B. (1957). Loss of recent memory after bilateral hippocampal lesions. *Journal of neurology, neurosurgery, and psychiatry*, *20*(1), 11–21. https://doi.org/10.1136/jnnp.20.1.11

Sen, A., Jette, N., Husain, M., & Sander, J. W. (2020). Epilepsy in older people. *Lancet (London, England), 395*(10225), 735–748. https://doi.org/10.1016/S0140-6736(19)33064-8

Sharma, A. K., Reams, R. Y., Jordan, W. H., Miller, M. A., Thacker, H. L., & Snyder, P. W. (2007). Mesial temporal lobe epilepsy: pathogenesis, induced rodent models and lesions. *Toxicologic pathology*, *35*(7), 984–999. https://doi.org/10.1080/01926230701748305

Slomianka, L., Amrein, I., Knuesel, I., Sørensen, J. C., & Wolfer, D. P. (2011). Hippocampal pyramidal cells: the reemergence of cortical lamination. *Brain structure & function*, *216*(4), 301–317. https://doi.org/10.1007/s00429-011-0322-0

Soltesz, I., & Losonczy, A. (2018). CA1 pyramidal cell diversity enabling parallel information processing in the hippocampus. *Nature neuroscience*, *21*(4), 484–493. https://doi.org/10.1038/s41593-018-0118-0

Sommer, W. (1880). Erkrankung des Ammonshorns als aetiologisches Moment der Epilepsie. *Archiv f. Psychiatrie 10*, 631–675. https://doi.org/10.1007/BF02224538

Squire L. R. (1992). Memory and the hippocampus: a synthesis from findings with rats, monkeys, and humans. *Psychological review*, *99*(2), 195–231. https://doi.org/10.1037/0033-295x.99.2.195

Srivastava, P. K., van Eyll, J., Godard, P., Mazzuferi, M., Delahaye-Duriez, A., Van Steenwinckel, J., Gressens, P., Danis, B., Vandenplas, C., Foerch, P., Leclercq, K., Mairet-Coello, G., Cardenas, A., Vanclef, F., Laaniste, L., Niespodziany, I., Keaney, J., Gasser, J., Gillet, G., Shkura, K., … Johnson, M. R. (2018). A systems-level framework for drug discovery identifies Csf1R as an anti-epileptic drug target. *Nature communications*, *9*(1), 3561. https://doi.org/10.1038/s41467-018-06008-4

Steinlein, O. K., & Noebels, J. L. (2000). Ion channels and epilepsy in man and mouse. *Current opinion in genetics & development*, *10*(3), 286–291. https://doi.org/10.1016/s0959-437x(00)00079-4

Steward, O., & Scoville, S. A. (1976). Cells of origin of entorhinal cortical afferents to the hippocampus and fascia dentata of the rat. *The Journal of comparative neurology*, *169*(3), 347–370. https://doi.org/10.1002/cne.901690306

Stuart, T., Butler, A., Hoffman, P., Hafemeister, C., Papalexi, E., Mauck, W. M., 3rd, Hao, Y., Stoeckius, M., Smibert, P., & Satija, R. (2019). Comprehensive Integration of Single-Cell Data. *Cell*, *177*(7), 1888–1902.e21. https://doi.org/10.1016/j.cell.2019.05.031

Svensson, V., Vento-Tormo, R., & Teichmann, S. A. (2018). Exponential scaling of single-cell RNA-seq in the past decade. *Nature protocols*, *13*(4), 599–604. https://doi.org/10.1038/nprot.2017.149

Tawarayama, H., Yamada, H., Amin, R., Morita-Fujimura, Y., Cooper, H. M., Shinmyo, Y., Kawata, M., Ikawa, S., & Tanaka, H. (2018). Draxin regulates hippocampal neurogenesis in the postnatal dentate gyrus by inhibiting DCC-induced apoptosis. *Scientific reports*, *8*(1), 840. https://doi.org/10.1038/s41598-018-19346-6

Thom M. (2014). Review: Hippocampal sclerosis in epilepsy: a neuropathology review. *Neuropathology and applied neurobiology, 40*(5), 520–543. https://doi.org/10.1111/nan.12150

Thom, M., Liagkouras, I., Martinian, L., Liu, J., Catarino, C. B., & Sisodiya, S. M. (2012). Variability of sclerosis along the longitudinal hippocampal axis in epilepsy: a post mortem study. *Epilepsy research*, *102*(1-2), 45–59. https://doi.org/10.1016/j.eplepsyres.2012.04.015

Thorvaldsdóttir, H., Robinson, J. T., & Mesirov, J. P. (2013). Integrative Genomics Viewer (IGV): high-performance genomics data visualization and exploration. *Briefings in bioinformatics*, *14*(2), 178–192. https://doi.org/10.1093/bib/bbs017

Tiefes, A. M., Hartlieb, T., Tacke, M., von Stülpnagel-Steinbeis, C., Larsen, L., Hao, Q., Dahl, H. A., Neubauer, B. A., Gerstl, L., Kudernatsch, M., Kluger, G. J., & Borggraefe, I. (2019). Mesial Temporal Sclerosis in SCN1A-Related Epilepsy: Two Long-Term EEG Case Studies. *Clinical EEG and neuroscience, 50*(4), 267–272.

https://doi.org/10.1177/1550059418794347

Tulving, E., & Markowitsch, H. J. (1998). Episodic and declarative memory: role of the hippocampus. *Hippocampus*, *8*(3), 198–204. https://doi.org/10.1002/(SICI)1098-1063(1998)8:3<198::AID-HIPO2>3.0.CO;2-G

Turski, W. A., Cavalheiro, E. A., Schwarz, M., Czuczwar, S. J., Kleinrok, Z., & Turski, L. (1983). Limbic seizures produced by pilocarpine in rats: behavioural, electroencephalographic and neuropathological study. *Behavioural brain research*, *9*(3), 315–335. https://doi.org/10.1016/0166-4328(83)90136-5

Valero, M., & de la Prida, L. M. (2018). The hippocampus in depth: a sublayer-specific perspective of entorhinal-hippocampal function. *Current opinion in neurobiology*, *52*, 107–114. https://doi.org/10.1016/j.conb.2018.04.013

Valero, M., Averkin, R. G., Fernandez-Lamo, I., Aguilar, J., Lopez-Pigozzi, D., Brotons-Mas, J. R., Cid, E., Tamas, G., & Menendez de la Prida, L. (2017). Mechanisms for Selective Single-Cell Reactivation during Offline Sharp-Wave Ripples and Their Distortion by Fast Ripples. *Neuron*, *94*(6), 1234–1247.e7. https://doi.org/10.1016/j.neuron.2017.05.032

Valero, M., Cid, E., Averkin, R. G., Aguilar, J., Sanchez-Aguilera, A., Viney, T. J., Gomez-Dominguez, D., Bellistri, E., & de la Prida, L. M. (2015). Determinants of different deep and superficial CA1 pyramidal cell dynamics during sharp-wave ripples. *Nature neuroscience*, *18*(9), 1281–1290. https://doi.org/10.1038/nn.4074

van der Maaten, L., and Hinton, G. (2008). Visualizing data using t-SNE. *Journal of Machine Learning Research*, *9*(11), 2579–2605. http://jmlr.org/papers/v9/vandermaaten08a.html

Vest, R. S., O'Leary, H., Coultrap, S. J., Kindy, M. S., & Bayer, K. U. (2010). Effective post-insult neuroprotection by a novel Ca(2+)/ calmodulin-dependent protein kinase II (CaMKII) inhibitor. *The Journal of biological chemistry*, *285*(27), 20675–20682. https://doi.org/10.1074/jbc.M109.088617

Vezzani, A., & Baram, T. Z. (2007). New roles for interleukin-1 Beta in the mechanisms of epilepsy. *Epilepsy currents*, *7*(2), 45–50. https://doi.org/10.1111/j.1535-7511.2007.00165.x

Wang, Z., Gerstein, M., & Snyder, M. (2009). RNA-Seq: a revolutionary tool for transcriptomics. Nature reviews. *Genetics*, *10*(1), 57–63. https://doi.org/10.1038/nrg2484

Wilhelm, B. T., & Landry, J. R. (2009). RNA-Seq-quantitative measurement of expression through massively parallel RNA-sequencing. *Methods (San Diego, Calif.)*, *48*(3), 249–257. https://doi.org/10.1016/j.ymeth.2009.03.016

Winden, K. D., Bragin, A., Engel, J., & Geschwind, D. H. (2015). Molecular alterations in areas generating fast ripples in an animal model of temporal lobe epilepsy. *Neurobiology of disease*, *78*, 35–44. https://doi.org/10.1016/j.nbd.2015.02.011

Wittner, L., Eross, L., Szabó, Z., Tóth, S., Czirják, S., Halász, P., Freund, T. F., & Maglóczky, Z. S. (2002). Synaptic reorganization of calbindin-positive neurons in the human hippocampal CA1 region in temporal lobe epilepsy. *Neuroscience*, *115*(3), 961–978. https://doi.org/10.1016/s0306-4522(02)00264-6

World Health Organization. (2019). Epilepsy: a public health imperative. *World Health Organization*. https://apps.who.int/iris/handle/10665/325293

Wyler, A. R., Dohan Jr, F. C., Schweitzer, J. B., & Berry III, A. D. (1992). A grading system for mesial temporal pathology (hippocampal sclerosis) from anterior temporal lobectomy. *Journal of Epilepsy*, *5*(4), 220-225. https://doi.org/10.1016/S0896-6974(05)80120-3

Yao, Z., van Velthoven, C., Nguyen, T. N., Goldy, J., Sedeno-Cortes, A. E., Baftizadeh, F., Bertagnolli, D., Casper, T., Chiang, M., Crichton, K., Ding, S. L., Fong, O., Garren, E., Glandon, A., Gouwens, N. W., Gray, J., Graybuck, L. T., Hawrylycz, M. J., Hirschstein, D., Kroll, M., … Zeng, H. (2021). A taxonomy of transcriptomic cell types across the isocortex and hippocampal formation. *Cell*, *184*(12), 3222–3241.e26. https://doi.org/10.1016/j.cell.2021.04.021

Yap, E. L., & Greenberg, M. E. (2018). Activity-Regulated Transcription: Bridging the Gap between Neural Activity and Behavior. *Neuron*, *100*(2), 330–348. https://doi.org/10.1016/j.neuron.2018.10.013

You, J. C., Muralidharan, K., Park, J. W., Petrof, I., Pyfer, M. S., Corbett, B. F., LaFrancois, J. J., Zheng, Y., Zhang, X., Mohila, C. A., Yoshor, D., Rissman, R. A., Nestler, E. J., Scharfman, H. E., & Chin, J. (2017). Epigenetic suppression of hippocampal calbindin-D28k by ΔFosB drives seizure-related cognitive deficits. *Nature medicine*, *23*(11), 1377–1383. https://doi.org/10.1038/nm.4413

Zabel, M. K., Zhao, L., Zhang, Y., Gonzalez, S. R., Ma, W., Wang, X., Fariss, R. N., & Wong, W. T. (2016). Microglial phagocytosis and activation underlying photoreceptor degeneration is regulated by CX3CL1-CX3CR1 signaling in a mouse model of retinitis pigmentosa. *Glia*, *64*(9), 1479–1491. https://doi.org/10.1002/glia.23016

Zeisel, A., Hochgerner, H., Lönnerberg, P., Johnsson, A., Memic, F., van der Zwan, J., Häring, M., Braun, E., Borm, L. E., La Manno, G., Codeluppi, S., Furlan, A., Lee, K., Skene, N., Harris, K. D., Hjerling-Leffler, J., Arenas, E., Ernfors, P., Marklund, U., & Linnarsson, S. (2018). Molecular Architecture of the Mouse Nervous System. *Cell*, *174*(4), 999–1014.e22. https://doi.org/10.1016/j.cell.2018.06.021

Zeisel, A., Muñoz-Manchado, A. B., Codeluppi, S., Lönnerberg, P., La Manno, G., Juréus, A., Marques, S., Munguba, H., He, L., Betsholtz, C., Rolny, C., Castelo-Branco, G., Hjerling-Leffler, J., & Linnarsson, S. (2015). Brain structure. Cell types in the mouse cortex and hippocampus revealed by single-cell RNA-seq. *Science (New York, N.Y.)*, *347*(6226), 1138–1142. https://doi.org/10.1126/science.aaa1934

Zheng, G. X., Terry, J. M., Belgrader, P., Ryvkin, P., Bent, Z. W., Wilson, R., Ziraldo, S. B., Wheeler, T. D., McDermott, G. P., Zhu, J., Gregory, M. T., Shuga, J., Montesclaros, L., Underwood, J. G., Masquelier, D. A., Nishimura, S. Y., Schnall-Levin, M., Wyatt, P. W., Hindson, C. M., Bharadwaj, R., … Bielas, J. H. (2017). Massively parallel digital transcriptional profiling of single cells. *Nature communications*, *8*, 14049. https://doi.org/10.1038/ncomms14049

Annex

The results of this Thesis work have been published in Cell Reports, in the annexed paper named "*Sublayer- and cell-type-specific neurodegenerative transcriptional trajectories in hippocampal sclerosis*" of which I am first co-author. However, this work has been done in collaboration with members of my laboratory and with researchers from other institutions. Here I describe the author contribution for each of the co-authors: Liset M. de la Prida and José P. López-Atalaya conceptualized the proyect. Liset M. de la Prida, José P. López-Atalaya, Álex Bayés and Ángel Barco designed the methodology. The experimentation was carried out by Elena Cid, Manuel Valero, Beatriz Gal, Daniel C. Medeiros, Carmen M. Navarrón, Luis Ballesteros-Esteban, Rita Reig-Viader, Aixa V. Morales, Iván Fernandez-Lamo and Daniel Gómez-Domínguez. The formal data analyses were performed Elena Cid, Ángel Márquez Galera, Manuel Valero, José P. López-Atalaya and Liset M. de la Prida. Ángel Márquez Galera and José P. López-Atalaya conducted all bioinformatic analysis of massively parallel sequencing data. Yasunori Hayashi and Masaaki Sato provided the Thy1.2-G-CaMP7-DsRed2 mouse strain. The original draft was written by Liset M. de la Prida and José P. López-Atalaya, after which Ángel Márquez Galera and Elena Cid actively joined the editing, revision and proofreading process. Liset M. de la Prida and José P. López-Atalaya acquired funding and supervised the experiments, analyses and progress of the project.

Cell Reports

Sublayer- and cell-type-specific neurodegenerative transcriptional trajectories in hippocampal sclerosis

Graphical abstract
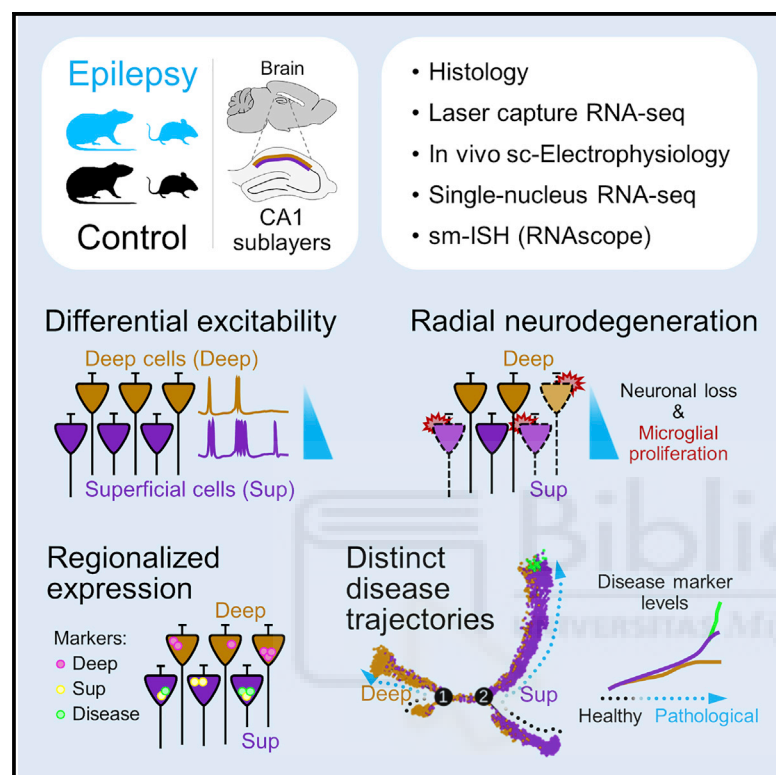
Authors

Elena Cid, Angel Marquez-Galera,
Manuel Valero, ..., Angel Barco,
Jose P. Lopez-Atalaya,
Liset M. de la Prida

Correspondence

jose.lopezatalaya@csic.es (J.P.L.-A.),
lmprida@cajal.csic.es (L.M.d.l.P.)

In brief

Cid et al. use a combination of techniques from single-cell recordings *in vivo* to bulk tissue and single-nucleus RNA-seq to reveal cell-type-specific segregation of neurodegenerative and epileptogenic processes in experimental epilepsy. They find that segregated disease-specific gene expression changes run differentially across cell types and sublayers of the hippocampal CA1 region.

Highlights

- Superficial CA1 pyramidal neurons are overactive in epileptic rodents

- Neurodegeneration-related gene signatures progress radially in the epileptic CA1

- Larger vulnerability of superficial CA1 pyramidal cells in experimental epilepsy

- Cell-type-specific disease trajectories characterize hippocampal sclerosis

CellPress

Cell Reports

Article

Sublayer- and cell-type-specific neurodegenerative transcriptional trajectories in hippocampal sclerosis

Elena Cid,[1,8] Angel Marquez-Galera,[2,8] Manuel Valero,[1] Beatriz Gal,[1,3] Daniel C. Medeiros,[1] Carmen M. Navarron,[2] Luis Ballesteros-Esteban,[1] Rita Reig-Viader,[4,5] Aixa V. Morales,[1] Ivan Fernandez-Lamo,[1] Daniel Gomez-Dominguez,[1] Masaaki Sato,[6] Yasunori Hayashi,[6,7] Àlex Bayés,[4,5] Angel Barco,[2] Jose P. Lopez-Atalaya,[2,*] and Liset M. de la Prida[1,9,*]

[1]Instituto Cajal, CSIC, 28002 Madrid, Spain
[2]Instituto de Neurociencias, Universidad Miguel Hernández-Consejo Superior de Investigaciones Científicas (UMH-CSIC), 03550 Sant Joan d'Alacant, Alicante, Spain
[3]Universidad Europea de Madrid, 28670 Villaviciosa de Odón, Madrid, Spain
[4]Institut d'Investigació Biomèdica San Pau, 08041 Barcelona, Spain
[5]Universitat Autònoma de Barcelona, 08193 Bellaterra, Cerdanyola del Vallès, Spain
[6]RIKEN Brain Science Institute, Wako, 351-0198 Saitama, Japan
[7]Department of Pharmacology, Kyoto University Graduate School of Medicine, 606-8501 Kyoto, Japan
[8]These authors contributed equally
[9]Lead contact
*Correspondence: jose.lopezatalaya@csic.es (J.P.L.-A.), lmprida@cajal.csic.es (L.M.d.l.P.)
 https://doi.org/10.1016/j.celrep.2021.109229

SUMMARY

Hippocampal sclerosis, the major neuropathological hallmark of temporal lobe epilepsy, is characterized by different patterns of neuronal loss. The mechanisms of cell-type-specific vulnerability and their progression and histopathological classification remain controversial. Using single-cell electrophysiology *in vivo* and immediate-early gene expression, we reveal that superficial CA1 pyramidal neurons are overactive in epileptic rodents. Bulk tissue and single-nucleus expression profiling disclose sublayer-specific transcriptomic signatures and robust microglial pro-inflammatory responses. Transcripts regulating neuronal processes such as voltage channels, synaptic signaling, and cell adhesion are deregulated differently by epilepsy across sublayers, whereas neurodegenerative signatures primarily involve superficial cells. Pseudotime analysis of gene expression in single nuclei and *in situ* validation reveal separated trajectories from health to epilepsy across cell types and identify a subset of superficial cells undergoing a later stage in neurodegeneration. Our findings indicate that sublayer- and cell-type-specific changes associated with selective CA1 neuronal damage contribute to progression of hippocampal sclerosis.

INTRODUCTION

Epilepsies are brain disorders characterized by an enduring predisposition to generate seizures with emotional and cognitive associated comorbidities. Despite significant therapeutic advances, one-third of affected individuals remain resistant to pharmacotherapy (Chen et al., 2018). Temporal lobe epilepsy (TLE), the most prevalent form of pharmacoresistant epilepsy, is frequently associated with hippocampal sclerosis (Blümcke et al., 2013). Hippocampal sclerosis is characterized by specific patterns of neuronal loss affecting different hippocampal subfields from the CA1 to CA3/4 areas, the hilus of the dentate gyrus, and superficial layers of the entorhinal cortex (Blümcke et al., 2009; Du et al., 1995; de Lanerolle et al., 2003). Factors such as epilepsy history, age of onset, and the relationship with early precipitating events may all influence the degree and severity of hippocampal sclerosis (Davies et al., 1996).

The most common form of hippocampal sclerosis (type 1; 60%–80% of TLE cases) shows severe neuronal loss of CA1, CA3, and CA4 pyramidal neurons and milder loss in CA2, with variability along the anteroposterior axis (Blümcke et al., 2013; Wyler et al., 1992). Other cell types, including microglia and astrocytes, are also affected (Blümcke et al., 2013; Morin-Brureau et al., 2018). In contrast, type 2 hippocampal sclerosis (10%–20% of cases) is associated with predominant CA1 neurodegeneration and minimal loss in other regions (Blümcke et al., 2013). Given the disparities between clinical series, there is no consensus on whether neuronal loss progresses over time (Blümcke et al., 2009; Davies et al., 1996). In addition, individual variabilities and anatomical inhomogeneities complicate classification (Coras et al., 2014; Rodrigues et al., 2015; Saghafi et al., 2018). For instance, patchy neuronal loss has been described in the CA1 region in some cases, whereas in others, it seems to adopt a more laminar profile
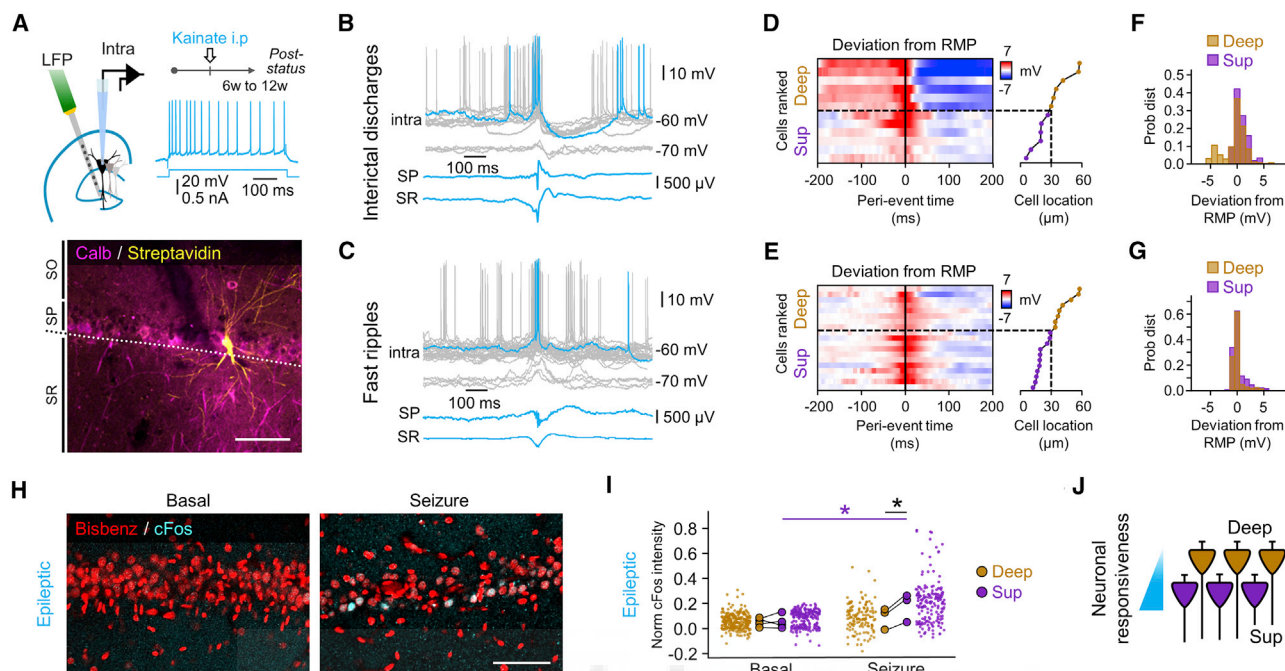
Figure 1. Differential responses of CA1 pyramidal cells during epileptiform activities

(A) Intracellular and multi-site local field potential (LFP) recordings from epileptic rats. Cells were identified with streptavidin and tested against Calbindin. Scale bar, 100 μm. SO, stratum oriens; SP, stratum pyramidale; SR; stratum radiatum.

(B) Intracellular activity during IID at different membrane potentials (gray traces). Traces are aligned by the peak of IID recorded at the SR. HFOs were recorded at the SP.

(C) Responses of the cell shown in (A) during SPW fast ripples.

(D) Deviation from the resting membrane potential (RMP) recorded in individual cells during IIDs (n = 12 cells). Red colors reflect depolarization and blue hyperpolarization. Cells are ranked by their distance to the SR and classified as deep and superficial (Sup) (subplot at right). The discontinuous line marks sublayer limits.

(E) Same as in D for SPW-fast ripples (n = 19 cells).

(F) Mean membrane potential responses around IID events showed differences between deep and Sup cells (Friedman χ^2 [1,333] = 28.7, p < 0.001). Data are from 6 deep and 6 Sup CA1 pyramidal cells.

(G) Same as in (G) for SPW fast ripple events. Note the larger after-event depolarization in Sup cells (Friedman χ^2 [1,333] = 14.67, p < 0.0001). Data are from 8 deep and 11 Sup CA1 pyramidal cells.

(H) cFos immunoreactivity in representative CA1 sections from one rat exhibiting bilateral forelimb clonus after sound stimulation (seizure) versus a non-stimulated epileptic rat with no observed seizure (basal). Scale bar, 80 μm.

(I) Intensity of c-Fos from all pyramidal cells in one confocal section per rat (small dots) and mean data per animal (larger dots). Significant interaction was confirmed for animals between groups and sublayers (p = 0.0044; n = 4 epileptic basal, n = 3 epileptic seizures). Post hoc differences: *p < 0.05.

(J) Schematic of electrophysiological and histopathological findings.

(Prada Jardim et al., 2018). In some affected individuals, cell loss concentrates in the CA4 region and the dentate gyrus and is frequently integrated in dual pathologies; e.g., TLE and malformations of cortical development, classified as type 3 hippocampal sclerosis (3%–7%) (Mathern et al., 1997). The mechanisms underlying specific vulnerability of diverse cells and their role in the histopathological landscape and clinical significance remain unknown.

Recent techniques and methods operating at single-cell resolution point to an exquisite cell-type-specific organization that is instrumental for brain function (Habib et al., 2016; Zeisel et al., 2015). In the hippocampus, the CA1 region is organized radially in two distinct sublayers with characteristic gene expression gradients along the anteroposterior and proximodistal axes (Cembrowski et al., 2016a; Dong et al., 2009; Slomianka et al., 2011). Functionally, superficial (closer to radia-

tum) and deep (closer to oriens) CA1 pyramidal neurons project differentially and diverge in their participation of sharp-wave ripple activity, theta-gamma oscillations, and behavioral-cognitive correlates (Soltesz and Losonczy, 2018; Valero and de la Prida, 2018). In spite of data suggesting critical regionalization of CA1 neuronal responses to ischemia, anoxia, and epilepsy (Morris et al., 1995; Valero et al., 2017; Wittner et al., 2002), little is known about their clinical relevance and potential relationship with neuronal vulnerability. Understanding the effect of cellular diversity and transcriptional changes in epilepsy progression may lend insights into more specific mechanisms toward new diagnostic and therapeutic opportunities (Pfisterer et al., 2020).

Here we combine gene expression profiling at the single-nucleus and microdissected tissue levels with single-cell electrophysiology to disclose epileptogenic and neurodegenerative

Cell Reports
Article

changes running differentially across CA1 sublayers in an experimental model of hippocampal sclerosis. Our study highlights the importance of leveraging cell type specificity to better understand the phenotypic complexities accompanying hippocampal sclerosis in epilepsy.

RESULTS

Large activity burden in superficial CA1 pyramidal cells during epileptiform activities

Single CA1 pyramidal cells were recorded intracellularly from anesthetized epileptic rats to evaluate their intrinsic excitability and activity during interictal discharges (IIDs), sharp-wave (SPW) fast ripples, and ictal discharges (Figures 1A–1C; Figures S1A and S1B). Recorded cells were identified post hoc (with streptavidin) and immunostained against Calbindin (Calb) to classify them as deep (negative) or superficial pyramidal cells (positive) (Figure 1A). SPW-associated high-frequency oscillation (HFO) events were detected automatically and classified as ripples (100–150 Hz), fast ripples (>150 Hz) and IID using amplitude and spectral information (Figures S1C and S1D), as before (Valero et al., 2017).

Intracellular activities recorded during IID events (n = 12 cells; Figure 1B) and SPW fast ripples (n = 19 cells; Figure 1C) were typically associated with consistent depolarization from the resting membrane potential (RMP), and firing of all pyramidal cells was examined (Figures 1D and 1E). A temporal analysis of membrane potential changes (30-ms bins) showed differences between cell types during both IID events (Figure 1F; Friedman χ^2 [1,333] = 28.7, p < 0.001) and SPW fast ripples (Figure 1G; Friedman χ^2 [1,333] = 14.67, p < 0.0001), with superficial cells consistently showing larger depolarization at the event peak. Post-event membrane potential responses recorded showed effect for the type of events (F(2,57) = 7.17, p = 0.0018), sublayer (F(1,57) = 5.44, p = 0.0236) and interaction (F(2,57) = 4.89, p = 0.0113). Post hoc Tukey tests confirmed significant smaller hyperpolarization (p = 0.0020) and a higher firing rate (p = 0.045) following IID events in superficial compared with deep cells. We found some minor differences of intrinsic excitability between cell types and groups (Table S1).

We reasoned that superficial pyramidal cells should be more steadily activated during seizures, given their poor post-event hyperpolarization. We exposed 3 epileptic rats to high-pitched sounds to promote convulsive seizures (pulses of 95–100 dB and 1- to 20-s duration at random intervals of 1–20 s during 10 min) (seizure group). This group was compared with 4 unstimulated epileptic rats without any observed clinical seizure (basal group). Animals were sacrificed after 1 h to evaluate expression of the immediate-early gene cFos (Figure 1H). Statistics per cell confirmed effects for interaction between groups and sublayer (p < 0.0001; 2-way ANOVA). Significant interaction was confirmed for animals (p = 0.0044) with post hoc differences between groups for superficial cells only (p = 0.0395) and between deep and superficial cells within the seizure group (p = 0.0117) (Figure 1I).

These results suggest higher responsiveness of superficial CA1 pyramidal cells during epileptiform activities in chronically epileptic rats (Figure 1J).

Sublayer regionalization of epilepsy-associated transcriptional responses

To investigate how the differential responsiveness of deep and superficial cells may relate with distinct transcriptional responses across sublayers, we performed RNA sequencing (RNA-seq) analysis of laser capture microdissection (LCM) samples from control (saline-injected) and epileptic rats (n = 3 replicates each; Figures 2A, S2A, and S2B; Table S2).

Analysis of LCM RNA-seq data revealed sublayer-specific genes common to control and epileptic animals (absolute $\log_2$ fold change [FC] > 0.5; adj. p < 0.01; Figure 2B; superficial versus deep samples). Among these, we retrieved *bona fide* marker genes of superficial (*Calb1*, *Grm1*, and *Syt17*) and deep CA1 pyramidal cells (*Ndst4*), consistent with previous data for mice (Cembrowski et al., 2016b, 2016a) (Figure S2C; see Figures S2D and S2E for validation by *in situ* hybridization). Sublayer gene expression analysis confirmed preserved regionalization in epileptic rats with only a subset of uncorrelated transcripts (FC > 0.5; adj. p < 0.01; Figure 2C, red dots; see Figure S2F for less stringent criteria: adj. p < 0.1). Strikingly, we found that some gene markers of other cell types in the hippocampus, including interneurons (*Sst*, *Vip*, and *Kit*), oligodendrocytes (*Mbp*, *Plp1*, and *Mobp*), astrocytes (*Aqp4*, *Gja1*, and *Gfap*), and homeostatic microglia (*Tgfbr1* and *Csf1r*), also exhibited sublayer differences, consistent with heterogeneous distribution of cell types across the CA1 radial axis (Figures 2B, 2C, and S2F) (see below).

Next, we investigated the transcriptional changes associated with epilepsy across CA1 sublayers (epileptic versus control samples per sublayer). We identified 103 significantly differentially expressed genes (DEGs) in the deep sublayer of epileptic versus control rats versus 376 DEGs in the superficial sublayer (FC > 0.5; adj. p < 0.01; Figure 2D). Although epilepsy-associated transcriptional changes run in similar directions in both sublayers (i.e., no counter-regulated genes), they were more exacerbated in the superficial CA1 (Figures 2D and S2H). Overall, we retrieved more upregulated than downregulated genes, particularly in the superficial (73% DEGs) versus the deep sublayer (57% DEGs) (Figure 2D, Venn diagrams on the right). Because of the small size of the gene set differentially regulated by epilepsy in the deep sublayer, a less stringent threshold was used to perform functional enrichment analysis with gene sets of equal sizes. We first required the genes to show a modest level of statistical significance (adj. p < 0.1) and ranked them by FC to retain the top 250 upregulated genes and top 250 downregulated genes. Functional enrichment analyses of these gene sets of equal size also revealed marked differences (Figure 2E).

Downregulated DEGs in epilepsy in the superficial CA1 sublayer show robust functional association with many Gene Ontology (GO) terms (adj. p < 0.05) linked to neuronal processes, such as synaptic transmission and neuron projection, including many well-known modulators of epileptogenic process, such as *Cacnb1*, *Cacnb4*, *Cacng2, Kcnq3*, *Kcnab1*, *Scn4b*, *Grin2a*, *Nptn*, and *Gria4* (Winden et al., 2015) (Figure 2E). Most of these Gene Ontology (GO) terms were significantly enriched only in the superficial CA1 sublayer (Figure 2E). Regarding upregulated genes in epilepsy, there were no GO terms significantly enriched using the gene set from the deep
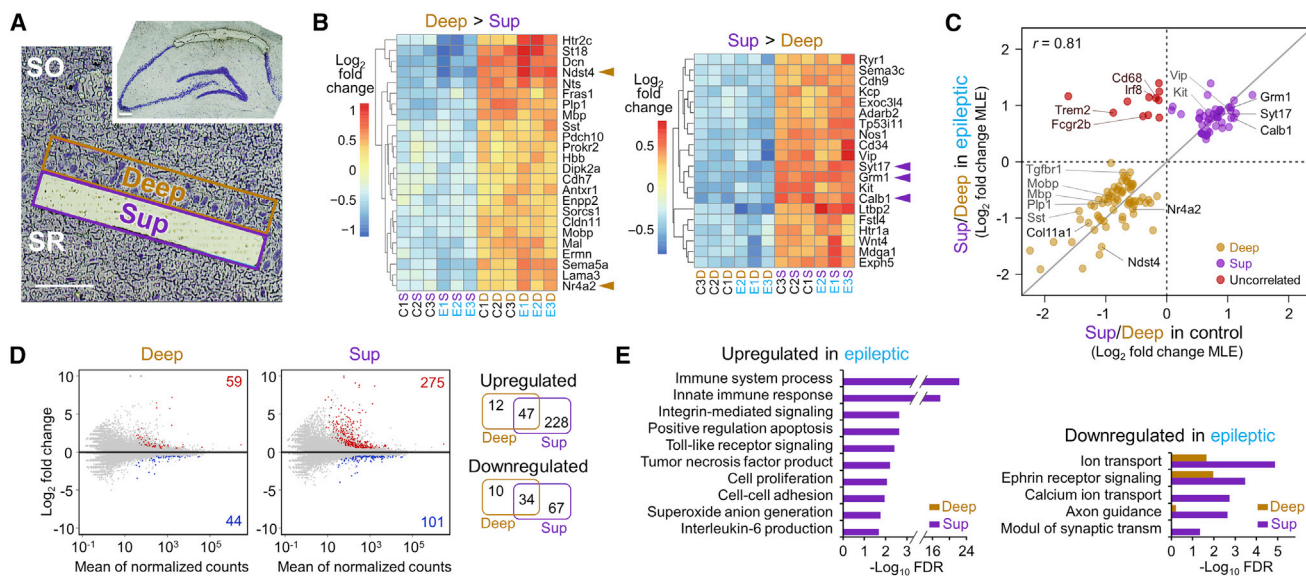
Figure 2. Bulk tissue gene expression profiling of the epileptic hippocampal area CA1 reveals regionalized transcriptional response

(A) Representative laser capture microdissection (LCM) sampling of the Sup CA1 sublayer. Scale bar, 100 μm.

(B) Heatmaps of DEGs in deep (left) and Sup CA1 sublayers (right) in three replicates from control (C) and epileptic (E) rats (FC > 0.5, adj. p < 0.01). Arrowheads point to *bona fide* gene markers of Sup (*Calb1*, *Grm1*, and *Syt17*) and deep (*Ndst4* and *Nr4a2*) pyramidal neurons. Note the presence of gene markers for interneurons (e.g., *Vip*, *Sst*, *Sema3c*, and *Kit*) and oligodendrocytes (*Plp1*, *Mbp*, *Mobp*, *Mal*, *Enpp2*, *Cldn11*, and *Ermn*).

(C) Scatterplot of DEGs between Sup and deep CA1 sublayers in control or epileptic rats (FC > 0.5, adj. p < 0.01). *Bona fide* gene markers of Sup (*Calb1*, *Grm1*, and *Syt17*) and deep (*Ndst4*, *Nr4a2*, *and Col11a1*) pyramidal neurons are highlighted (black text and bold font). Also shown are marker genes for interneurons (*Sst*, *Vip*, and *Kit*), oligodendrocytes (*Mbp*, *Mobp*, and *Plp1*), astrocytes (*Aqp4* and *Gja1*), and microglia (*Tgfbr1*). Note the presence of a subset of uncorrelated transcripts, including canonical markers of microglia cells (*Trem2*, *Irf8*, *Fcgr2b*, and *Cd68*), at the Sup sublayer in epileptic rats (red). MLE, maximum-likelihood estimate.

(D) MA plots showing epilepsy-associated significantly upregulated (red) and downregulated (blue) genes in deep and Sup CA1 sublayers (FC > 0.5, adj. p < 0.01) (left). Venn diagrams show the overlap of upregulated (top) and downregulated (bottom) genes between epileptic and control in Sup and deep sublayers of CA1.

(E) GO analysis of the top 250 upregulated and downregulated genes in deep and Sup sublayers in epilepsy (adj. p < 0.1 and then ranked by FC).

sublayer (adj. p < 0.05). Strikingly, significantly upregulated transcripts in the superficial sublayer of epileptic CA1 show a strong functional association with immune and inflammatory responses, including cytokine production, cell migration, cell proliferation, and programmed cell death (e.g., *Tlr3*, *Tlr7*, *C1qa*, *Csf1r*, *Tgfb1*, *Cd74*, *Cd86*, *Itgax*, *Itgam*, *Itgb2*, *Casp1*, *Casp4*, *Nlrc4*, *Pycard*, and *Tnfrsf1b*) (Figure 2E). Upregulated genes in the superficial CA1 sublayer of epileptic animals include core components of the inflammasome, such as *Nlrc4*, *Casp1*, and *Casp4*, which, upon activation, can promote pyroptosis, a pro-inflammatory form of lytic cell death (McKenzie et al., 2020). The transcript levels of the cysteine protease *Casp3*, a central effector of apoptosis, was also found to be upregulated specifically in the epileptic CA1 (global effect, adj. p < 0.05; superficial, adj. p = 0.0612; deep, adj. p = 0.6443). Thus, differential gene expression analysis suggests that the nature and severity of transcriptional responses to TLE may segregate radially across CA1.

Cell type deconvolution of LCM RNA-seq data suggests sublayer-specific neurodegeneration associated with microglia

Given the sublayer heterogeneity of biological processes revealed by bulk-tissue LCM RNA-seq, we reasoned that they might reflect different contributions by discrete cellular popula-

tions within the CA1 sample and/or changes in cell type composition in response to epilepsy.

To address this point, we reanalyzed a published dataset of single-cell RNA-seq (scRNA-seq) from 3,005 barcoded individual cells from the mouse somatosensory S1 cortex and CA1 regions (Zeisel et al., 2015; Figure S2I). We first performed unsupervised consensus clustering to identify major cell types in CA1 and canonical marker genes (Figures S2J and S2K). Next, to identify cell-type-specific gene signatures in bulk tissue RNA-seq data, we used scRNA-seq expression levels for the top 250 DEGs between CA1 sublayers of control and epileptic rats to summarize the cells by linear dimensionality reduction with principal-component analysis (Figure 3A). In addition, we also performed pairwise correlations and hierarchical clustering for these gene sets (Figure 3A). In control animals, these analyses revealed that gene signatures of distinct cell types, including pyramidal neurons, astrocytes, and oligodendrocytes, were prominent in the CA1 deep layer, whereas genes enriched in the superficial sublayer were mostly associated with pyramidal neurons and interneurons. In sharp contrast, we noticed strong upregulation of a core gene signature that included many known microglial markers (Micro; e.g., *Tyrobp*, *Trem2*, *Irf8*, *Irf5*, *Fcgr2b*, *Cd74*, *Cd68*, *Itgam*, and *Arpc1b*) and was specific to the superficial layer of the epileptic CA1 (Figures 3A and 3C). We further confirmed these findings using a different scRNA-seq dataset from the Allen Brain Map portal

Cell Reports
Article
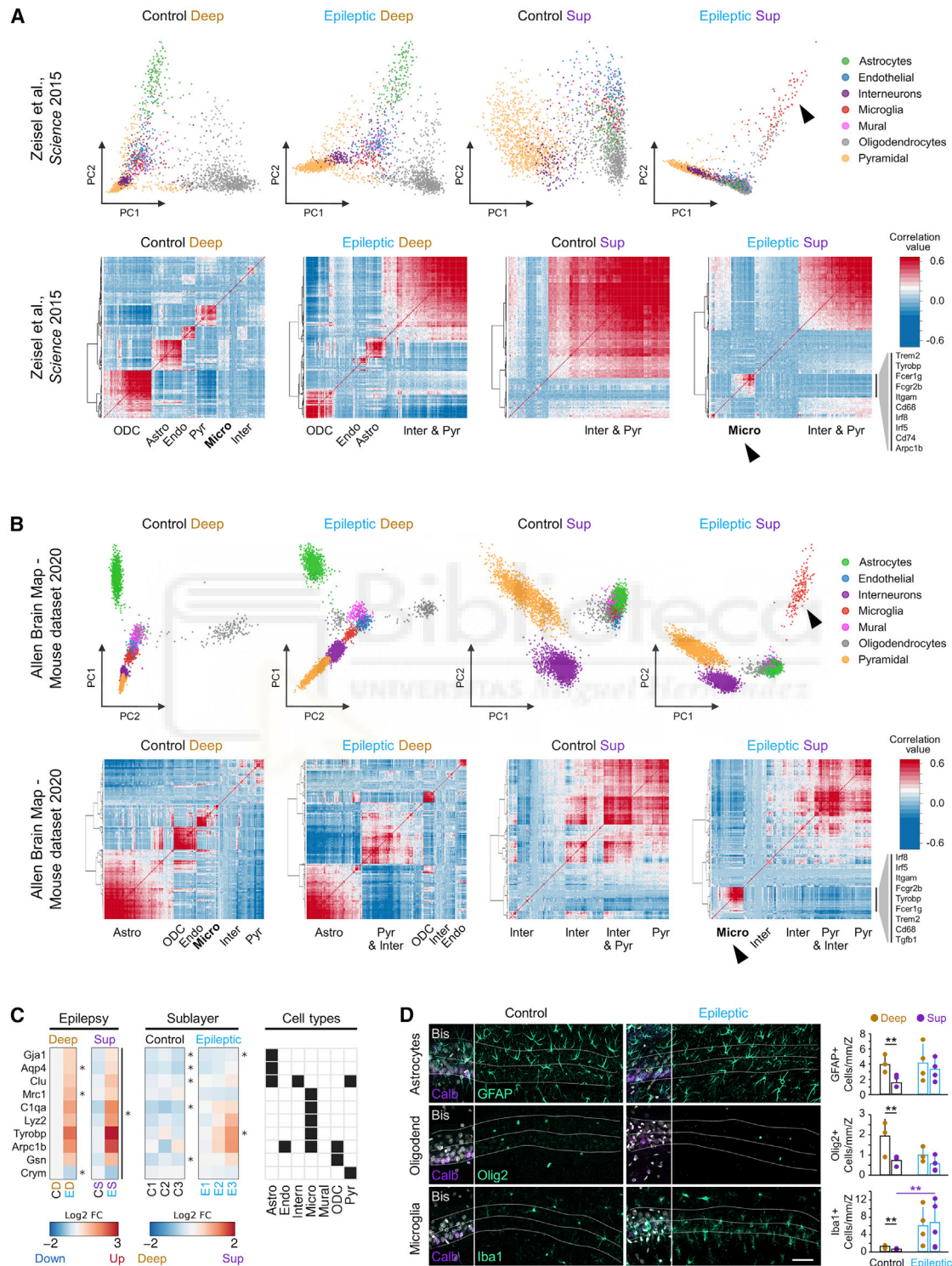
Figure 3. Microglia subpopulations underlie the transcriptional signature of Sup CA1 in epilepsy

(A and B) Subpopulation signatures inferred by deconvolution of bulk tissue transcriptome profiles. Gene sets were the top 250 DEGs between Sup and deep CA1 sublayers in epileptic and control rats (as indicated) identified in bulk tissue RNA-seq. For the selected genes, normalized expression was retrieved from publicly available scRNA-seq data from the mouse CA1 hippocampal region (Zeisel et al., 2015) (A) or the Allen Brain Map portal (Mouse Whole Cortex and Hippocampus SMART-seq [2019] with 10x-SMART-seq taxonomy [2020]) (B), and single cells were summarized by linear dimensionality reduction using principal-component

(legend continued on next page)

(Mouse Whole Cortex and Hippocampus SMART-seq [2019]) with 10x-SMART-seq taxonomy (2020) (Figure 3B). To evaluate this *in situ*, we performed immunofluorescence staining against protein markers for microglia (Iba1), astrocytes (glial fibrillary acidic protein [GFAP]), and oligodendrocytes (Olig2) and quantified their density across sublayers (Figure 3D, left). We confirmed the presence of physiological segregation of glial cell types across the CA1 sublayers (control) and changes in TLE, with between-groups differences reaching significance for microglia (Figure 3D, right).

Prompted by these results, we dissected the contribution of microglia-associated transcripts in our sample. We noticed that most of the uncorrelated transcripts in the comparison of sublayer-enriched genes across conditions were highly expressed in microglia (red dots in Figures 2C and S2F; see microglia-specific genes in Figure S2G). Thus, we evaluated their potential functional effect by building the microglial sensome (Hickman et al., 2013), which was upregulated profoundly in the superficial sublayer of epileptic rats (Figure S3A). Moreover, evaluation of microglia-neuron interactions via ligand-receptor pairing confirmed sublayer-specific effects (Figure S3B). For example, in the epileptic superficial CA1 subfield, we found dysregulated expression of the transcript encoding the CD200 receptor, whose expression in neurons provides a "don't eat me" signal that reduces microglial activation (Hoek et al., 2000). Similarly, *Cx3cl1*, a neuronal chemokine that dampens the microglia inflammatory response and neurotoxicity, was also strongly downregulated, whereas *C3* and *Csf1* transcripts were upregulated in the superficial CA1 sublayer (Biber et al., 2007; Luo et al., 2013). In contrast, the epileptic deep CA1 sublayer showed a much weaker microglia signature, and only *Cx3cl1* was found to be downregulated (Figure S3B).

Our analyses reveal heterogeneous distribution of resident cell types across the CA1 radial axis of the normal hippocampus. Strikingly, we identified critical changes in the epileptic hippocampus, including local accumulation of reactive microglia and changes of key modulators of the neuronal immune response specifically at the superficial sublayer.

CA1 hippocampal sclerosis is degenerative and sublayer specific

Given the results described above, we sought to evaluate the anatomical landscape of CA1 hippocampal sclerosis. Previously, we reported a significant reduction of linear cell density concen-

trated at the CA1 region in the systemic kainate model of TLE in rats, more consistent with sclerosis type 2 (Inostroza et al., 2011). To precisely evaluate CA1 sublayers, we combined immunostaining against the CA1 marker Wfs1 with the superficial marker Calbindin (Figure 4A). Proximal, intermediate, and distal CA1 segments were evaluated separately in tissue from 10 control and 10 epileptic rats (1 section per animal from −3.2 to −4.8 mm from the bregma). To avoid effects of hippocampal atrophy over cell density per area, we chose to evaluate the linear density of cells along the *stratum pyramidale* (SP) (cells per millimeter).
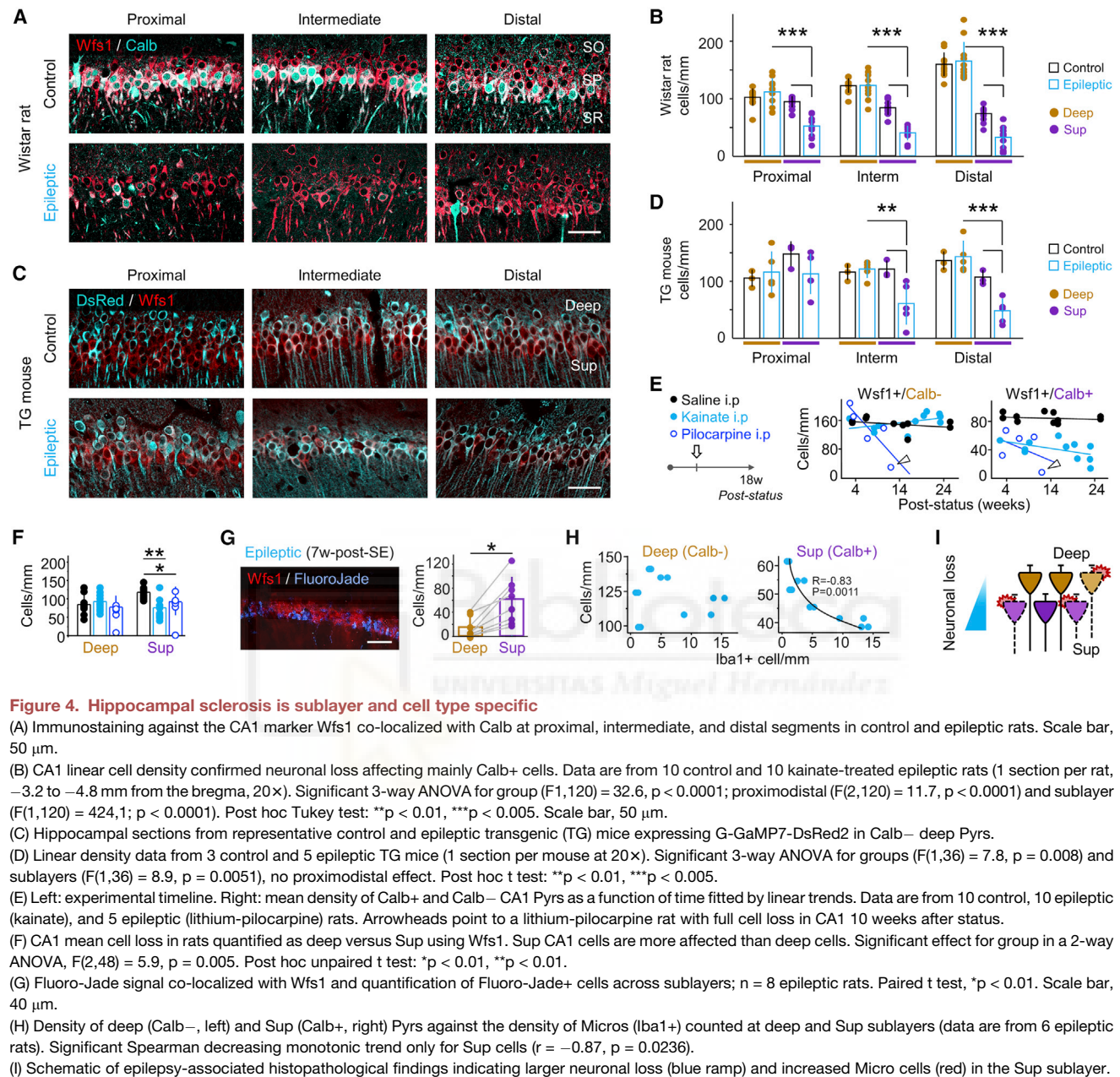
Cell loss in all three segments was mostly restricted to Calb+ superficial CA1 pyramidal cells in chronically epileptic rats (Figure 4B; 3-way ANOVA for group, sublayer, and proximodistal effects, all significant at $p < 0.0001$; post hoc Tukey test, $p < 0.001$). Because Calbindin immunoreactivity may be affected during epileptogenesis (You et al., 2017), we exploited the transgenic mouse line Thy1.2-G-CaMP7-DsRed2 with restricted expression on deep pyramidal cells (Figure 4C). Using this line, we estimated superficial cells as Wfs1+/DsRed2− and deep cells as Wfs1+/DsRed2+. Estimated global error by off-target Calb+/DsRed2+ expression was at 12% (10% proximal, 10% intermediate, 16% distal). We found similar regionalization of neuronal loss at the intermediate and distal segments of chronic epileptic mice using co-localization between DsRed2 and Wfs1 (Figure 4D, left; n = 3 control, n = 5 epileptic; 6–8 weeks post-status; significant interaction between group and sublayer, $p = 0.0006$; post hoc t test, $p < 0.01$).

Given a potential interaction between expression of Calbindin and aging (Iacopino and Christakos, 1990), we evaluated temporal trends of CA1 cell loss in epileptic rats, where a time-dependent decrease of Calb+ cells was appreciated ($r = −0.52$, $p = 0.097$, Pearson correlation), but not for control animals ($p = 0.66$; Figure 4E). We also examined the sublayer-specific vulnerability of CA1 neurons in the lithium-pilocarpine model in rats (Curia et al., 2008), which is more consistent with type 1 hippocampal sclerosis (Inostroza et al., 2011). Notably, pilocarpine-treated rats showed a similar reduction of Calb+ CA1 pyramidal cells early along epileptogenesis ($p = 0.0003$, n = 5 rats, 2–13 weeks post-status; Figure 4E, note full cell loss after 10 weeks post-status, arrowhead). Finally, to fully exclude an interaction with Calbindin immunoreactivity, we evaluated Wfs1+ cell density at deep and superficial sublayers by relying only on anatomical criteria (location within the sublayer) and found consistent

---

analysis (PCA) (top panels). Cells are colored by population membership (STAR Methods). Also shown are heatmaps of pairwise correlation for selected gene sets using scRNA-seq data, as indicated above (bottom panels). *Bona fide* markers of distinct cell types were detected in clusters of highly correlated genes representing cell type gene signatures convoluted in the bulk tissue RNA-seq (Pyr, pyramidal cell; Inter, interneuron; ODC, oligodendrocytes; Astro, astrocytes; Endo, endothelial cells; Micro, microglia; Mural, mural cells). Gene signatures of different types of cells (e.g., Pyrs, Astros, and ODCs) in the deep CA1 sublayer of control and epileptic rats lead to segregation of the cells in the corresponding PCAs and heatmap of the pairwise correlation matrix. Note the radial distribution of distinct cell types in the CA1 region in control and epileptic rats. Also note the presence of a strong gene signature of Micros in the Sup CA1 sublayer of epileptic rats (arrowhead). Names of highly correlated genes enriched in Micros are shown (Zeisel et al., 2018).

(C) Heatmaps of significantly differentially expressed cell marker genes (Figures S2I–S2K) in epilepsy in the deep or Sup sublayer (left panels), heatmap showing the sublayer effect in control and epileptic groups (paired design) for cell-marker genes modulated in epilepsy (center panels), and cell types associated with each marker gene (right panel). Pyr, pyramidal cells. *adj. $p < 0.1$.

(D) Representative sections of control and epileptic rats immunostained against GFAP (Astros), Olig2 (ODCs), and Iba1 (Micros) (left panels). The leftmost section for each condition shows co-localization between the cell type marker (cyan), Calb (purple), and bisbenzimide (Bis; white). Bar plots show quantification of astrocyte (GFAP+), ODC (Olig2+), and Micro (Iba1+) linear cell density across sublayers and groups. Shown are significant differences in interaction between sublayer and groups for Astros ($F_{(1,5)} = 10.1$, $p = 0.022$) and Micros ($F_{(1,5)} = 7.4$, $p = 0.042$) with post hoc differences at deep and Sup layers in the control group, the effect of the sublayer for ODCs ($F_{(1,5)} = 23.8$, $p = 0.0045$), and differences between groups only for Micro cells. Data are from 3 control and 4 epileptic rats. *$p < 0.05$, **$p < 0.01$, post hoc tests. Scale bar, 60 μm.

Cell Reports
Article

Figure 4. Hippocampal sclerosis is sublayer and cell type specific

(A) Immunostaining against the CA1 marker Wfs1 co-localized with Calb at proximal, intermediate, and distal segments in control and epileptic rats. Scale bar, 50 μm.

(B) CA1 linear cell density confirmed neuronal loss affecting mainly Calb+ cells. Data are from 10 control and 10 kainate-treated epileptic rats (1 section per rat, −3.2 to −4.8 mm from the bregma, 20×). Significant 3-way ANOVA for group ($F_{1,120}$) = 32.6, p < 0.0001; proximodistal ($F_{(2,120)}$ = 11.7, p < 0.0001) and sublayer ($F_{(1,120)}$ = 424,1; p < 0.0001). Post hoc Tukey test: **p < 0.01, ***p < 0.005. Scale bar, 50 μm.

(C) Hippocampal sections from representative control and epileptic transgenic (TG) mice expressing G-GaMP7-DsRed2 in Calb− deep Pyrs.

(D) Linear density data from 3 control and 5 epileptic TG mice (1 section per mouse at 20×). Significant 3-way ANOVA for groups ($F_{(1,36)}$ = 7.8, p = 0.008) and sublayers ($F_{(1,36)}$ = 8.9, p = 0.0051), no proximodistal effect. Post hoc t test: **p < 0.01, ***p < 0.005.

(E) Left: experimental timeline. Right: mean density of Calb+ and Calb− CA1 Pyrs as a function of time fitted by linear trends. Data are from 10 control, 10 epileptic (kainate), and 5 epileptic (lithium-pilocarpine) rats. Arrowheads point to a lithium-pilocarpine rat with full cell loss in CA1 10 weeks after status.

(F) CA1 mean cell loss in rats quantified as deep versus Sup using Wfs1. Sup CA1 cells are more affected than deep cells. Significant effect for group in a 2-way ANOVA, $F_{(2,48)}$ = 5.9, p = 0.005. Post hoc unpaired t test: *p < 0.01, **p < 0.01.

(G) Fluoro-Jade signal co-localized with Wfs1 and quantification of Fluoro-Jade+ cells across sublayers; n = 8 epileptic rats. Paired t test, *p < 0.01. Scale bar, 40 μm.

(H) Density of deep (Calb−, left) and Sup (Calb+, right) Pyrs against the density of Micros (Iba1+) counted at deep and Sup sublayers (data are from 6 epileptic rats). Significant Spearman decreasing monotonic trend only for Sup cells (r = −0.87, p = 0.0236).

(I) Schematic of epilepsy-associated histopathological findings indicating larger neuronal loss (blue ramp) and increased Micro cells (red) in the Sup sublayer.

results in both TLE models (Figure 4F; 2-way ANOVA for group, p = 0.005).

To further confirm sublayer-specific neurodegeneration, we combined Fluoro-Jade staining, which characteristically labels degenerating cells, with Wfs1 immunostaining in sections from epileptic rats (n = 8 epileptic rats) and again observed stronger neurodegeneration in superficial sublayers (Figure 4G; paired t test, p = 0.0017). Notably, double immunostaining against Calb and the microglial marker Iba1 revealed an inverse correlation of the amount of microglia and the density of superficial pyramidal neurons, consistent with a decreasing monotonic trend (Calb+; r = −0.87, p = 0.0236; Spearman correlation but not for deep cells [Calb−]; Figure 4H). This result indicates that loss of

superficial pyramidal neurons is strongly associated with local accumulation of microglia.

Our results support the idea that hippocampal sclerosis results from specific interactions between different cell types in a particular niche (i.e., superficial CA1 pyramidal cells and activated microglia), leading to regionalized neurodegenerative signatures in the sclerotic CA1 (Figure 4I).

Single-nucleus RNA-seq confirms cell-type-specific neurodegeneration of CA1 pyramidal cells

To gain more insights into the transcriptional activity patterns underlying hippocampal sclerosis, we performed unbiased high-throughput RNA-seq of isolated single-nucleus RNA-seq

(snRNA-seq) (Figure 5A). We analyzed the transcriptomes of 6,739 single high-quality CA1 barcoded nuclei derived from 2 control and 2 epileptic mice (control, 3,661 nuclei; epilepsy, 3,078 nuclei). Consistent with recent reports (Habib et al., 2016; Zeisel et al., 2015), barcoded nuclei were automatically classified into 13 clusters, which were then aggregated into six major cell classes: excitatory neurons, interneurons, oligodendrocytes, microglia, oligodendrocyte precursor cells, and astrocytes (Figures S4A and S4B; see Figure S4C for control versus epileptic and Figure S4D for unique molecular identifier (UMI) levels and number of genes per cell type; Table S3).

We focused on pyramidal CA1 neurons, which represented 80% of the cell population (5,347 nuclei: 2,934 control and 2,413 epileptic). After two clustering rounds (Figure S4E), we identified deep and superficial pyramidal cells from control (1,123 deep, 1,810 superficial) and epileptic (878 deep and 1,469 superficial) samples and a small population of pyramidal nuclei that were mostly epilepsy-specific (Pyr_ES; 67 nuclei: 66 from epileptic CA1, 1 from control CA1) (Figure 5B). Notably, clustering exhibited consistent distribution of markers for deep (e.g., *Ndst4* and *Col11a1*) and superficial pyramidal neurons (e.g., *Calb1* and *Epha3*) (Figures S4F and S4G). The specific population of Pyr_ES cells showed total UMI values well above the quality threshold (>500 UMIs) and a number of annotated genes lying within the control and epileptic ranges (Figure S4H), excluding potential artifacts. Differential expression analysis of Pyr_ES cells against all detected cells, excluding deep and superficial pyramidal neurons, revealed enrichment of pyramidal CA1 marker genes such as *Gria2*, *Rasgrf1*, *Camkv*, and *Brd9*, along with other transcripts enriched in excitatory neurons, including *Epha6*, *Hs6st3*, *Cntnap2*, *Kcnh7*, *Kcnip4*, and *Meg3*, which confirmed their pyramidal nature (Figures S4I and S4J). Similar to our LCM RNA-seq observations at the tissue level, we found consistent correlation of sublayer-specific genes in control and epileptic samples (Figures 5C, 5D, S5).

Next, we sought to identify gene programs underlying the differential vulnerability of deep and superficial CA1 pyramidal cell in response to epilepsy (adj. p < 0.05). Although statistical evidence of this analysis is limited by the small sample size, it provided useful prospective hypotheses and identified many epilepsy-related transcriptional changes. Many transcripts common to both cell types were associated with modulation of synaptic transmission, synapse organization, and regulation of membrane potential (Figures 5E and 5F, common genes in black). Single-nucleus differential expression analysis also revealed striking differences between superficial and deep cells of genes involved in synaptic signaling and ion membrane transport (Figures 5E and 5F). To exclude effects of different sample sizes between groups and cell types, we evaluated the top-ranked 300 DEGs and found similar GO families to be involved differentially (Figure S6A). Deregulated genes in superficial cells in epilepsy showed a strong functional association that was related to the gamma-aminobutyric acid (GABA) signaling pathway, calcium ion transport, potassium ion transport, regulation of glutamatergic synaptic transmission, axon growth and guidance, and synapse assembly. We also noted cell-type-specific changes in genes

related to neuronal survival. For instance, we found significant upregulation of death-associated protein kinase 1 (*Dapk1*) specifically in superficial CA1 neurons (Bialik and Kimchi, 2006; Figure 5G). Conversely, genes associated with the pro-survival receptors TrkB (*Ntrk2*) and TrkC (*Ntrk3*) and sortilin-related VPS10 domain-containing receptor 3 (*Sorcs3*) were upregulated exclusively in deep cells (Huang and Reichardt, 2001; Pfisterer and Khodosevich, 2017; Figure S6B). Other genes regulating neuronal vulnerability to insults were found to be deregulated in both populations of CA1 pyramidal neurons. These include the anti-apoptotic genes *Akt3*, *Chl1*, and *Spag5* and the pro-apoptotic gene *Nkain2* (He et al., 2020; Katic et al., 2017; Tawarayama et al., 2018; Figures 5G and S6B).

For some transcripts, we noted significant differential expression in epilepsy-specific Pyr_ES cells and chose to focus on this small cluster (Figure 5B, green). Compared with control pyramidal cells, Pyr_ES cells showed transcriptional dysregulation of the GO families that were altered in superficial and deep CA1 neurons in epilepsy (Figure S6C). To avoid confounding effects caused by the small sample size, we focused on transcripts identified as differentially expressed between Pyr_ES and all other epileptic cells that were well represented in both populations (i.e., detected in at least 50% of cells per group; pct.1 > 0.5 and pct.2 > 0.5 over test result). Notably, many of these transcripts were upregulated more in Pyr_ES neurons compared with other epileptic cells, including the previously mentioned apoptotic-related genes *Spag5*, *Chl1*, and *NKain2* (Figures 5G, 5H, and S6B).

To validate these findings at the single-cell level *in situ*, we used specific RNA-based probes (RNAscope) for sublayer-specific (*Dcc*) and group-specific (*Dapk1* and *Spag5*) transcripts in combination with Wfs1 immunostaining to label CA1 pyramidal cells in coronal brain sections of control and epileptic mice (n = 5 control, n = 5 epileptic mice). As expected, we observed fluorescence-labeled spots restricted to the somata of CA1 pyramidal neurons (Figures 5I, 5J, S6D, and S6E). Quantification of RNAscope revealed sublayer effects of *Dcc* (2-way ANOVA $F_{(1,8)}$ = 21.59, p = 0.0017) with significant post hoc differences between layers in both groups (p < 0.05; see also distribution per cells in Figure 5K, small dots). In contrast, for *Dapk1* ($F_{(1,8)}$ = 12.99, p = 0.0069) and *Spag5* ($F_{(1,8)}$ = 10.53, p = 0.0118), we found that significant differences between groups involved mainly the superficial sublayer, in line with our snRNA-seq results (Figure 5K).

Our analysis confirmed profound transcriptional changes related to neuronal excitability and neurodegeneration in epileptic CA1 pyramidal neurons. These functions appear to be segregated across deep and superficial cell types, consistent with electrophysiological, LCM RNA-seq, and histological data. Notably, snRNA-seq analysis revealed disease-associated genes that were highly cell type specific, including some with key functions in neuronal survival. Hence, epilepsy-induced cell-type-specific regulation of genes with key roles in synaptic plasticity and survival is a potential molecular link between differential activity burden and vulnerability across the CA1 radial axis, leading to regionalized hippocampal sclerosis.
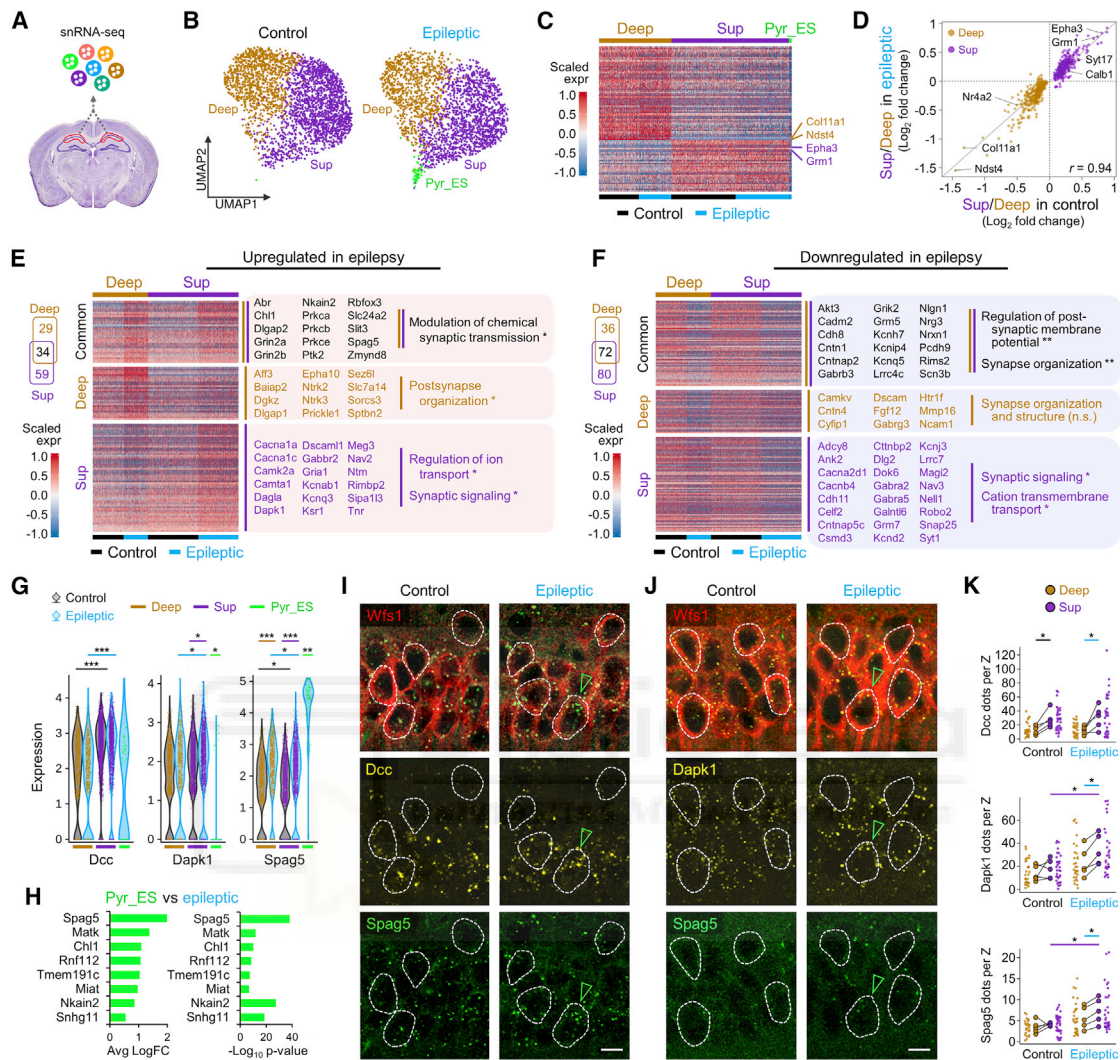
Figure 5. snRNA-seq profiling of the normal and epileptic CA1 area

(A) Nuclei were isolated from the CA1 region of adult mice and purified by flow cytometry for single-nucleus RNA-seq (snRNA-seq).

(B) Uniform manifold approximation and projection (UMAP) plots of CA1 Pyrs subtypes segregated by condition (control and epileptic). Pyr_ES, epilepsy specific.

(C) Heatmap showing normalized expression for principal gene markers for deep and Sup neurons in control and epileptic mice (96 enriched genes: 62 deep, 34 Sup; absolute log FC > 0.25; min.pct = 0.5; adj. p < 10^{-30}). Note the presence of a subset of cells with differential gene expression corresponding to the Pyr_ES cell population (green).

(D) Significantly enriched genes in Sup and deep CA1 neurons in control mice and their relative level of enrichment in epileptic animals (adj. p < 0.05, 493 genes). Gene expression levels of CA1 neuronal subtype-specific enriched genes are preserved in epilepsy.

(E) Venn diagram and heatmap of DEGs upregulated in epilepsy (adj. p < 0.05, Wilcoxon rank sum test). The heatmap shows normalized expression levels for upregulated DEGs that are common (34 genes), specific to deep (29 genes), or Sup (59 genes) CA1 neurons. Representative genes and associated significant GO terms are shown. FDR *adj. p < 0.05 (Fisher's exact test).

(F) Same as in (E) for downregulated genes.

(G) Violin plot of normalized expression value for selected genes in deep and Sup neurons in epilepsy (blue) and control (black). Wilcoxon rank-sum test; *p < 0.05, **p < 10^{-10}, ***p < 10^{-50}, #p < 10^{-100}. Expression levels in Pyr_ES cells are also shown (green).

(H) FC (left) and significance (right) for most upregulated genes in Pyr_ES compared with epileptic CA1 Pyrs (absolute log FC > 0.5 and min.pct = 0.5).

(I) Immunostaining against the CA1 marker Wfs1 and multiplexed RNAscope for *Dcc* and *Spag5* transcripts. Cells with their somata in the confocal plane are outlined. Note significant accumulation of *Spag5* in an epileptic cell (green arrowhead). Scale bar, 10 μm.

(J) Same as in (I) for *Dapk1* and *Spag5* transcripts.

(K) Quantification of *Dcc*, *Dapk1*, and *Spag5* per cell (small dots) and mouse (5 control and 5 epileptic); post hoc paired t tests, *p < 0.05.

Pseudotemporal ordering reveals sublayer-specific neurodegenerative progression

Based on the data above, we speculated that epilepsy-related responses and degenerative signals might evolve distinctly across cell types and sublayers. This may be especially critical for cell death programs accompanying hippocampal sclerosis. To glean insights into these transitional states, we used manifold learning leveraged in nearest-neighbor information to automatically organize cells in trajectories along a principal tree, reflecting progression of associated biological processes (Qiu et al., 2017a).

Low dimensional embedding of the automatically learned underlying trajectory produced a spanning tree, revealing a topological structure with four main branches (A, B, D, and E) and two bifurcation points (1 and 2; Figure 6A). Most nuclei at branches A and B were from cells identified as deep, whereas branches D and E were populated mostly by superficial cells (Figure 6B). Interestingly, control and epileptic cells were distributed differently. Branches A and D were mostly populated by control pyramidal cells, whereas branches B and E contained the vast majority of epileptic cells (Figures 6C and 6D). The trajectory topology suggested that the transcriptional state of single cells progresses along sublayer-specific disease trajectories from a basal state (branches A and D) to the epileptic condition (branches B and E) (Figure 6C). Notably, epilepsy-specific Pyr_ES cells were retrieved at the end of the superficial epileptic E path, suggesting that they may be superficial neurons at a terminal pathological state (Figure 6B, green arrowhead).

To identify mechanisms underlying single-cell transcriptional changes from health to disease, we performed quantitative comparison of gene expression kinetics across trajectories in each cellular population (DDRTree method) (Qiu et al., 2017b). By comparing the top-ranked 250 DEGs in deep (maximum false discovery rate [FDR] adj. p = 8.94×10^{-4}, likelihood ratio test) versus superficial cells (maximum FDR adj. p = 5.8×10^{-19}), we found about 50% of genes (124 genes) associated with epilepsy carrying significant cell-type-specific trajectories. Consistent with our previous results, we found that genes deregulated in epilepsy in superficial CA1 neurons show tight functional association among them, leading to a high proportion of significantly enriched ontology terms compared with genes deregulated in deep CA1 neurons (Figures 6E and 6F). Again, significantly enriched GO terms were related to structural and functional neuronal plasticity. Interestingly, pseudotemporal kinetics also revealed marked differences in the progression across sublayers of genes with important functions in regulating neuronal survival. For instance, the gene transcript levels of *Dapk1* showed a robust increase in superficial epileptic cells, whereas the gene expression levels of the pro-survival receptors TrkB (*Ntrk2*) and TrkB (*Ntrk3*), along with other genes with key functions in neurons, such as *Sorcs3* and *Aff3*, were upregulated specifically in deep pyramidal cells (Figures 6G and S6F). Other genes also related to neuronal vulnerability, such as *Camk2a* and *Nrg3*, displayed similar changes along the disease trajectory in both cell types (Figures 6G and S6F). Strikingly, the subset of apoptosis-related genes *Spag5*, *Matk*, and *Chl1* reached their maximal expression level in Pyr_ES at the end of the transcriptional trajectory in superficial cells (Figures 6G, 6H, and S6F, green).

DISCUSSION

Our work identifies sublayer-specific transcriptional changes in experimental hippocampal sclerosis. Using a combination of techniques, we found that acquired TLE involves heterogeneous biological processes running across deep and superficial CA1 pyramidal cells. Our data suggest that epileptogenesis and the accompanying hippocampal sclerosis are evolving processes that affect the transcriptional state of neurons in a cell-type-specific manner.

Hippocampal sclerosis is a heterogeneous histopathological entity (Blümcke et al., 2013). The prognosis value of certain subtypes has been debated, but emerging data suggest that it deserves further consideration in light of cell type specificity (Prada Jardim et al., 2018). Superficial and deep CA1 pyramidal cells are innervated differently by local-circuit GABAergic interneurons, express different neuromodulatory receptors, project differentially to cortical and subcortical regions, and participate distinctly in hippocampal oscillations (Cembrowski et al., 2016a; Soltesz and Losonczy, 2018; Valero and de la Prida, 2018). The more sustained excitability of superficial pyramidal cells (in terms of post-event depolarization and increased firing rate) and their consistent stronger expression of the immediate-early gene-associated protein c-Fos after individual seizures suggest that they have a larger activity burden compared with deep cells (Figure 1). Although our snRNA-seq analysis identified many transcripts regulated differentially between deep and superficial CA1 neurons that may underlie pro-epileptogenic changes in intrinsic excitability, microcircuit mechanisms are key contributors to these differences. First, perisomatic inhibition by parvalbumin (PV) basket cells is remarkably higher in deep compared with superficial cells (Soltesz and Losonczy, 2018; Valero et al., 2015). Second, superficial cells are more likely to be driven by presynaptic CA3 activity than deep cells (Valero et al., 2015). Similarly, direct inputs from layer III pyramidal neurons in the medial entorhinal cortex are biased by deep CA1 cells, whereas projections from the lateral entorhinal cortex are stronger in superficial cells (Masurkar et al., 2017). Given loss of medial layer III inputs and sprouting of lateral inputs together with specific cannabinoid type 1 receptors pathways (Laurent et al., 2015; Maroso et al., 2016), it is very likely that these changes contribute to more sustained activation of superficial cells in the epilepsy context.

Transcriptional dysregulation is a central feature of most neurodegenerative diseases. Our transcriptional profiling in laser-microdissected CA1 deep and superficial sublayers (LCM RNA-seq) revealed strong regionalized responses to acquired epilepsy. We found significantly larger transcriptional changes of GO terms associated with immune and inflammatory processes, cytokine production, and programmed cell death in the superficial sublayer (Figure 2). This includes *Cx3cr1*, *P2ry12*, and *Il18*, among other genes described previously, playing major roles in microglial activation and neurodegeneration associated with epilepsy (Ali et al., 2015; Eyo et al., 2014; Vezzani and Baram, 2007). For the deep pyramidal sublayer, transcriptional changes were milder in general and mostly involved deregulation of genes associated with changes in excitability, homeostatic regulation, and synaptic signaling, such as *Kcnh7*, *Kcnip4*,

Cell Reports
Article
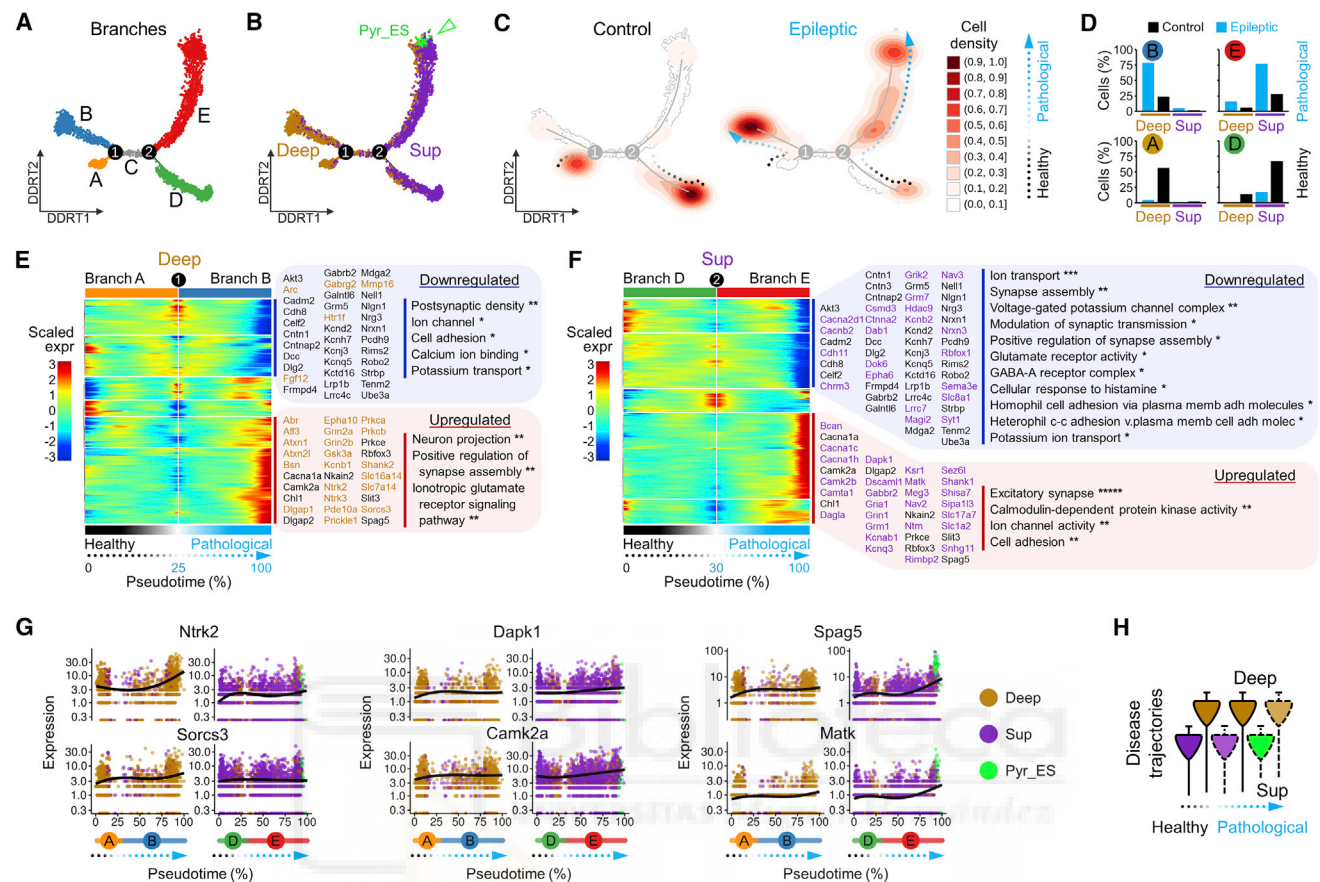
Figure 6. Pseudotemporal ordering of transcriptional changes unfolds separate disease trajectories across CA1 sublayers

(A) UMAP plot of pseudotemporal trajectory analysis of Pyr subpopulations along with discriminative dimensionality reduction via learning a tree(DDRTree) coordinates uncovers four major branches (A, B, D, and E) and segregated from two branchpoints (1 and 2).

(B) Distribution of Pyr subpopulations (deep, Sup, and Pyr_ES) across pseudotime trajectories. An arrowhead points to Pyr_ES cells located at the endpoint of branch E.

(C) Distribution of Pyr subpopulations across pseudotime trajectories by condition (control and epileptic).

(D) Distribution of Pyr subtypes across the trajectory topology.

(E) Heatmap of the top-ranked branched expression analysis modeling (BEAM) significant changes through progression across the trajectory from branch A (basal state) to B (epilepsy) (deep cells). Each row indicates the standardized kinetic curves of a gene.

(F) Same as (E) for the Sup-specific trajectory from basal state (branch D) to the epileptic condition (branch E).

(G) Pseudotime kinetics across disease trajectory for selected DEGs in epilepsy.

(H) Schematic of disease trajectories from control to epilepsy.

Scn3b, and *Gabrb3* (Dixit et al., 2016; Steinlein and Noebels, 2000). Many of these changes were confirmed by snRNA-seq analysis (Figure 5), which disclosed significant upregulation of the *Dapk1* specifically in superficial CA1 neurons (Bialik and Kimchi, 2006), whereas genes associated with the pro-survival receptors TrkB (*Ntrk2*) and TrkC (*Ntrk3*) and *Sorcs3* were mostly upregulated in deep cells (Huang and Reichardt, 2001; Pfisterer and Khodosevich, 2017).

By leveraging unsupervised branched expression learning, we identified deviating transcriptional disease trajectories in deep and superficial pyramidal cells (Figure 6). Some of the GO terms involved suggest that transition from the normal to the epileptic condition in deep cells is more likely associated with changes in synaptic signaling and excitability (i.e., they reflect microcircuit alterations), whereas superficial cells move differentially along

transcriptional changes affecting cell-cell communication (i.e., neuron-microglia interactions). Such different latent trends might suggest that deep and superficial cells are at different stages in the neurodegenerative process or being affected by pathways leading to differential vulnerability. For instance, although we found deregulated expression of genes associated with apoptotic pathways that were common to both cell types in response to epilepsy (i.e., *Akt3*, *Nrg3*, and *Camk2a*) (Ashpole and Hudmon, 2011; He et al., 2020; Kanekura et al., 2005; Tawarayama et al., 2018; Vest et al., 2010), genes related to cell death were found to be deregulated specifically in superficial or deep neurons. In superficial cells, epilepsy resulted in decreased expression of brain-derived neurotrophic factor (*Bdnf*) and increased transcript levels of the pro-apoptotic pathway activator *Dapk1* (Bialik and Kimchi, 2006). Conversely,

in deep pyramidal neurons, epilepsy led to a robust increase in expression of the gene encoding the pro-survival receptors TrkB (*Ntrk2*) and TrkC (*Ntrk3*) (Huang and Reichardt, 2001; Pfisterer and Khodosevich, 2017). Interestingly, pseudotime analysis mapped some control cells along the epileptic branches in both sublayers, suggesting that latent sublayer-specific transcriptional processes might actually be running along life (Bishop et al., 2010).

Our snRNA-seq analysis also disclosed an epilepsy-specific pyramidal cell population, Pyr_ES, which accumulated at the end of the superficial trajectory branch (Figure 6B, arrowhead). This subset of pyramidal cells displayed remarkable expression of neurodegeneration-related transcripts such as *Cdk5*, *Ckb*, *Matk*, *Chl1*, and *Spag5* (Patrick et al., 1999). The presence of cells with very high numbers of *Spag5* molecules in the superficial sublayer of the epileptic CA1 was confirmed by combined immunofluorescence and single-molecule amplification methods. Our results indicate that genes dysregulated more in epilepsy are expressed specifically by a vulnerable subset of pyramidal neurons undergoing later stages of neurodegeneration by the time of sampling. We propose that Pyr_ES cells reflect the accumulated pro-epileptic transitional changes leading to epileptogenesis and neurodegeneration, as suggested by their extreme location along disease trajectories.

Our results identify previously unobserved heterogeneity in the neuronal patterns of activity of deep and superficial CA1 pyramidal neurons in epilepsy, show specific gene expression signatures across CA1 deep and superficial sublayers that are associated with neuronal loss and hippocampal sclerosis, reveal disease trajectories of deep and superficial CA1 pyramidal neurons in epilepsy, and uncover the underlying transcriptional programs. By dissecting the transcriptional landscape across CA1 sublayers in epilepsy, our work offers insights into the mechanisms regulating epileptogenesis and highlights the importance of leveraging cell type specificity to better understand the phenotypic complexities accompanying hippocampal sclerosis in epilepsy.

STAR★METHODS

Detailed methods are provided in the online version of this paper and include the following:

- KEY RESOURCES TABLE
- RESOURCE AVAILABILITY
  - Lead contact
  - Materials availability
  - Data and code availability
- EXPERIMENTAL MODEL AND SUBJECT DETAILS
- METHOD DETAILS
  - EEG recordings and analysis
  - *In vivo* recording and labeling of single cells
  - Analysis of intracellular single-cell recordings
  - cFos immunostaining and analysis
  - Laser capture microdissection (LCM) and RNA isolation
  - LCM RNA-seq library construction and sequencing
  - LCM RNA-seq data analysis

- LCM RNA-seq single-cell informed data analysis
- Single-nuclei isolation
- Single-nucleus RNA sequencing
- snRNA-seq analysis
- Cell trajectories and pseudotime analysis
- Cell-type immunostaining and analysis
- FluoroJade staining
- *In situ* hybridization analysis
- RNAscope analysis
- QUANTIFICATION AND STATISTICAL ANALYSIS

SUPPLEMENTAL INFORMATION

Supplemental information can be found online at https://doi.org/10.1016/j.celrep.2021.109229.

AUTHOR CONTRIBUTIONS

Conceptualization, L.M.d.l.P. and J.P.L.-A.; methodology, L.M.d.l.P., J.P.L.-A., A. Bayés, and A. Barco; investigation, E.C., M.V., B.G., D.C.M., C.M.N., L.B.-E., R.R.-V., A.V.M., I.F.-L., and D.G.-D.; formal analysis, E.C., A.M.-G., M.V., J.P.L.-A., and L.M.d.l.P.; software, A.M.-G., and J.P.L.-A.; resources, Y.H., and M.S.; writing – original draft, L.M.d.l.P. and J.P.L.-A.; writing – reviewing & editing, L.M.d.l.P., J.P.L.-A., E.C., and A.M.-G.; funding acquisition, L.M.d.l.P. and J.P.L.-A.; supervision, L.M.d.l.P. and J.P.L.-A.

DECLARATION OF INTERESTS

The authors declare no competing interests.

REFERENCES

Ali, I., Chugh, D., and Ekdahl, C.T. (2015). Role of fractalkine-CX3CR1 pathway in seizure-induced microglial activation, neurodegeneration, and neuroblast production in the adult rat brain. Neurobiol. Dis. *74*, 194–203.

Anders, S., Pyl, P.T., and Huber, W. (2015). HTSeq–a Python framework to work with high-throughput sequencing data. Bioinformatics *31*, 166–169.

Ashpole, N.M., and Hudmon, A. (2011). Excitotoxic neuroprotection and vulnerability with CaMKII inhibition. Mol. Cell. Neurosci. *46*, 720–730.

Cell Reports
Article

Benjamini, Y., and Hochberg, Y. (1995). Controlling the False Discovery Rate: A Practical and Powerful Approach to Multiple Testing. J. R. Stat. Soc. B Methodol. *57*, 289–300.

Bialik, S., and Kimchi, A. (2006). The death-associated protein kinases: structure, function, and beyond. Annu. Rev. Biochem. *75*, 189–210.

Biber, K., Neumann, H., Inoue, K., and Boddeke, H.W.G.M. (2007). Neuronal 'On' and 'Off' signals control microglia. Trends Neurosci. *30*, 596–602.

Bishop, N.A., Lu, T., and Yankner, B.A. (2010). Neural mechanisms of ageing and cognitive decline. Nature *464*, 529–535.

Blümcke, I., Kistner, I., Clusmann, H., Schramm, J., Becker, A.J., Elger, C.E., Bien, C.G., Merschhemke, M., Meencke, H.-J., Lehmann, T., et al. (2009). Towards a clinico-pathological classification of granule cell dispersion in human mesial temporal lobe epilepsies. Acta Neuropathol. *117*, 535–544.

Blümcke, I., Thom, M., Aronica, E., Armstrong, D.D., Bartolomei, F., Bernasconi, A., Bernasconi, N., Bien, C.G., Cendes, F., Coras, R., et al. (2013). International consensus classification of hippocampal sclerosis in temporal lobe epilepsy: a Task Force report from the ILAE Commission on Diagnostic Methods. Epilepsia *54*, 1315–1329.

Butler, A., Hoffman, P., Smibert, P., Papalexi, E., and Satija, R. (2018). Integrating single-cell transcriptomic data across different conditions, technologies, and species. Nat. Biotechnol. *36*, 411–420.

Cembrowski, M.S., Bachman, J.L., Wang, L., Sugino, K., Shields, B.C., and Spruston, N. (2016a). Spatial Gene-Expression Gradients Underlie Prominent Heterogeneity of CA1 Pyramidal Neurons. Neuron *89*, 351–368.

Cembrowski, M.S., Wang, L., Sugino, K., Shields, B.C., and Spruston, N. (2016b). Hipposeq: a comprehensive RNA-seq database of gene expression in hippocampal principal neurons. eLife *5*, e14997.

Chen, Z., Brodie, M.J., Liew, D., and Kwan, P. (2018). Treatment Outcomes in Patients With Newly Diagnosed Epilepsy Treated With Established and New Antiepileptic Drugs: A 30-Year Longitudinal Cohort Study. JAMA Neurol. *75*, 279–286.

Cid, E., and de la Prida, L.M. (2019). Methods for single-cell recording and labeling in vivo. J. Neurosci. Methods *325*, 108354.

Coras, R., Pauli, E., Li, J., Schwarz, M., Rössler, K., Buchfelder, M., Hamer, H., Stefan, H., and Blumcke, I. (2014). Differential influence of hippocampal subfields to memory formation: insights from patients with temporal lobe epilepsy. Brain *137*, 1945–1957.

Curia, G., Longo, D., Biagini, G., Jones, R.S.G., and Avoli, M. (2008). The pilocarpine model of temporal lobe epilepsy. J. Neurosci. Methods *172*, 143–157.

Davies, K.G., Hermann, B.P., Dohan, F.C., Jr., Foley, K.T., Bush, A.J., and Wyler, A.R. (1996). Relationship of hippocampal sclerosis to duration and age of onset of epilepsy, and childhood febrile seizures in temporal lobectomy patients. Epilepsy Res. *24*, 119–126.

de Lanerolle, N.C., Kim, J.H., Williamson, A., Spencer, S.S., Zaveri, H.P., Eid, T., and Spencer, D.D. (2003). A retrospective analysis of hippocampal pathology in human temporal lobe epilepsy: evidence for distinctive patient subcategories. Epilepsia *44*, 677–687.

Dixit, A.B., Banerjee, J., Srivastava, A., Tripathi, M., Sarkar, C., Kakkar, A., Jain, M., and Chandra, P.S. (2016). RNA-seq analysis of hippocampal tissues reveals novel candidate genes for drug refractory epilepsy in patients with MTLE-HS. Genomics *107*, 178–188.

Dobin, A., Davis, C.A., Schlesinger, F., Drenkow, J., Zaleski, C., Jha, S., Batut, P., Chaisson, M., and Gingeras, T.R. (2013). STAR: ultrafast universal RNA-seq aligner. Bioinformatics *29*, 15–21.

Dong, H.-W., Swanson, L.W., Chen, L., Fanselow, M.S., and Toga, A.W. (2009). Genomic-anatomic evidence for distinct functional domains in hippocampal field CA1. Proc. Natl. Acad. Sci. USA *106*, 11794–11799.

Du, F., Eid, T., Lothman, E.W., Köhler, C., and Schwarcz, R. (1995). Preferential neuronal loss in layer III of the medial entorhinal cortex in rat models of temporal lobe epilepsy. J. Neurosci. *15*, 6301–6313.

Eyo, U.B., Peng, J., Swiatkowski, P., Mukherjee, A., Bispo, A., and Wu, L.J. (2014). Neuronal hyperactivity recruits microglial processes via neuronal NMDA receptors and microglial P2Y12 receptors after status epilepticus. J. Neurosci. *34*, 10528–10540.

Habib, N., Li, Y., Heidenreich, M., Swiech, L., Avraham-Davidi, I., Trombetta, J.J., Hession, C., Zhang, F., and Regev, A. (2016). Div-Seq: Single-nucleus RNA-Seq reveals dynamics of rare adult newborn neurons. Science *353*, 925–928.

He, J., Green, A.R., Li, Y., Chan, S.Y.T., and Liu, D.X. (2020). SPAG5: An Emerging Oncogene. Trends Cancer *6*, 543–547.

Hickman, S.E., Kingery, N.D., Ohsumi, T.K., Borowsky, M.L., Wang, L.C., Means, T.K., and El Khoury, J. (2013). The microglial sensome revealed by direct RNA sequencing. Nat. Neurosci. *16*, 1896–1905.

Hoek, R.H., Ruuls, S.R., Murphy, C.A., Wright, G.J., Goddard, R., Zurawski, S.M., Blom, B., Homola, M.E., Streit, W.J., Brown, M.H., et al. (2000). Downregulation of the macrophage lineage through interaction with OX2 (CD200). Science *290*, 1768–1771.

Huang, E.J., and Reichardt, L.F. (2001). Neurotrophins: roles in neuronal development and function. Annu. Rev. Neurosci. *24*, 677–736.

Huang, W., Sherman, B.T., and Lempicki, R.A. (2009). Systematic and integrative analysis of large gene lists using DAVID bioinformatics resources. Nat. Protoc. *4*, 44–57.

Huber, W., Carey, V.J., Gentleman, R., Anders, S., Carlson, M., Carvalho, B.S., Bravo, H.C., Davis, S., Gatto, L., Girke, T., et al. (2015). Orchestrating high-throughput genomic analysis with Bioconductor. Nat. Methods *12*, 115–121.

Iacopino, A.M., and Christakos, S. (1990). Specific reduction of calcium-binding protein (28-kilodalton calbindin-D) gene expression in aging and neurodegenerative diseases. Proc. Natl. Acad. Sci. USA *87*, 4078–4082.

Inostroza, M., Cid, E., Brotons-Mas, J., Gal, B., Aivar, P., Uzcategui, Y.G., Sandi, C., and Menendez de la Prida, L. (2011). Hippocampal-dependent spatial memory in the water maze is preserved in an experimental model of temporal lobe epilepsy in rats. PLoS ONE *6*, e22372.

Jefferys, J.G.R., Menendez de la Prida, L., Wendling, F., Bragin, A., Avoli, M., Timofeev, I., and Lopes da Silva, F.H. (2012). Mechanisms of physiological and epileptic HFO generation. Prog. Neurobiol. *98*, 250–264.

Kanekura, K., Hashimoto, Y., Kita, Y., Sasabe, J., Aiso, S., Nishimoto, I., and Matsuoka, M. (2005). A Rac1/phosphatidylinositol 3-kinase/Akt3 anti-apoptotic pathway, triggered by AlsinLF, the product of the ALS2 gene, antagonizes Cu/Zn-superoxide dismutase (SOD1) mutant-induced motoneuronal cell death. J. Biol. Chem. *280*, 4532–4543.

Katic, J., Loers, G., Tosic, J., Schachner, M., and Kleene, R. (2017). The cell adhesion molecule CHL1 interacts with patched-1 to regulate apoptosis during postnatal cerebellar development. J. Cell Sci. *130*, 2606–2619.

Kiselev, V.Y., Kirschner, K., Schaub, M.T., Andrews, T., Yiu, A., Chandra, T., Natarajan, K.N., Reik, W., Barahona, M., Green, A.R., and Hemberg, M. (2017). SC3: consensus clustering of single-cell RNA-seq data. Nat. Methods *14*, 483–486.

Laurent, F., Brotons-Mas, J.R., Cid, E., Lopez-Pigozzi, D., Valero, M., Gal, B., and de la Prida, L.M. (2015). Proximodistal structure of theta coordination in the dorsal hippocampus of epileptic rats. J. Neurosci. *35*, 4760–4775.

Li, H., Handsaker, B., Wysoker, A., Fennell, T., Ruan, J., Homer, N., Marth, G., Abecasis, G., and Durbin, R.; 1000 Genome Project Data Processing Subgroup (2009). The Sequence Alignment/Map format and SAMtools. Bioinformatics *25*, 2078–2079.

Liao, Y., Wang, J., Jaehnig, E.J., Shi, Z., and Zhang, B. (2019). WebGestalt 2019: gene set analysis toolkit with revamped UIs and APIs. Nucleic Acids Res. *47*, W199–W205.

Love, M.I., Huber, W., and Anders, S. (2014). Moderated estimation of fold change and dispersion for RNA-seq data with DESeq2. Genome Biol. *15*, 550.

Luo, J., Elwood, F., Britschgi, M., Villeda, S., Zhang, H., Ding, Z., Zhu, L., Alabsi, H., Getachew, R., Narasimhan, R., et al. (2013). Colony-stimulating factor 1 receptor (CSF1R) signaling in injured neurons facilitates protection and survival. J. Exp. Med. *210*, 157–172.

Maroso, M., Szabo, G.G., Kim, H.K., Alexander, A., Bui, A.D., Lee, S.-H., Lutz, B., and Soltesz, I. (2016). Cannabinoid Control of Learning and Memory through HCN Channels. Neuron *89*, 1059–1073.

Masurkar, A.V., Srinivas, K.V., Brann, D.H., Warren, R., Lowes, D.C., and Siegelbaum, S.A. (2017). Medial and Lateral Entorhinal Cortex Differentially Excite Deep versus Superficial CA1 Pyramidal Neurons. Cell Rep. *18*, 148–160.

Mathern, G.W., Kuhlman, P.A., Mendoza, D., and Pretorius, J.K. (1997). Human fascia dentata anatomy and hippocampal neuron densities differ depending on the epileptic syndrome and age at first seizure. J. Neuropathol. Exp. Neurol. *56*, 199–212.

McInnes, L., Healy, J., and Melville, J. (2018). UMAP: Uniform Manifold Approximation and Projection for Dimension Reduction. arXiv, arXiv:1802.03426. https://arxiv.org/abs/1802.03426.

McKenzie, B.A., Dixit, V.M., and Power, C. (2020). Fiery Cell Death: Pyroptosis in the Central Nervous System. Trends Neurosci. *43*, 55–73.

Morin-Brureau, M., Milior, G., Royer, J., Chali, F., Le Duigou, C., Savary, E., Blugeon, C., Jourdren, L., Akbar, D., Dupont, S., et al. (2018). Microglial phenotypes in the human epileptic temporal lobe. Brain *141*, 3343–3360.

Morris, M.E., Baimbridge, K.G., el-Beheiry, H., Obrocea, G.V., and Rosen, A.S. (1995). Correlation of anoxic neuronal responses and calbindin-D28k localization in stratum pyramidale of rat hippocampus. Hippocampus *5*, 25–39.

Patrick, G.N., Zukerberg, L., Nikolic, M., de la Monte, S., Dikkes, P., and Tsai, L.H. (1999). Conversion of p35 to p25 deregulates Cdk5 activity and promotes neurodegeneration. Nature *402*, 615–622.

Pfisterer, U., and Khodosevich, K. (2017). Neuronal survival in the brain: neuron type-specific mechanisms. Cell Death Dis. *8*, e2643.

Pfisterer, U., Petukhov, V., Demharter, S., Meichsner, J., Thompson, J.J., Batiuk, M.Y., Martinez, A.A., Vasistha, N.A., Thakur, A., Mikkelsen, J., et al. (2020). Identification of epilepsy-associated neuronal subtypes and gene expression underlying epileptogenesis. Nat. Commun. *11*, 5038.

Prada Jardim, A., Liu, J., Baber, J., Michalak, Z., Reeves, C., Ellis, M., Novy, J., de Tisi, J., McEvoy, A., Miserocchi, A., et al. (2018). Characterising subtypes of hippocampal sclerosis and reorganization: correlation with pre and postoperative memory deficit. Brain Pathol. *28*, 143–154.

Qiu, X., Mao, Q., Tang, Y., Wang, L., Chawla, R., Pliner, H.A., and Trapnell, C. (2017a). Reversed graph embedding resolves complex single-cell trajectories. Nat. Methods *14*, 979–982.

Qiu, X., Hill, A., Packer, J., Lin, D., Ma, Y.A., and Trapnell, C. (2017b). Single-cell mRNA quantification and differential analysis with Census. Nat. Methods *14*, 309–315.

Rodrigues, G.R., Kandratavicius, L., Peixoto-Santos, J.E., Monteiro, M.R., Gargaro, A.C., Geraldi, C. de V.L., Velasco, T.R., and Leite, J.P. (2015). Increased frequency of hippocampal sclerosis ILAE type 2 in patients with mesial temporal lobe epilepsy with normal episodic memory. Brain *138*, e359.

Saghafi, S., Ferguson, L., Hogue, O., Gales, J.M., Prayson, R., and Busch, R.M. (2018). Histopathologic subtype of hippocampal sclerosis and episodic memory performance before and after temporal lobectomy for epilepsy. Epilepsia *59*, 825–833.

Scandaglia, M., Lopez-Atalaya, J.P., Medrano-Fernandez, A., Lopez-Cascales, M.T., Del Blanco, B., Lipinski, M., Benito, E., Olivares, R., Iwase, S., Shi, Y., and Barco, A. (2017). Loss of Kdm5c Causes Spurious Transcription and Prevents the Fine-Tuning of Activity-Regulated Enhancers in Neurons. Cell Rep. *21*, 47–59.

Slomianka, L., Amrein, I., Knuesel, I., Sørensen, J.C., and Wolfer, D.P. (2011). Hippocampal pyramidal cells: the reemergence of cortical lamination. Brain Struct. Funct. *216*, 301–317.

Soltesz, I., and Losonczy, A. (2018). CA1 pyramidal cell diversity enabling parallel information processing in the hippocampus. Nat. Neurosci. *21*, 484–493.

Steinlein, O.K., and Noebels, J.L. (2000). Ion channels and epilepsy in man and mouse. Curr. Opin. Genet. Dev. *10*, 286–291.

Stuart, T., Butler, A., Hoffman, P., Hafemeister, C., Papalexi, E., Mauck, W.M., 3rd, Hao, Y., Stoeckius, M., Smibert, P., and Satija, R. (2019). Comprehensive Integration of Single-Cell Data. Cell *177*, 1888–1902.e21.

Tawarayama, H., Yamada, H., Amin, R., Morita-Fujimura, Y., Cooper, H.M., Shinmyo, Y., Kawata, M., Ikawa, S., and Tanaka, H. (2018). Draxin regulates hippocampal neurogenesis in the postnatal dentate gyrus by inhibiting DCC-induced apoptosis. Sci. Rep. *8*, 840.

Thom, M., Liagkouras, I., Martinian, L., Liu, J., Catarino, C.B., and Sisodiya, S.M. (2012). Variability of sclerosis along the longitudinal hippocampal axis in epilepsy: a post mortem study. Epilepsy Res. *102*, 45–59.

Thorvaldsdóttir, H., Robinson, J.T., and Mesirov, J.P. (2013). Integrative Genomics Viewer (IGV): high-performance genomics data visualization and exploration. Brief. Bioinform. *14*, 178–192.

Valero, M., and de la Prida, L.M. (2018). The hippocampus in depth: a sublayer-specific perspective of entorhinal-hippocampal function. Curr. Opin. Neurobiol. *52*, 107–114.

Valero, M., Cid, E., Averkin, R.G., Aguilar, J., Sanchez-Aguilera, A., Viney, T.J., Gomez-Dominguez, D., Bellistri, E., and de la Prida, L.M. (2015). Determinants of different deep and superficial CA1 pyramidal cell dynamics during sharp-wave ripples. Nat. Neurosci. *18*, 1281–1290.

Valero, M., Averkin, R.G., Fernandez-Lamo, I., Aguilar, J., Lopez-Pigozzi, D., Brotons-Mas, J.R., Cid, E., Tamas, G., and Menendez de la Prida, L. (2017). Mechanisms for Selective Single-Cell Reactivation during Offline Sharp-Wave Ripples and Their Distortion by Fast Ripples. Neuron *94*, 1234–1247.e7.

van der Maaten, L., and Hinton, G. (2009). Visualizing Data using t-SNE. J. Mach. Learn. Res. *9*, 2579–2605.

Vest, R.S., O'Leary, H., Coultrap, S.J., Kindy, M.S., and Bayer, K.U. (2010). Effective post-insult neuroprotection by a novel Ca(2+)/ calmodulin-dependent protein kinase II (CaMKII) inhibitor. J. Biol. Chem. *285*, 20675–20682.

Vezzani, A., and Baram, T.Z. (2007). New roles for interleukin-1 Beta in the mechanisms of epilepsy. Epilepsy Curr. *7*, 45–50.

Winden, K.D., Bragin, A., Engel, J., and Geschwind, D.H. (2015). Molecular alterations in areas generating fast ripples in an animal model of temporal lobe epilepsy. Neurobiol. Dis. *78*, 35–44.

Wittner, L., Eross, L., Szabó, Z., Tóth, S., Czirják, S., Halász, P., Freund, T.F., and Maglóczky, Z.S. (2002). Synaptic reorganization of calbindin-positive neurons in the human hippocampal CA1 region in temporal lobe epilepsy. Neuroscience *115*, 961–978.

Wyler, A.R., Curtis Dohan, F., Schweitzer, J.B., and Berry, A.D. (1992). A grading system for mesial temporal pathology (hippocampal sclerosis) from anterior temporal lobectomy. J. Epilepsy *5*, 220–225.

You, J.C., Muralidharan, K., Park, J.W., Petrof, I., Pyfer, M.S., Corbett, B.F., LaFrancois, J.J., Zheng, Y., Zhang, X., Mohila, C.A., et al. (2017). Epigenetic suppression of hippocampal calbindin-D28k by ΔFosB drives seizure-related cognitive deficits. Nat. Med. *23*, 1377–1383.

Zeisel, A., Muñoz-Manchado, A.B., Codeluppi, S., Lönnerberg, P., Manno, G., La Juréus, A., Marques, S., Munguba, H., He, L., Betsholtz, C., et al. (2015). Cell types in the mouse cortex and hippocampus revealed by single-cell RNA-seq. Science *347*, 1138–1142.

Zeisel, A., Hochgerner, H., Lönnerberg, P., Johnsson, A., Memic, F., van der Zwan, J., Häring, M., Braun, E., Borm, L.E., La Manno, G., et al. (2018). Molecular Architecture of the Mouse Nervous System. Cell *174*, 999–1014.e22.

Cell Reports
Article

STAR★METHODS

KEY RESOURCES TABLE

REAGENT or RESOURCE	SOURCE	IDENTIFIER
Antibodies		
Rabbit anti-calbindin D-28k	Swant	Cat# CB38; RRID: AB_10000340
Mouse anti-calbindin D-28k	Swant	Cat# 300; RRID: AB_10000347
Rabbit anti-Wfs1	Proteintech	Cat# 11558-1-AP; RRID: AB_2216046
Rabbit anti-Iba1	Wako	Cat# 019-19741; RRID: AB_839504
Rabbit anti-GFAP	Sigma	Cat# G9269; RRID: AB_477035
Rabbit anti-Olig2	Millipore	Cat# AB9610; RRID: AB_570666
Rabbit anti-cFos	Santa Cruz Biotechnology	Cat# sc-52; RRID: AB_2106783
Alexa Fluor633 goat anti-rabbit IgG	Thermo Fisher	Cat# A21070; RRID: AB_2535731
Alexa Fluor488 donkey anti-mouse IgG	Thermo Fisher	Cat# A21202; RRID: AB_141607
Alexa Fluor488 goat anti-mouse IgG	Jackson Immunoresearch	Cat# 115-545-003; RRID: AB_2338840
Rhodamine Red goat anti-mouse IgG	Jackson Immunoresearch	Cat# 115-295-003; RRID: AB_2338756
Alexa Fluor488-conjugated streptavidin	Jackson Immunoresearch	Cat# 016-540-084; RRID: AB_2337249
Chemicals, peptides, and recombinant proteins		
BSA	Sigma	A7906
EDTA	Sigma	607-429-00-8
PBS	VWR	E404-200 TABS
Tris-HCl	Sigma	T5941
NaCl	VWR	7647-14-5
MgCl2	Sigma	M2670
IGEPAL	Sigma	I8896
ARCTURUS PicoPure RNA isolation kit	Thermo Fisher Scientific	KIT0204
RNase-free DNase set	QIAGEN	79254
Bisbenzimide H33258	Sigma-Aldrich	Cat# B2883; CAS: 23491-45-4
Neurobiotin tracer	Vector Labs	Cat# SP-1120
FluoroJade C dye	Sigma	AG325
DPX mountant	VWR	360294H
ProLong Gold antifade mountant	ThermoFisher Scientific	P10144
Critical commercial assays		
Chromium single cell 3′ library & gel bead kit v2	10x Genomics	cat#: 120237 (v2)
Chromium i7 multiplex kit	10x Genomics	N/A
Chromium single cell A chip kit	10x Genomics	cat#: 120236
TruSeq stranded mRNA library prep kit	Illumina	cat#: RS-122-2101/2
HiSeq sequencing kit TruSeq v4	Illumina	cat#: FC-401-4003
RNAscope fluorescent multiplex reagent kit	ACD	320850
Deposited data		
LCM-RNA-seq	Gene Expression Omnibus (NCBI)	GSE143555
snRNA-seq	Gene Expression Omnibus (NCBI)	GSE143560
Experimental models: organisms/strains		
Mouse: Thy1.2-G-CaMP7-DsRed2	RIKEN Bioresources Center	stock RBRCO6579
Mouse: Calb1-2A-dgCre-D	Jackson Labs	N/A
Mouse: TdTomato reporter line Ai9	Jackson Labs	Stock No:007905
Rat: Wistar	Instituto Cajal Animal facility	N/A
Mouse: C57BL/6	Instituto Cajal Animal facility	N/A

Continued

REAGENT or RESOURCE	SOURCE	IDENTIFIER
Oligonucleotides		
Wfs1-forw (5′CATCCCCAACAACCTGTTCC)	Sigma	NM_031823.1, bp 783-1631
Wfs1-rev (5′ACACCAGGTAGGGCACCACC)	Sigma	N/A
Ndst4-forw (5′ATACATCCAAAACTGATCCCAC)	Sigma	XM_006233274.2, bp 536-1024
Ndst4-rev (5′AAAAGCACTGGCTGGTAGGTAG)	Sigma	N/A
Syt17-forw (5′ACACATCCAAGTCCACATACAG)	Sigma	NM_138849.1, bp 378-1118
Syt17-rev (5′GTGTACCAGCTGGATTTTCACA)	Sigma	N/A
Hrt1a-forw (5′CTTTCTATATCCCGCTGTTGCT)	Sigma	J05276.1, bp 730-1663
Hrt1a-rev (5′CACACAGATACTAGTGGTTCTC)	Sigma	N/A
Scn7a-for (5′GATTATTTCTTCCCTTGTGTATGC)	Sigma	NM_131912.1, bp 2812-3550
Scn7a-rev (5′CTAAAGTCATCTTCGCTCAAGG)	Sigma	N/A
Recombinant DNA		
Mm-Spag5	ACD	505691
Mm-Dcc-C3	ACD	427491-C3
Mm-Dapk1-C3	ACD	880221-C3
RNAscope 3-plex positive control probe-Mm	ACD	320881
RNAscope 3-plex negative control probe	ACD	320871
Software and algorithms		
Sequencer Software HiSeq Control Software	Illumina, Inc	https://support.illumina.com/sequencing/sequencing_instruments/hiseq_2500/downloads.html?langsel=/us
R	R Foundation for Statistical Computing	https://www.R-project.org/; RRID: SCR_001905
RStudio	RStudio, PBC	https://www.rstudio.com/; RRID: SCR_000432
FastQC	Simon Andrews	https://www.bioinformatics.babraham.ac.uk/projects/fastqc; RRID: SCR_014583
STAR	Dobin et al., 2013	https://code.google.com/archive/p/rna-star; RRID: SCR_004463
Samtools	Li et al., 2009	http://samtools.sourceforge.net; RRID: SCR_002105
HTSeq	Anders et al., 2015	https://htseq.readthedocs.io/en/master/; RRID: SCR_005514
DESeq2	Love et al., 2014	http://www.bioconductor.org/packages/release/bioc/html/DESeq2.html; RRID: SCR_015687
Cell Ranger	Huang et al., 2009	https://david.ncifcrf.gov; RRID: SCR_017344
Seurat	Butler et al., 2018; Stuart et al., 2019	http://satijalab.org/seurat/; RRID: SCR_016341
Monocle 2	Qiu et al., 2017a, 2017b	http://cole-trapnell-lab.github.io/monocle-release; RRID: SCR_016339
DAVID Bioinformatics	Huang et al., 2009	https://david.ncifcrf.gov; RRID: SCR_001881
Webgestalt	Liao et al., 2019	http://www.webgestalt.org; RRID: SCR_006786
MATLAB 2016b	Mathworks	https://www.mathworks.com; RRID: SCR_001622
ImageJ	NIH Image	https://imagej.net/ImageJ; RRID: SCR_003070
SPSS Statistics	IBM	https://www.ibm.com/products/spss-statistics; RRID: SCR_002865
Other		
Resource website for the LCM RNA-seq data	This paper	http://lopezatalayalab.in.umh-csic.es/CA1_Sublayers_&_Epilepsy
Resource website for the snRNA-seq data	This paper	http://lopezatalayalab.in.umh-csic.es/CA1_SingleNuclei_&_Epilepsy
Silicon probes: 16-channel linear; 100 μm inter-spacing; 413 μm2 electrode area	Neuronexus	A1x16-5mm-100-413

Cell Reports
Article

RESOURCE AVAILABILITY

Lead contact

Further information and requests for reagents and resources may be directed to the lead contact, Dr. Liset M de la Prida (lmprida@cajal.csic.es).

Materials availability

This study did not generate any new unique reagents.

Data and code availability

No unpublished custom code, software or algorithm was used in this study. Freely available software and algorithms used for analysis are listed in the resource table. Some analyses were specifically designed for the purpose of this paper using routines written in MATLAB 7.10 (MathWorks). All custom scripts and data contained in this manuscript are available upon request from the Lead Contact. The accession number for the bulk-tissue transcriptome (LCM RNA-seq) and single-nuclei RNA-seq (snRNA-seq) data reported in this paper is Gene Expression Omnibus (GEO) database: GSE143555 (LCM RNA-seq) https://www.ncbi.nlm.nih.gov/geo/query/acc.cgi?acc=GSE143555; GSE143560 (snRNA-seq) https://www.ncbi.nlm.nih.gov/geo/query/acc.cgi?acc=GSE143560. Two open web applications provide visualization of transcriptomic data: LCM RNA-seq data: http://lopezatalayalab.in.umh-csic.es/CA1_Sublayers_&_Epilepsy. snRNA-seq data: http://lopezatalayalab.in.umh-csic.es/CA1_SingleNuclei_&_Epilepsy.

EXPERIMENTAL MODEL AND SUBJECT DETAILS

All experimental protocols and procedures were performed according to the Spanish legislation (R.D. 1201/2005 and L.32/2007), the European Communities Council Directives of 1986 (86/609/EEC) and 2003 (2003/65/CE) for animal research, and were approved by the Ethics Committee of the Instituto Cajal.

Adult male Wistar rats (180–200 g; 6-8 weeks postnatal), as well as wild-type C57 and transgenic mice (20-25 g; 8-9 weeks postnatal), were treated with multiple intraperitoneal injections of kainate (5 mg/kg) at hourly intervals until they reached *status* epilepticus. Transgenic mouse lines included the Thy1.2-G-CaMP7-DsRed2 (c57BL/6J-Tg(Thy1-G-CaMP7-DsRed2)492Bsi, stock RBRCO6579, RIKEN) and the Calb1-Cre (Jackson Lab, stock No:023531; Calb1-2A-dgCre-D) crossed with the tdTomato reporter line (Jackson Lab, stock No:007905; Ai9). The *status* was defined as a condition of continuous seizures lasting longer than 30 min. In a subset of rats, the lithium-pilocarpine model was used. These rats were i.p. injected with pilocarpine hydrochloride 12–24 h after the injection of lithium chloride (127 mg/kg, i.p.). Between one and four doses of 10 mg/kg pilocarpine were injected every 30 min until the *status* epilepticus was reached. Diazepam (4 mg/kg) was injected 1 h post-*status* to stop convulsions in all animals. They received intraperitoneal injections of 5% dextrose in saline (2.5 ml) and their diet was supplemented with fruit and powder milk during the following 2–3 days. After 3 days, animals behaved normally and were housed individually. Control animals were injected with saline and received treatments similar to epileptic animals.

Animals used in this study were examined in the chronic phase of the *status epilepticus* model of TLE (2-23 weeks post-*status*) when they already exhibited spontaneous seizures and interictal discharges (IID) (Figures S1A and S1B). In epileptic rats and mice, these events were typically associated with high-frequency oscillations (HFOs; Figure S1B), which are considered biomarkers of epileptogenesis (Jefferys et al., 2012; Valero et al., 2017). We focused on the dorsal hippocampus given the major role in associated cognitive comorbidities of epilepsy and more consistent neuronal loss as compared to ventral (Thom et al., 2012; Valero et al., 2017). In some epileptic animals, we aimed to induce convulsive seizures using high-pitched sounds (pulses of 95-100 dB and 1-20 s duration at random intervals of 1-20 s during 10 min). A convulsive motor seizure was defined according to clinical criteria, as sustained and repeated forelimbs automatisms with or without falling. Control animals did never exhibit convulsive seizures using this protocol.

METHOD DETAILS

EEG recordings and analysis

To evaluate epileptogenesis, some rats and mice were implanted with either intracranial 16-channel silicon probes or skull EEG-grid of 32-channels (Neuronexus) under isoflurane anesthesia (1.5%–2% mixed in oxygen 400–800 ml/min). Jeweler's screws were inserted into the skull for providing additional anchoring and reference/ground connections (over the cerebellum). The implant was secured with dental cement. Animals were recovered from anesthesia and returned to home cages.

For recordings, EEG signals were pre-amplified (4x gain) and recorded with a 32-channel AC amplifier (Axona), further amplified by 100, filtered by analog means at 1 Hz to 5 kHz, and sampled at 20 kHz/channel with 12 bits precision. EEG recordings were synchronized with a ceiling video camera (30 frames/s) to track the animal position in space.

Analysis of electrophysiological signals was implemented in MATLAB 9.3 (MathWorks). EEG signals from the frontal and parietal electrodes were used to identify theta periods during running (band-pass 4-12 Hz) and periods of immobility characterized by low frequency delta activity (0.5-4 Hz). Forward-backward-zero-phase finite impulse response (FIR) filters of order 512 were used to

preserve temporal relationships between channels and signals. Spectral values fitted to 1/f were similar between groups for frequencies > 150 Hz. HFO events were defined from the bandpass filtered signal (80-120 Hz) by thresholding (> 4 SDs). The power spectra were evaluated in a window of ± 0.2 ms around each detected event. Time-frequency analysis was performed by applying the multitaper spectral estimation in sliding windows with 97.7% overlap and frequency resolution of 10 Hz in the 90-600 Hz frequency range. HFO activity was evaluated as the power integral in the 80-120 Hz band.

We used a combination of features to identify HFO events automatically and to classify them in different categories (Valero et al., 2017) (Figure S1). First, we identified large amplitude transient (< 100 ms) discharges using LFP and current-source-density signals (CSD, i.e., the second spatial derivative) at the SR and SLM. Second, we identified HFO events at the SP by frequency thresholding over 100 Hz. Then we used spectral indices such as entropy and fast ripple indices from candidate HFO events at SP together with amplitude information from LFP and CSD signals at SR to classify events as: a) SPW-ripples (low amplitude; 100-150 Hz); b) SPW-fast ripples (medium amplitude, > 150 Hz) and IID-HFO (larger amplitude, > 100 Hz). Events not meeting criteria were left unclassified. Surface EEG recordings from mice were analyzed similarly, by using channels over the dorsal hippocampus or at the frontal cortex to identify HFO events and channels over the parietal cortex using selected segments of the EEG.

In vivo recording and labeling of single cells

Rats were anesthetized with urethane (1.2 g/kg, i.p.), fastened to the stereotaxic frame and warmed to keep their body temperature at 37°C. Two bilateral craniotomies of ~1 mm diameter were performed for CA3 stimulation (AP: −1.2 mm, ML: 2.9 mm) and CA1 recordings (AP: −3.7 mm; ML: 3 mm). The dura was gently removed, the *cisterna magna* was drained and the craniotomy covered with warm agar to reinforce stability.

A 16-channel silicon probes (NeuroNexus Tech; 100 μm interspaced, 413 μm² contact) was advanced perpendicular along the CA1-DG-CA3c axis guided by extracellular stimulation and electrophysiological hallmarks. Concentric bipolar electrodes were advanced 3.5 mm with 30° in the coronal plane to stimulate CA3. Stimulation consisted of biphasic square pulses (0.2 ms duration, 0.05-1.2 mA every 5 s). Extracellular signals were pre-amplified (4x gain) and recorded with a 16(32)-channel AC amplifier (Multichannel Systems), further amplified by 100, analogically filtered at 1Hz to 5 kHz, and sampled at 20 kHz/channel with 12 bits precision with a Digidata 1440. A subcutaneous Ag/AgCl wire in the neck served as reference. Recording and stimulus position was confirmed by post hoc histological analysis.

Intracellular recording and labeling were obtained in current-clamp mode using sharp pipettes (1.5 mm/0.86 mm outer/inner diameter borosilicate glass; A-M Systems, Inc) filled with 1.5 M potassium acetate and 2% Neurobiotin (Vector Labs, Inc; 50-100 MΩ) (Cid and de la Prida, 2019). Signals were acquired with an intracellular amplifier (Axoclamp 900A) at 100x gain. The resting potential, input resistance and amplitude of action potentials was monitored all over the course of experiments.

After data collection, Neurobiotin was ejected using 500 ms depolarizing pulses at 1-3 nA at 1 Hz for 10-45 min. Animals were perfused with 4% paraformaldehyde (PFA) and 15% saturated picric acid in 0.1 M, pH 7.4 phosphate buffered saline (PBS). Brains were postfixed overnight at room temperature (RT), washed in PBS and serially cut in 70 μm coronal sections (Leica VT 1000S vibratome). Sections containing the stimulus and probe tracks were identified with a stereomicroscope (S8APO, Leica). Sections containing Neurobiotin-labeled cells were localized by incubating them in 1:400 Alexa Fluor 488-conjugated streptavidin (Jackson ImmunoResearch 016-540-084) with 1% Triton X-100 in PBS (PBS-Tx) for 2 hours at room temperature (RT). To evaluate morphological features of single cells, sections containing the somata of recorded cells were processed with Triton 1% in PBS, blocked with 10% fetal bovine serum (FBS) in PBS-Tx and incubated overnight at RT with the primary antibody solution containing rabbit anti-Calbindin (1:500, CB D-28k, Swant CB-38) or mouse anti-Calbindin (1:1000, CB D-28k, Swant 300) antibodies with 1% FBS in PBS-Tx. After three washes in PBS-Tx, sections were incubated for 2 hours at RT with appropriate secondary antibodies: goat anti-rabbit Alexa Fluor 633 (1:500, Invitrogen, A21070), and goat anti-mouse Alexa Fluor488 (Jackson Immunoresearch, 115-545-003) or goat anti-mouse Rhodamine Red (1:200, Jackson ImmunoResearch, 115-295-003) in PBS-Tx-1% FBS. Following 10 min incubation with bisbenzimide H33258 (1:10000 in PBS, Sigma, B2883) for nuclei labeling, sections were washed and mounted on glass slides in Mowiol (17% polyvinyl alcohol 4-88, 33% glycerin and 2% thimerosal in PBS).

All morphological analyses were performed blindly to electrophysiological data. The distance from the cell soma to radiatum was measured from confocal images using information from Calbindin and bisbenzimide staining. All pyramidal cells included in this study were localized within the CA1 region. Calbindin immunostaining was used to estimate the width of the superficial sub-layer from the border to the stratum radiatum. Superficial cells were defined based on the location of the soma within the calbindin sublayer, independently on their immunoreactivity (Valero et al., 2015). The border with radiatum was estimated for each section and the distance from the recorded cell somata was measured using ImageJ (NIH Image).

Analysis of intracellular single-cell recordings

Interictal discharges and sharp-waves associated with HFO events (ripples or fast ripples) recorded simultaneously to the intracellular membrane potential were detected as explained before. The timing of these events was used to identify the corresponding membrane potential deflections. Time-frequency analysis of HFO events was performed by applying the multitaper spectral estimation in sliding windows with 97.7% overlap and frequency resolution of 10 Hz in the 90-600 Hz frequency range (only the 100-600 Hz range is shown) to data sweeps aligned by sharp-wave ripple events (±1 s). Membrane potential responses of single-cells were evaluated in peri-event plots before (−200 to −150 ms), during (±50 ms) and after (150 to 200 ms) HFO events.

Cell Reports
Article

Passive electrophysiological properties (input resistance, membrane decay and capacitance) of neurons recorded intracellularly *in vivo* were measured using 500 ms currents step in current-clamp mode. Cells with intracellular action potential amplitude smaller than 40 mV were excluded. Resting membrane potential and input resistance were estimated by linear regression between baseline potential data and the associated holding current. Intrinsic firing properties, including action potential threshold, half-width duration and AHP were estimated from the first spike in response to depolarizing current pulses of 0.2 nA amplitude and 500 ms duration. The sag and maximal firing rate were calculated from current pulses of $\pm$ 0.3 nA amplitude. A bursting index was defined as the ratio of the number of complex spikes (minimum of 3 spikes < 8 ms inter-spike interval) over the total number of spikes recorded during theta activity.

cFos immunostaining and analysis

To evaluate immediate-early gene expression associated to sound-induced convulsive seizures, animals were perfused 1 hour after and their brains cut in 70 μm coronal sections. Selected sections were stained against c-Fos using a polyclonal antibody at 1:250 (Santa Cruz Biotechnology sC-52) and bisbenzimide. Using one 20x confocal mosaic per animal, we quantified cFos intensity at CA1 pyramidal cells by delineating single-cell nuclei stained with bisbenzimide in one confocal plane (ImageJ). The mean intensity of cFos signal from each cell was then normalized by subtracting the background (set at 0) and dividing by the maximal positive signal in the mosaic, which was always at granule cell level (set at 1). No significant differences of background were observed across sections. Delineated cells were ranked by their distance to radiatum to classify them as deep or superficial, according to standard measurements of Calb1-layer thickness.

Laser capture microdissection (LCM) and RNA isolation

Brains from 3 control and 3 epileptic rats were dissected, longitudinally cut in half (separating both hemispheres), wrapped in aluminum foil and immediately frozen in liquid nitrogen. To avoid circadian effects on gene expression all samples were collected in the morning before noon and conserved at -80°C until use. The hippocampal region of each hemisphere was cut in 20 μm slices in a cryostat (Leica) (chamber temperature: -20°C; block temperature: -30°C) and placed on 1.0 mm PEN-membrane covered slides (Carl Zeiss). Slides were conserved at -20°C until use. Right before microdissection, slides were dried with vapor of liquid nitrogen. The CA1 cell layer was microdissected with a Leica 6000 laser microdissector through a 40x non-oil immersion objective to obtain cell bodies of superficial and deep sublayers separately (Figure 2A). Microdissected deep and superficial areas were collected in different empty caps of 0.5 mL Eppendorf tubes. After microdissection, samples were processed following ARCTURUS PicoPure RNA Isolation Kit (Thermo Fisher Scientific) instructions in order to extract and isolate total RNA. Briefly, 50 μl of extraction buffer was added into the cap, incubated at 42°C for 30 min, centrifuged at 800 x G for 2 min and stored at -80°C. The same volume of 70% ethanol was added to the cell extract and the mixture was pipetted into a pre-conditioned RNA purification column. The column was centrifuged 2 min at 100 x G and 30 s at 16000 x G, and washed with 100 μl of Wash Buffer 1. To completely eliminate DNA, the purification column was treated with 40 μl of DNase (diluted 1/8 in RDD Buffer) (QIAGEN), incubated 15 min and centrifuged at 8000 x G for 15 s. Then the column was washed twice with 100 μl of Wash Buffer 2, and centrifuged at 8000 x G after the first wash and at 16000 x G after the second one. Finally, RNA was eluted into a new 0.5 μl Eppendorf tube by adding 11 μl of elution buffer onto the column membrane, incubating the column for 1 min at room temperature, and centrifuging the column for 1 min at 1000 x G and at 16000 x G immediately after. Total RNA samples were stored at -80°C. RNA integrity number (RIN) was similar in control (4.7 $\pm$ 0.8) and epileptic rats (5.7 $\pm$ 0.5; p = 0.07; 3 replicates x 2 sublayers per group), as well as for deep (5.2 $\pm$ 0.9) and superficial sublayers (5.3 $\pm$ 0.1; p = 0.81; n = 6 replicates per sublayers).

LCM RNA-seq library construction and sequencing

RNA preparation for sequencing deep and superficial CA1 sublayers from control and epileptic rats was performed as described in Scandaglia et al. (2017). The twelve samples were sequenced according to manufacturer instructions in a HiSeq2500 sequencer (Illumina, Inc). Libraries were strand specific (reverse) and sequenciation was performed in paired-end configuration with a read length of 75 bp. Library size of read pairs for the different samples analyzed was between 47 and 59 Million reads. RNA-seq data can be accessed at the GEO repository (GSE143555).

LCM RNA-seq data analysis

Alignment quality control of sequenced samples (LCM RNA-seq) was assessed with FastQC (v.0.11.3) (Babraham Institute) and RNA-seq tracks were visualized using IGV (v.2.3.57) (Thorvaldsdóttir et al., 2013). LCM RNA-seq reads were mapped to the rat genome (Rnor_6.0.83) using STAR (v.2.5.0c) (Dobin et al., 2013), and files were further processed with Samtools (v.0.1.19). Aligned reads were counted to gene transcripts using HTSeq (v.0.6.1) (Anders et al., 2015). Differential expression analysis was performed using DESeq2 (v.1.10.0) (Love et al., 2014) of the bioconductor suite (Huber et al., 2015) in the R (v.3.2.2) statistical computing platform. The experimental design consisted in two factors (treatment and anatomical area) and there was also grouped samples (samples from different anatomical areas (minus (deep) and plus (superficial) that were obtained from individual mice). Genes were considered differentially expressed at Benjamini-Hochberg (BH) adj. p < 0.05 and FC > 0.3 (Benjamini and Hochberg, 1995), except otherwise specified. GO analysis was performed using DAVID (v.6.8) bioinformatics platform (Huang et al., 2009).

LCM RNA-seq single-cell informed data analysis

Single-cell RNA-seq data from Zeisel et al. (2015) was reanalyzed with consensus cluster SC3 algorithm (Kiselev et al., 2017). From the original 3,005 cells, pyramidal and interneurons were removed from somatosensory cortex, resulting in a total of 2,442 cells. Remaining cells were re-analyzed downstream with SC3. Clustering stability was optimal for 6 clusters. One cluster presented high heterogeneity (mixed population cluster), and was reanalyzed with the optimal clustering stability (5 clusters). Marker genes were tested for every cluster with Wilcoxon signed rank test. Top 10 genes with the area under the receiver operating characteristic (ROC) curve (AUC) power > 0.85 and with the adj. $p < 0.01$ from both cluster analyses were selected, with a total of 69 bona fide population markers. Based on the markers, populations were fused/splitted and 3 populations were isolated in the first clustering (pyramidal neurons, interneurons and oligodendrocytes) and 4 more in the second (astrocytes, endothelial cells, microglia and mural cells). Sixteen outlier cells were removed by total_counts, total_features or pct_counts_spike criteria, remaining 2,426 cells with a high correspondence with the original classification: Astrocytes (155 cells), Endothelial (177 cells), Interneurons (174 cells), Microglia (85 cells), Mural (56 cells), Oligodendrocytes (804 cells) and Pyramidal (975 cells). Next, to capture convoluted gene signatures on LCM RNA-seq we used gene sets of equal size that were differentially regulated between superficial and deep sublayers of control and epileptic rats. To obtain these gene sets, we first filtered the genes by significance (adj. $p < 0.1$), then significantly differentially regulated genes were ranked by fold-change, and top 250 differentially regulated genes for each sublayer and condition, were retained for further analysis. We then, obtained normalized gene expression from scRNA-seq data for these gene sets and performed linear dimensionality reduction by principal component analysis to summarize and visualize the cells in the low-dimensional space. We also performed Pearson pairwise correlation and hierarchical clustering for these gene sets across all cells, to capture cell-type specific gene signatures that were mapped to major cell types in CA1 by using previously identified cell markers.

Single-cell RNA-seq data from Allen Brain Map portal - Mouse Whole Cortex and Hippocampus SMART-seq (2019) with 10x-SMART-seq taxonomy (2020) (http://portal.brain-map.org/atlases-and-data/rnaseq/mouse-whole-cortex-and-hippocampus-smart-seq) was downloaded and subsetted as follows: from the original 76,533 cells, cells from hippocampal region were retained, and subsequently, cells from CA2, CA3, DG or empty subclass were removed. Then, cells of subclasses Astro, Micro-PVM, Endo, Oligo or VLMC were added. This initial filtering led a total of 5,506 cells. Of these, cells tagged by subclass as CA1-ProS (1,592 cells), Astro (976 cells), Lamp5 (864 cells), Vip (462 cells), Sncg (416 cells), Sst (266 cells), Oligo (236 cells), Endo (213 cells), Micro-PVM (176 cells), VLMC (159 cells), Pvalb (69 cells) were retained for further analysis, while cells tagged by subclass as SUB-ProS (29 cells), L2 IT RHP (21), NP SUB (9), L2/3 IT CTX-1 (3), L5 IT TPE-ENT (3), Sst Chodl (3), L2/3 IT ENTl (2), L6 CT CTX (2), Meis2 (2), L2/3 IT CTX-2 (1), L2/3 IT PPP (1), L6b CTX (1) were removed because of their low cell number and/or mismatch with CA1 or glial cells. The remaining 5,429 cells were grouped in their corresponding major cell populations as follows: Astrocytes (Astro) (976 cells), Endothelial (Endo) (213 cells), Interneurons (Lamp5, Pvalb, Sncg, Sst, Vip) (2077 cells), Microglia (Micro-PVM) (176 cells), Mural (VLMC) (159 cells), Oligodendrocytes (Oligo) (236 cells) and Pyramidal (CA1-ProS) (1,592 cells). Next, we proceed as indicated before to capture convoluted gene signatures on LCM RNA-seq by using normalized expression data from this scRNA-seq dataset, for differentially regulated between superficial and deep sublayers of control and epileptic rats.

Single-nuclei isolation

We accurately isolated single nuclei from 2 control and 2 epileptic Calb1::CrexTdTomato young adult mice. We used these animals to facilitate identification of the CA1 region under a fluorescent scope. Animals were sacrificed 12 weeks after the kainate/saline administration by cervical dislocation and brains were dissected and cut in 300 um thick slices in a vibratome covered by ice cold HBBS 1x. As in LCM studies, samples were collected before noon to avoid circadian effects. The dorsal CA1 region were manually dissected from 4 consecutive slices and put altogether into 400 μL of ice-cold MACS buffer (0,5% BSA, 2 mM EDTA, PBS 1x). CA1 portions were transferred to a dounce homogenizer (20404 Lab Unlimited) containing 400 μL of MACS buffer and were homogenized 12-15 times each with the pestle. The cell suspension was transferred to a 2 mL Eppendorf tube and centrifuge 15 min 500 x G 4°C. Cell pellets were resuspended in 500 μL of lysis buffer (10 mM Tris-HCL, 10 mM NaCl, 3 mM $MgCl_2$, 0,1% IGEPAL) and kept 5 min on ice. Samples were then spun down at 500 x G for 30 min in a pre-chilled centrifuge. The nuclei pellet was resuspended in PBS 1x 1% BSA and then 15,000 nuclei were purified by flow cytometry in a BD FACS Aria III. The whole process was carried out at 4°C.

Single-nucleus RNA sequencing

Purified intact nuclei from mouse hippocampal CA1 area were processed through all steps to generate stable cDNA libraries. For every sample, 15,000 nuclei were loaded into a Chromium Single Cell A Chip (10x Genomics) and processed following the manufacturer's instructions. Single-nuclei RNA-seq libraries were prepared using the Chromium Single Cell 3′ Library & Gel Bead kit v2 and i7 Multiplex kit (10x Genomics). Pooled libraries were then loaded on a HiSeq2500 instrument (Illumina) and sequenced to obtain 75 bp paired-end reads following manufacturer instructions. On sequencing depth, 262 million fragments were generated for the control condition and 296 for the epileptic dataset. Libraries reached a sequencing saturation of 86.9% for control and 91.2% for epilepsy condition. snRNA-seq data can be accessed at the GEO repository (GSE143560).

snRNA-seq analysis

Quality control of sequenced reads was performed using FastQC (Babraham Institute). Sequenced samples were processed using the Cell Ranger (v.2.2.0) pipeline (10x Genomics) and aligned to the GRCm38 (mm10) mouse reference genome customized to count

Cell Reports
Article

reads in introns (pre-mRNA) over the Ensembl gene annotation version 94. Barcodes with total unique molecular identifier (UMI) count > 10% of the 99th percentile of the expected recovered cells were selected for further analysis. Using this criterion, we retrieved 3,661 (control), 3,078 (epileptic) high quality nuclei per sample. Mean reads per nucleus were 71,449 (control) and 96,150 (epileptic). Median genes per nucleus were 71,449 (control) and 96,150 (epileptic). Minimum UMI count per nucleus were 710 (control), 540 (epileptic), well above the typical quality standards in single-cell/nucleus sequencing. Single-nucleus RNA-seq data were subsequently pre-processed and further analyzed in R (v.3.4.4) using Seurat (v.2.3.4) (Butler et al., 2018; Stuart et al., 2019). Filtering parameters were as follows: genes, nCell < 5; cells, nGene < 200. Data were then normalized using global-scaling normalization (method: LogNormalize, scale.factor = 10,000).

An initial exploratory analysis was performed on each dataset separately. This analysis retrieved a similar number of clusters in each dataset that were approximately equal in size. We next combined both datasets using the function MergeSeurat. Highly variable genes (HVGs) were detected using FindVariableGenes function with default parameters. Then, normalized counts on HVGs were scaled and centered using ScaleData function with default parameters. Principal component analysis (PCA) was performed over the first ranked 1,000 HVGs. Plots of the two principal components of the PCA, where cells were colored by dataset, excluded the presence of batch effects. Cluster detection was carried out with Louvain algorithm in FindClusters function, using 20 first PCA dimensions and resolution of 0.6 (the default number in Seurat and the optimal according to cell number, data dispersion and co-expression of previously reported cell markers). Plots of the two principal components of the PCA where cells were colored by dataset of origin excluded the presence of batch effects.

This analysis identified 13 clusters. CA1 pyramidal neurons populated three of these clusters: one cluster was enriched in bona fide gene markers of deep cells (*Ndst4*, *Coll11a1*) whereas a second one was enriched in canonical markers of superficial cells (*Calb1*, *Epha3*). The third cluster showed a mixed identity. An additional round of clustering segmented this population in three additional clusters that were enriched in deep and superficial markers, respectively, and a third cluster that could not be annotated based on the presence of gene markers of CA1 sublayer neurons. The vast majority of cells within this cluster (66/67) were from epileptic mice (Pyr_ES). Next, the FindMarkers function was used to identify gene markers and to determine the cell populations represented by each cluster. Finally, cell subtypes were manually aggregated based on the presence of canonical markers of known cell types into six distinct major cell types: excitatory neurons (Excit); inhibitory neurons (Inter); oligodendrocytes (ODC); oligodendrocyte progenitor cells (OPCs); microglia (Microglia); astrocytes (Astro).

Visualization and embedding were performed using stochastic nearest neighbors (tSNE) (van der Maaten and Hinton, 2009) and uniform manifold approximation and projection (UMAP) (McInnes et al., 2018) methods over PCA using the 20 first PCA dimensions. UMAP plots of gene expression show normalized count (UMIs) per nucleus. The equalized expression between fixed percentiles was plotted according to the following criterion: the minimum expression was adjusted to 5% and the maximum expression was adjusted to 95% in all UMAP expression plots. To evaluate effects of epilepsy, datasets from both conditions were merged and HVGs were identified for each dataset as above indicated. Only HVGs that were detected in all datasets were used to perform visualization and embedding as described above. Clustering was performed on merged dataset from both conditions and populations were identified combining these results with clustering information obtained in control and epileptic datasets separately, together with co-expression of population markers.

Differential expression analysis (DEA) was used to identify population gene markers. For DEA, the nuclei of each population were contrasted against all the other nuclei in the merged dataset using Wilcoxon Rank Sum test on normalized counts. For epilepsy effect analysis, in the merged dataset, the nuclei of each population from the epileptic dataset were contrasted against all the other nuclei of the same population in control using Wilcoxon Rank Sum test on normalized counts. GO functional enrichment analyses were performed using DAVID (v.6.8) bioinformatics platform (Huang et al., 2009). All DEA and functional enrichment analyses applies False Discovery Rate (FDR) method by BH post hoc p adjustment, except otherwise specified.

Cell trajectories and pseudotime analysis

The disease pseudotime analysis was performed using Monocle 2 (v.2.8.0) (Qiu et al., 2017a, 2017b). First, the Seurat merged dataset was transformed to Monocle object and cells from Pyr_CA1 were subset. The size factor and dispersion of the subset was estimated, and data was normalized and preprocessed. Genes under the minimum level detection threshold of 0.1 and detected in less than 10 cells were filtered with the function setOrderingFilter. Genes defining how a cell progress through a pseudo-time disease trajectory were selected with the function differentialGeneTest (Monocle's main differential analysis routine). 2,579 genes (64,68% of a total of 3,987 genes considered as expressed) were significative with FDR adj. p < 1% for the combination of factors: ~SeuratCluster+Condition, and thus, defined the high dimensional space for pseudotemporal trajectory analysis.

Discriminative dimensionality reduction with trees (DDRTree) reduction algorithm learns the principal graph and specifies the trajectory. DDRTree was applied inside the function reduceDimension, and got the default parameters: norm_method = "log," pseudo_expr = 1, relative_expr = TRUE, auto_param_selection = TRUE (automatically calculate the proper value for the ncenter (number of centroids)) and scaling = TRUE (scale each gene before running trajectory reconstruction). Prior the dimensional reduction, the function reduceDimension also performed a variance-stabilization of the data (because the expressionFamily of the data was negbinomial.size). Finally, the cells were ordered according to pseudo-time with the function orderCells, which added a pseudo-time value and state for each cell; together encode where each cell maps to the trajectory.

For enrichment analysis on pseudotime trajectories, top-ranked 250 branched expression analysis modeling (BEAM) significant changes through the progression across the disease trajectory for each sublayer were clusterized and GO enrichment analyses on upregulated and downregulated clusters were performed using DAVID (v.6.8) bioinformatics platform (Huang et al., 2009).

Cell-type immunostaining and analysis

To evaluate the contribution of different cell-types to hippocampal sclerosis, control and epileptic rats and mice were perfused with 4% paraformaldehyde (PFA) and 15% saturated picric acid in 0.1 M PBS, pH 7.4. Brains were postfixed overnight and cut in 70 μm coronal sections (Leica VT 1000S vibratome). Sections containing the dorsal-intermediate hippocampus were processed with Triton 1% in PBS and blocked with 10% fetal bovine serum (FBS) in PBS-Tx. Sections were incubated overnight at RT with 1% FBS PBS-Tx solution containing primary antibodies against a battery of cell-type specific markers. The list of antibodies includes: rabbit anti-calbindin (1:1000, CB D-28k, Swant CB-38) or mouse anti-calbindin (1:500, CB D-28k, Swant 300) to identify superficial CA1 pyramidal cells; rabbit anti-Wfs1 (1:500, Protein Tech, 11558-1-AP) for CA1 pyramidal cells; rabbit anti-Iba1 (1:1000, Wako, 019-19741) for microglia; rabbit anti-GFAP (1:1000, Sigma, G9269) for astrocytes; rabbit anti-Olig2 (1:200, Millipore, AB9610) for oligodendrocytes. After three washes in PBS-Tx, sections were incubated for 2 hours at RT with appropriate secondary antibodies: goat anti-rabbit Alexa Fluor633 (1:200, ThermoFisher, A-21070), and donkey anti-mouse Alexa Fluor488 (1:200, ThermoFisher, A-21202) or goat anti-mouse Rhodamine Red (1:200, Jackson ImmunoResearch, 115-295-003) in PBS-Tx-1%FBS. Following 10 min incubation with bisbenzimide H33258 (1:10000 in PBS, Sigma, B2883) for nuclei labeling, sections were washed and mounted on glass slides in Mowiol (17% polyvinyl alcohol 4-88, 33% glycerin and 2% thimerosal in PBS).

To acquire multichannel fluorescence stacks from recorded cells, a confocal microscope (Leica SP5) with LAS AF software v2.6.0 build 7266 (Leica) was used. The following channels (fluorophore, laser and excitation wavelength, emission spectral filter) were used: a) bisbenzimide, Diode 405 nm, 415–485 nm; b) Alexa Fluor 488 nm, Argon 488 nm, 499–535 nm; c) Rhodamine Red / Alexa Fluor 568 / Texas Red, DPSS 561 nm, 571–620 nm; d) Alexa Fluor 633, HeNe 633 nm, 652–738 nm; and objectives HC PL APO CS 10.0 × 0.40 DRY UV, HCX PL APO lambda blue 20.0 × 0.70 IMM UV and HCX PL APO CS 40.0 × 1.25 OIL UV were used.

FluoroJade staining

To evaluate neurodegenerating neurons we used coronal sections from epileptic rats perfused at different time points post-*status*. Selected sections were immunostained against Wfs1 followed by FluoroJade staining. To this purpose, sections were pretreated for 5 min with 1% sodium hydroxide in 80% ethanol, followed by 70% ethanol (2 min) and distilled water (2 min). Sections were then incubated 10 min in 0.06% potassium permanganate, rinsed in distilled water and immersed into 0.0001% solution of FluoroJade C dye (Sigma AG325) in 0.1% acetic acid (pH 3.5) for 10 min. After a brief wash in distilled water, they were mounted on gelatin-coated slides, air-dried, coverslipped with DPX and examined under a confocal microscope as described above. FluoroJade positive cells exhibited bright green fluorescence.

In situ hybridization analysis

Selected sections from control and epileptic rats were processed for *in situ* hybridization using standard methods. Briefly, riboprobes were prepared from Rat *Enpp2* cDNA (Image clone ID 7115236) and using RT-PCR from rat adult hippocampus to prepare *Wfs1* (NM_031823.1, from bp 783 to 1631), *Ndst4* (XM_006233274.2, from bp 536 to 1024), *Syt17* (NM_138849.1, from bp 378 to 1118), *Hrt1a* (J05276.1, from bp 730 to 1663) and *Scn7a* (NM_131912.1, from bp 2812 to 3550) cDNAs. Similar riboprobes were used in sections from normal and epileptic mice. Riboprobe hybridization was detected using alkaline phosphatase–coupled anti-digoxigenin Fab fragments (Sigma). Hybridized sections were mounted in glycerol and photographed using a Nikon stereoscope and a DCC Nikon camera.

RNAscope analysis

Control and epileptic mice were perfused with 4% paraformaldehyde (PFA) and 15% saturated picric acid in 0.1 M PBS, pH 7.4. Brains were post-fixed overnight and cut in 50 μm coronal sections (Leica VT 1000S vibratome) which were kept at −20°C in a solution of 30% glycerol and 30% etylenglycol in PBS. RNAscope Fluorescent Multiplex Assay (Advanced Cell Diagnostics) was carried out according to the manufacturer's protocols. Briefly, sections containing the dorsal-intermediate hippocampus (around −2 μm AP from Bregma) were washed in PBS-Tx, and mounted onto SuperFrost Plus microscope slides (10149870, ThermoFisher Scientific). They were then dehydrated at 60°C follow by ethanol, pretreated with a target retrieval solution (322000, ACD) and protease III (322340, ACD), and co-hybridized with *Spag5* (Mm-Spag5, 505691, ACD) and *Dcc* (Mm-Dcc-C3, 427491, ACD) or *Dapk1* (Mm-Dapk1-C3, 880221-C3, ACD) probes. Finally, the amplification steps (RNAscope Fluorescent Multiplex Detection reagents, 320851, ACD) were followed, using Atto 550 for *Spag5* and Atto 647 for *Dcc* or *Dapk1* as fluorescent labels. The RNAscope 3-plex positive control probe set (320881, ACD), with probes to Polr2a, PPIB and UBC, was used to confirm preservation of sample RNA. The negative control probe to bacterial DapB (320871) was used to establish non-specific labeling.

Following the RNAscope protocol, sections were blocked for 30 min with 10% FBS in PBS-Tx, and incubated overnight at RT with rabbit anti-Wfs1 (1:500, Protein Tech, 11558-1-AP) in 1% FBS PBS-Tx. After three washes in PBS, sections were incubated for 2 h with donkey anti-rabbit Alexa Fluor488 (1:200, ThermoFisher Scientific, A-21206) in 1% FBS PBS-Tx, washed twice in PBS and mounted using ProLong Gold Antifade mountant (ThermoFisher Scientific, P10144).

Cell Reports
Article

Multichannel fluorescence stacks were achieved in a confocal microscope (Leica SP5) with LAS AF software v2.6.0 build 7266 (Leica), with a 40x objective (HCX PL APO CS 40.0 × 1.25 OIL UV), at 0.5 μm z-interval. Pinhole was set at 1 Airy, and following channels settings were applied for each fluorophore (excitation wavelength, emission spectral filter): Argon (488 nm, 499–553 nm) for Alexa Fluor488, DPSS (561 nm, 570–630 nm) for Atto 550, and HeNe (633 nm, 645–740 nm) for Atto 647. Diode (405 nm, 415–485 nm) was used as an unstained channel to identify autofluorescent material, which can be abundant in epileptic tissue. Images were acquired at 8 bits, 387.5 × 387.5 μm (1024 × 1024 pixels) in size. Brightness and contrast were adjusted with the ImageJ Fiji software (NIH Image).

To estimate the amount of *Dapk1*, *Spag5* and *Dcc* transcripts per cell, a total of 5 control and 5 epileptic animals (12 cells per animal) were analyzed. Each ROI was drawn in one confocal plane as the outline of a pyramidal cell soma at their maximum diameter based on Wfs1 immunoreactivity, using ImageJ. Only those cells focused within the first 10 μm were selected to avoid reduction of the signal due to depth in the section. In either *Dapk1*, *Spag5* or *Dcc* channels, single signal dots were counted, and clusters were converted to dot number as suggested by the manufacturer (ACD): (total intensity - average background intensity x area)/single dot average intensity.

QUANTIFICATION AND STATISTICAL ANALYSIS

Statistical analyses were performed with MATLAB, SPPSS and using the computing environment R (R Development Core Team, 2005, http://www.R-project.org). No statistical method was used to predetermine sample sizes. Normality and homoscedasticity were evaluated with the Kolmogorov–Smirnov and Levene's tests, respectively. The exact number of replications for each experiment is detailed in text and figures. Several ways ANOVAs or Friedman tests were applied. Post hoc comparisons were evaluated with the Tukey-Kramer, Student or Wilcoxon tests. Deep-superficial trends were evaluated using Spearman correlation and tested against 0 (i.e., no correlation was the null hypothesis) at $p < 0.05$ (two sided).

Supplemental information

Sublayer- and cell-type-specific

neurodegenerative transcriptional

trajectories in hippocampal sclerosis

Elena Cid, Angel Marquez-Galera, Manuel Valero, Beatriz Gal, Daniel C. Medeiros, Carmen M. Navarron, Luis Ballesteros-Esteban, Rita Reig-Viader, Aixa V. Morales, Ivan Fernandez-Lamo, Daniel Gomez-Dominguez, Masaaki Sato, Yasunori Hayashi, Àlex Bayés, Angel Barco, Jose P. Lopez-Atalaya, and Liset M. de la Prida

SUPPLEMENTAL INFORMATION
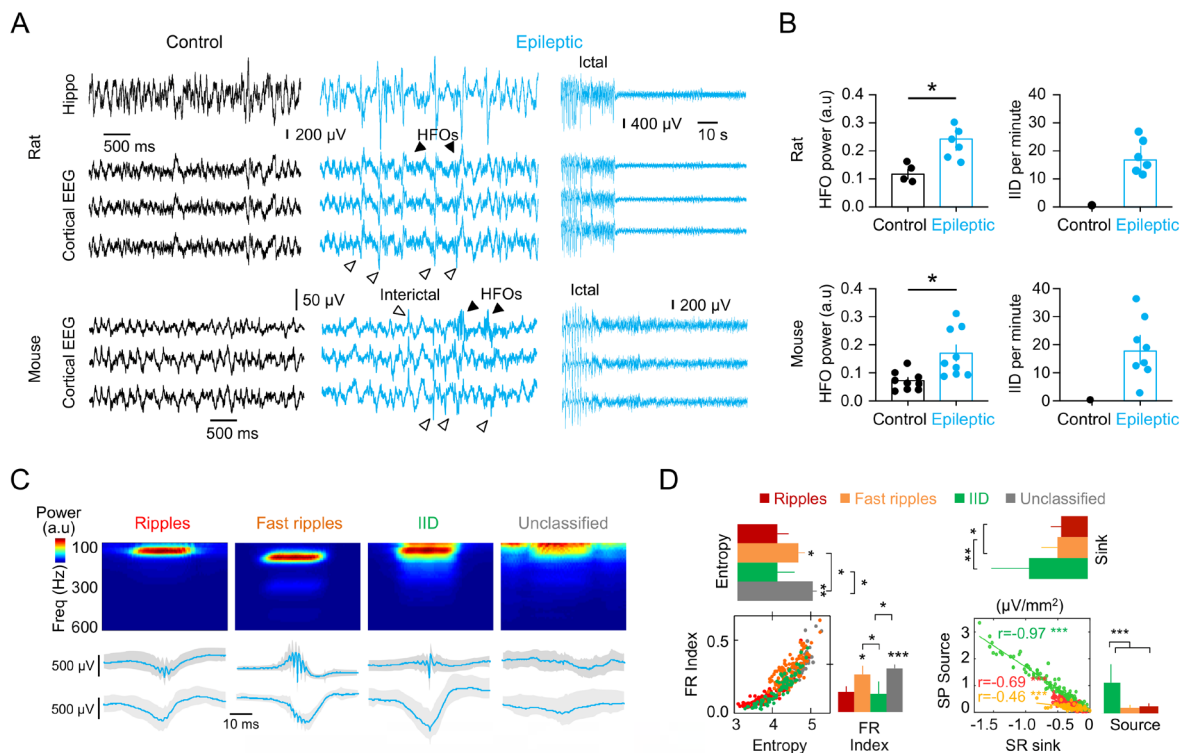
Figure S1. Electrophysiological Analysis, Related to Figure 1.
(A) Cortical EEG and/or intrahippocampal recordings from epileptic rats and mice allowed evaluation of neurophysiological changes accompanying acquired epilepsy. Simultaneous cortical and hippocampal recordings are shown for rats, while cortical EEG is shown for mice. Note interictal discharges (IID) and high-frequency oscillations (HFOs) in epileptic animals recorded both intracranially and at the cortical surface over the hippocampus. The small size of the mouse brain and connectivity between the hippocampus and prefrontal cortex facilitates recording of HFOs at scalp. The late stage of a seizure recorded in both animals is shown to highlight ictal discharges.
(B) Quantification of the HFO power and IID rate in rats and mice 6 weeks after status. IID rate was evaluated from 20 min sessions in epileptic animals. Data from 1 session from 6 rats and 3 sessions from 3 mice. *, $p < 0.05$ unpaired t-test.
(C) Sharp-wave (SPW) associated HFO events recorded from the dorsal hippocampus of urethane anesthetized epileptic rats were automatically detected and separated as ripples (100-150 Hz), fast ripples (> 150 Hz) and IID using amplitude and spectral information. Some events were left unclassified.
(D) Quantitative separation of ripples, fast ripples and IID events. Spectral indices such as entropy and fast ripple indices were combined with information on the amplitude of current-source density (CSD) signals. IID were clearly separated from SPW events using CSD amplitude of sinks and sources. Asterisks reflect significant differences from post hoc Tukey tests as *, $p < 0.05$; **, $p < 0.01$ and ***, $p < 0.001$.

Figure S2. CA1 Sublayer-Specific Gene Expression Profiling by LCM RNA-seq, Related to Figure 2 and Figure 3.

(A) Bar graph showing per-sample sequencing depth. Note similar library size of about 50 x 10^6 fragments per sample in both groups (paired-end sequencing).

(B) Principal component analysis of normalized rlog counts. Note pairwise clustering of deep and superficial samples from the same animals and significant separation between control and epileptic replicates, suggesting that transcriptional variability underlie between-group differences.

(C) Scatterplot showing differentially expressed genes between superficial and deep manually sorted neurons from mice (false discovery ratio, FDR adj. p < 0.1; data from Cembrowski et al., 2016) against change in mRNA expression for these genes in bulk-tissue LCM RNA-seq data from rats (y-axis) (this study). Colored points indicate genes that were differentially expressed across sublayers in both species.

(D) In situ hybridizatrion (ISH) of the dorsal CA1 specific marker *Wfs1*, the superficial sublayer marker *Syt17* and deep sublayer marker *Ndst4* in representative hippocampal sections from control and epileptic rats and mice. Note sublayer markers are not all-or-none, but rather reflect a gradient distribution. Scale bar, 100 μm.

(E) Allen Brain Atlas (ABA) ISH sections showing additional genes differentially regulated in deep and superficial sublayers in mouse. Note regionalization of some interneuron-specific genes such as *Sst* and *Vip*, as well as non-neuronal genes such as *Mbp*. Scale bar, 100 μm.

(F) Scatter plot of genes differentially expressed between superficial and deep CA1 sublayers in control or epileptic rats (adj. p value < 0.1). Names of bona fide gene markers of superficial (*Calb1, Grm1, Syt17*) and deep (*Ndst4, Nr4a2, Col11a1*) pyramidal neurons are highlighted (black text and bold font). Shown in the plot is also the names of known cell-type marker genes (grey). (Interneurons – *Sst*, *Vip*, *Kit*, Oligodendrocytes – *Mbp*, *Mobp*, *Plp1*, Astrocytes – *Aqp4*, *Gfap*, *Gja1*, Microglia – *Csf1r*, *Tgfbr1*). Note also the presence of a subset of uncorrelated transcripts including canonical markers of microglia cells (*Trem2*, *Irf8*, *Fcgr2b*, *Cd68*), at the superficial sublayer in epileptic rats (red). MLE: maximum-likelihood estimate.

(G) Bar plot of the eleven cell-type-specific uncorrelated DEGs from Figure 2C showing expression levels in single cells from the mouse CA1 area (Zeisel et al., 2015) (see Methods section).

(H) Scatter plot showing changes in gene expression in CA1 superficial and deep CA1 sublayers in epilepsy (global effect: 732 unregulated, 185 downregulated genes (adj. p < 0.01 and $\log_2$ fold change > 0.5).

(I) Single-cell consensus clustering (SC3) analysis (Kiselev et al., 2017) was performed on publicly available single-cell RNA-seq data from mouse cortex and hippocampus (Zeisel et al., 2015) to cluster the cells and to identify marker genes. Next, scRNA-seq data for genes identified in LCM RNA-seq analyses (gene lists of top 250 differentially expressed genes between CA1 sublayers of control and epileptic rats) was used to deconvolve bulk-tissue LCM RNA-seq by identifying the presence of co-expressed genes at the single cell level containing marker genes.

(J) Pairwise correlations of the average expression for the 69 cell-type gene markers obtained using SC3 on single-cell RNA-seq data from Zeisel et al., (2015).

(K) Bar plot showing expression levels as $\log_2$(molecules/cell) for the 69 cell type gene markers at single cell level (x-axis) across the seven major cell types identified using SC3. Pyr, pyramidal neurons; Inter, interneurons; ODC, oligodendrocytes; Astro, astrocytes; Endo, endothelial cells; Micro, microglia; Mural, mural cells.

Figure S3. Transcriptional Changes Associated with Microglia in The Epileptic CA1 (Bulk-Tissue LCM RNA-seq), Related to Figure 2 and Figure 3.

(A) Heatmaps of log$_2$ fold changes for genes annotated to the microglial sensome (Hickman et al., 2013). Log$_2$ fold change values are for the epilepsy effect in superficial and deep sublayers (Epilepsy), and for sublayer effect in control and epileptic mice (Sublayer). *, Adj. p < 0.1. Gene Ontology: Biological Process annotation (GO:BP) is shown at the foremost right (black squares). The list continues from left to right.

(B) Schematic diagram illustrating neuron-glia interactions via ligand-receptor pairings. Neuronal ligands (diamonds) and microglia receptors (circles) are color coded by expression log$_2$ fold change (see color scheme legend) in the comparison between superficial and deep sublayer in control (top-left) and epileptic (top-right) CA1, and for epilepsy effect in deep (bottom-left) and superficial (bottom-right) CA1 sublayer. *, Adj. p < 0.1.

Figure S4. Transcriptional Profiling at Single-Nucleus Level Unfolds Heterogeneity of Excitatory Pyramidal Neurons in The Basal and Epileptic Hippocampal CA1 Area, Related to Figure 5.
(A) Uniform Manifold Approximation and Projection (UMAP) plot from snRNA-seq transcriptional profiling showing 6 major cell classes identified and annotated in our CA1 samples.
(B) Heatmap of cell-type marker genes (168 enriched genes with AUC power >= 0.55) scaled expression per single-nucleus across identified cell populations.
(C) UMAP plot of the snRNA-seq datasets split by condition.
(D) Violin plots showing distribution of nUMI (left) and nGene (right) per major populations as indicated in the legend.
(E) UMAP plot clustering of the CA1 pyramidal cell population took two rounds. In the first round, nuclei were automatically separated in three main subclusters: deep cells, superficial cells and a third cluster of pyramidal neurons (Pyr_CA1). In the second round, the subsetted Pyr_CA1 cells were sorted as deep and superficial and epilepsy-specific Pyr_ES cells (green).
(F) UMAP plot of the pyramidal cell class colored by normalized expression levels for the indicated subpopulation gene markers.
(G) UMAP plot of the subsetted Pyr_CA1 pyramidal cells. Note separation of deep and superficial cells, as well as the epilepsy-specific pyramidal cell subpopulation (Pyr_ES).

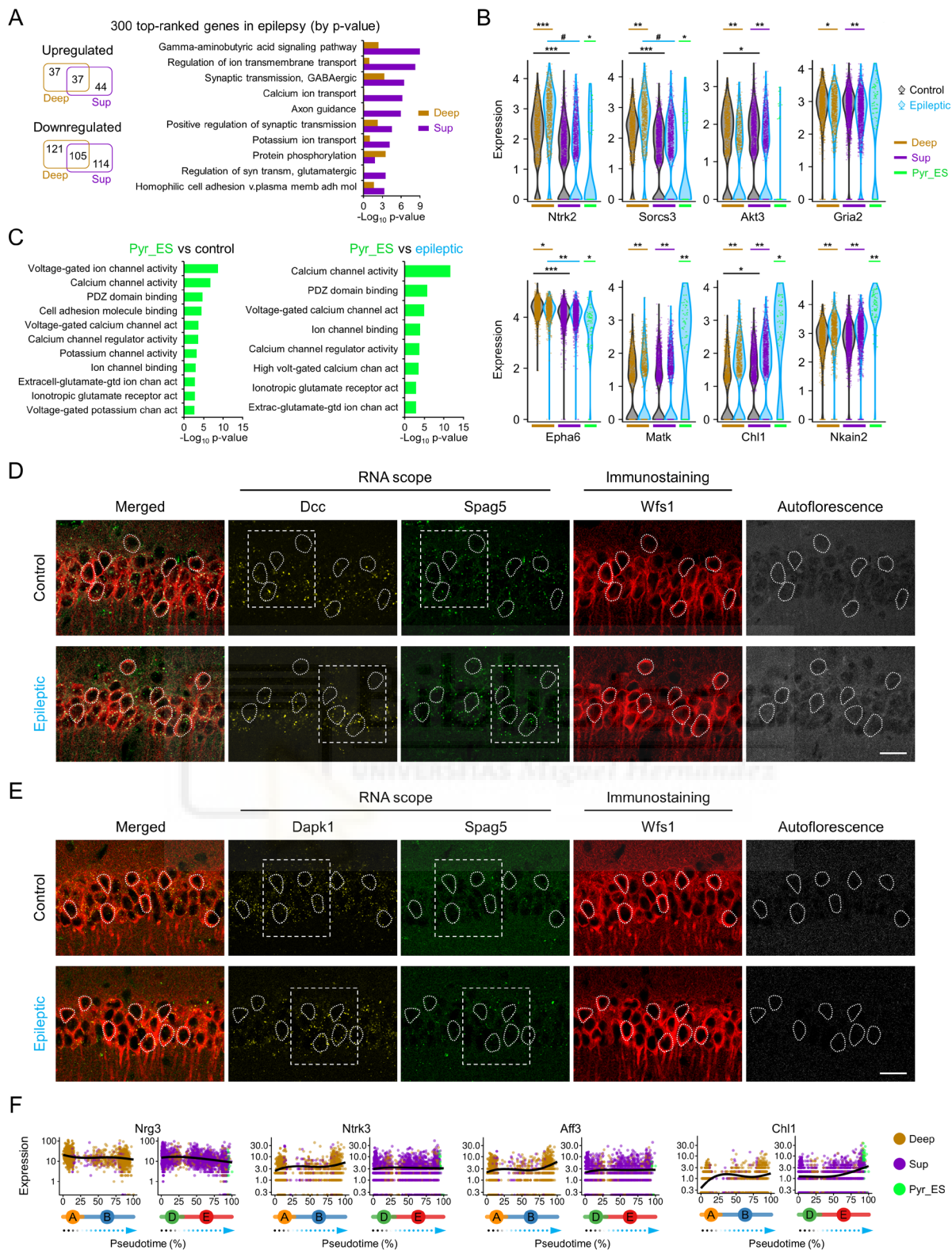**(H)** Box plots showing nUMI (left) and nGene (right) per cell in the epilepsy-specific population Pyr_ES population.
(I) Confirmation of cell-type specific gene mapping of sorted cells.
(J) Proportions of the distinct cell types and populations identified across conditions (control and epilepsy). Note the epilepsy-specific population Pyr_ES (light green).

Figure S5. Overlap Between LCM RNA-seq and snRNA-seq Sublayer-Specific Results, Related to Figure 2 and Figure 5.

(A) Venn diagram showing overlap in genes identified as significantly enriched in superficial (Sup LCM RNA-seq) and deep sublayer (Deep LCM RNA-seq) by bulk-tissue CA1 sublayer-specific tissue gene expression profiling (LCM RNA-seq) or snRNA-seq. Many sublayer- and cell-subtype significantly enriched transcripts were common across species (rat, mouse) and technologies (bulk-tissue RNA-seq, snRNA-seq).

(B) GO analysis and heatmap showing average of normalized expression for genes significantly enriched in deep CA1 neurons (snRNA-seq) in the control animals.

(C) Same as in B for genes significantly enriched in superficial CA1 neurons (snRNA-seq) in the control animals.

Figure S6. Gene profiling at single cell nuclei reveals transcriptional changes in superficial and deep CA1 neurons in experimental epilepsy, Related to Figure 5 and Figure 6.
(A) Venn diagram and GO terms of top-ranked 300 genes modulated in epilepsy.
(B) Violin plots showing normalized expression value (normalized log transformed UMIs) by condition (control, black; epilepsy, blue) and population (deep, occher; superficial, purple; Pyr_ES, light-green) for selected genes modulated in epilepsy. Note specific upregulation in Pyr_ES cells of *Matk*, *Chl1*, and *Nkain2*. *, $p < 0.05$; **, $p < 10^{-10}$; ***, $p < 10^{-50}$ (Wilcoxon rank sum test).

(C) Bar chart of significant GO:BP terms for most upregulated genes in Pyr_ES when compared with control (left) and epileptic (right) CA1 pyramidal cells (absolute $\log_2$ fold change > 0.5 and min.pct = 0.5).

(D) Combined RNAscope and Wfs1 immunostaining analysis of *Dcc* and *Spag5* in situ. Neurons having their soma cut transversally by the confocal plane are outlined. Discontinuous line boxes identify the region expanded in Figure 5. The channel 405 nm was used to control for autofluorescent signals across channels, which are characteristic of epileptic tissue (rightmost). Scale bar, 10 μm.

(E) Same for *Dapk1* and *Spag5*.

(F) Examples of pseudotemporal kinetics across disease trajectory for significantly modulated genes in epilepsy related to neuronal survival (*Nrg3*, *Ntrk3*, *Aff3, Chl1*).

NEURODEGENERATIVE TRAJECTORIES IN A MODEL OF EPILEPSY WITH HIPPOCAMPAL SCLEROSIS

Ángel Márquez Galera
PhD Thesis
Supervised by Dr. José Pascual López-Atalaya Martínez

Summary

Temporal lobe epilepsy (TLE), the most common form of focal epilepsy, is a chronic disorder of the nervous system which is characterized by recurrent, unprovoked focal seizures that originate in the temporal lobe of the brain. Hippocampal sclerosis (HS), the major neuropathological hallmark of temporal lobe epilepsy, is characterized by different patterns of neuronal loss and is associated with cognitive impairment and drug resistance. One of the areas most affected by hippocampal sclerosis is the CA1 subfield, a layered structure consisting of a superficial and a deep sublayer. However, the mechanisms leading to CA1 hippocampal sclerosis are unknown. Using single-cell electrophysiology *in vivo* and immediate-early gene expression, we reveal that superficial CA1 pyramidal neurons are overactive in epileptic rodents. Bulk tissue and single-nucleus expression profiling disclose sublayer-specific transcriptomic signatures. These analyses reveal that superficial sublayer is more severely affected by epilepsy, showing a prominent neurodegeneration-associated transcriptomic signature that was characterized by upregulation of microglia reactive response and cell cycle genes, and downregulation of neuronal plasticity genes. Pseudotime analysis of gene expression in single nuclei and *in situ* validation reveal separated trajectories from health to epilepsy across cell types and identify a subset of superficial cells undergoing a later stage in neurodegeneration. Our findings indicate that sublayer- and cell-type-specific changes associated with selective neuronal damage in CA1 contribute to progression of hippocampal sclerosis, with neurons populating the superficial CA1 sublayer being much more vulnerable than those in the deep sublayer. In addition, we have introduced a protocol that leverages existing single-cell expression data to deconvolve lists of differentially expressed genes from highly heterogeneous tissues into cell-type-specific gene expression patterns. We have made all the data from this study accessible as public resources through interactive websites that facilitate exploration of analysis results.

Keywords

epilepsy; temporal lobe epilepsy; hippocampal sclerosis; neurodegenerative trajectories; single-nucleus RNA-seq; microdissected tissue RNA-seq; *in vivo* single-cell electrophysiology; gene expression *in situ* hybridization; transcriptomic data visualization app; cell type specificity; DEGs deconvolution into gene patterns.

INSTITUTO DE NEUROCIENCIAS